National Library of Canada
Acquisitions and Bibliographic Services Branch
395 Wellington Street
Ottawa, Ontario
K1A 0N4

Bibliothèque nationale du Canada
Direction des acquisitions et des services bibliographiques
395, rue Wellington
Ottawa (Ontario)
K1A 0N4

Your file Votre référence

Our file Notre référence

NOTICE

The quality of this microform is heavily dependent upon the quality of the original thesis submitted for microfilming. Every effort has been made to ensure the highest quality of reproduction possible.

If pages are missing, contact the university which granted the degree.

Some pages may have indistinct print especially if the original pages were typed with a poor typewriter ribbon or if the university sent us an inferior photocopy.

Reproduction in full or in part of this microform is governed by the Canadian Copyright Act, R.S.C. 1970, c. C-30, and subsequent amendments.

AVIS

La qualité de cette microforme dépend grandement de la qualité de la thèse soumise au microfilmage. Nous avons tout fait pour assurer une qualité supérieure de reproduction.

S'il manque des pages, veuillez communiquer avec l'université qui a conféré le grade.

La qualité d'impression de certaines pages peut laisser à désirer, surtout si les pages originales ont été dactylographiées à l'aide d'un ruban usé ou si l'université nous a fait parvenir une photocopie de qualité inférieure.

La reproduction, même partielle, de cette microforme est soumise à la Loi canadienne sur le droit d'auteur, SRC 1970, c. C-30, et ses amendements subséquents.

Canada

UNIVERSITY OF ALBERTA

STUDIES OF THE MECHANISM OF ELECTROSPRAY IONIZATION MASS SPECTROMETRY

BY

LIANG TANG

A thesis submitted to the faculty of Graduate Studies and Research in partial fulfillment of the requirements for the degree of DOCTOR OF PHILOSOPHY

DEPARTMENT OF CHEMISTRY

Edmonton, Alberta

FALL 1993

National Library of Canada
Acquisitions and Bibliographic Services Branch
395 Wellington Street
Ottawa, Ontario
K1A 0N4

Bibliothèque nationale du Canada
Direction des acquisitions et des services bibliographiques
395, rue Wellington
Ottawa (Ontario)
K1A 0N4

Your file Votre référence

Our file Notre référence

The author has granted an irrevocable non-exclusive licence allowing the National Library of Canada to reproduce, loan, distribute or sell copies of his/her thesis by any means and in any form or format, making this thesis available to interested persons.

L'auteur a accordé une licence irrévocable et non exclusive permettant à la Bibliothèque nationale du Canada de reproduire, prêter, distribuer ou vendre des copies de sa thèse de quelque manière et sous quelque forme que ce soit pour mettre des exemplaires de cette thèse à la disposition des personnes intéressées.

The author retains ownership of the copyright in his/her thesis. Neither the thesis nor substantial extracts from it may be printed or otherwise reproduced without his/her permission.

L'auteur conserve la propriété du droit d'auteur qui protège sa thèse. Ni la thèse ni des extraits substantiels de celle-ci ne doivent être imprimés ou autrement reproduits sans son autorisation.

ISBN 0-315-88229-8

Canada

UNIVERSITY OF ALBERTA

RELEASE FORM

NAME OF AUTHOR: LIANG TANG

TITLE OF THESIS: STUDIES OF THE MECHANISM OF ELECTROSPRAY IONIZATION MASS SPECTROMETRY

DEGREE: DOCTOR OF PHILOSOPHY

YEAR THIS DEGREE GRANTED: 1993

Permission is hereby granted to the University of Alberta library to reproduce single copies of this thesis and to lend or sell such copies for private, scholarly or scientific research purposes only.

The author reserves all other publication and other rights in association with the copyright in the thesis, and except as hereinbefore provided neither nor any substantial portion thereof may be printed or otherwise reproduced in any material form whatever without the author's prior written permission.

Tang Liang

September 27, 1993

UNIVERSITY OF ALBERTA

FACULTY OF GRADUATE STUDIES AND RESEARCH

The undersigned certify that they have read, and recommend to the Faculty of Graduate Studies and Research for acceptance, a thesis entitled STUDIES OF THE MECHANISM OF ELECTROSPRAY IONIZATION MASS SPECTROMETRY submitted by LIANG TANG in partial fulfillment of the requirements for the degree of DOCTOR OF PHILOSOPHY.

P. Kebarle

Dr. Paul Kebarle

Frederick F. Cantwell

Dr. Frederick F. Cantwell

H B Dunford

Dr. H. Brian Dunford

Dr. John Gray

Gary Horlick

Dr. Gary Horlick

Jan Sunner

Dr. Jan Sunner

September 27, 1993

To my parents, my wife and my son

ABSTRACT

The two major processes in electrospray mass spectrometry (ESMS) are the formation of charged droplets and the formation of gas phase ions.

Measurements of the total electrospray current, I, from solutions of the electrolytes HCl and NaCl, in methanol and water respectively, demonstrate that the current I increases with the conductivity σ of the solution. The relationship, $I = A\sigma^n = A(\lambda_m^\circ C)^n$, where A is a constant, λ_m° is the limiting molar conductivity of the given electrolyte at concentration C and $n \approx 0.22$ has been found. Thus, while electrolytes with higher λ_m° give higher ion currents for a given concentration, differences between electrolytes are small due to the low value of n. The applicability of this equation supports the electrophoretic mechanism in the formation of charged droplets in electrospray.

The dependence of the mass analyzed ion intensities, I_A and I_B, of analytes A^+ and B^+ for a variety of concentrations, $[A^+]$ and $[B^+]$, in the same methanol solution have been determined in several series of experiments. The equation $I_{(A^+ ms)} = pf \frac{k_A[A^+]}{k_A[A^+] + k_B[B^+]} I$ where p is a constant expressing the efficiency of the mass spectrometer for sampling the gas phase ions current and f is the efficiency of conversion of droplet charge to gas phase ions, is proposed and coefficient k values obtained for the ions, Li^+, Na^+, K^+, Cs^+, NH_4^+, several protonated alkaloids, $(Ethyl)_4N^+$, $(n\text{-}Propyl)_4N^+$, $(n\text{-}Butyl)_4N^+$, $n\text{-}C_7H_{15}NH_3^+$, $n\text{-}C_{11}H_{23}NH_3^+$, were obtained. The observed coefficients, k, depend on the surface activities of the analytes when $[A^+]$ and $[B^+]$ are in the range 10^{-8} to 5×10^{-6} mol/L and on the ion evaporation rate constants and surface activities for $[A^+]$ and $[B^+]$ in the

range 5×10^{-5} to 10^{-2} mol/L. Ion evaporation rates predicted by the Iribarne equation follow the same pattern as the experimental coefficients but the exact predictions of the equation could not be confirmed or disproved.

Rates of solvent loss from the droplets and the fission of the droplets due to Rayleigh instability are also included in the analysis. It is verified that charged droplets begin to produce gas phase ions after most solvent has evaporated.

ACKNOWLEDGMENT

I wish to express my sincere appreciation to Professor Paul Kebarle for his advice and encouragement throughout the course of this work.

I would especially thank Dr. Allan Hogg for providing me valuable assistance and advice on mass spectrometric techniques.

The helpful suggestions and comments from Dr. Arthur T. Blades during my research are greatly appreciated. I should also thank everyone in Professor Kebarle' research group, in particular, Dr. Stephen Anderson for his help with the upgraded data system on the SCIEX mass spectrometer.

I would also like to express my appreciation to the contributions from chemistry department, mass spectrometry laboratory, machine shop, electronic shop, glass shop and all other supporting staff.

The financial assistance provided by the University of Alberta and the National Research Council of Canada is acknowledged.

TABLE OF CONTENTS

CHAPTER PAGE

1. General Introduction 1
   1.1 Electrospray phenomena. 1
   1.2 Ionization methods widely used in analytical mass spectrometry . . . 2
   1.3 Electrospray mass spectrometry and its status in the development . . 5
   1.4 References. 11
2. Effect of the Conductivity of the Electrosprayed Solution on the Electrospray Current. Factors Determining Analyte Sensitivity in Electrospray Mass Spectrometry. 15
   2.1 Introduction 15
   2.2 Experimental 20
      a. Total ion current measurement. 20
      b. Electrolyte solutions and conductivity measurements. 22
   2.3 Results and Discussion. 22
      a. Electrospray current. Dependence on conductivity of solution, limiting molar conductivity and concentration of electrolyte. 22
      b. Comparison with the Hendricks equation for the electrospray current I. 27
      c. Dynamic range of detected analyte ion intensity in ESMS. 30
   2.4 Conclusions. 37
   2.5 Appendix Conductivity at high electric fields. 38
   2.6 References 43
3. Dependence of Ion Intensity in Electrospray Mass Spectrometry on the Concentration of the Analytes in the Electrosprayed Solution 45
   3.1. Introduction. 45
   3.2 Experimental. 49

3.3 Results and Discussion. 57
I. Behavior when electrolytes are at higher, 10^{-5}-10^{-3} M, concentrations 57
a. Experiments where the analyte ion concentration is constant and a second electrolyte, B^+, is present in increasing concentrations. 57
b. Experiments where concentration is increased and [A] = [B] 67
II. Behavior when electrolytes are at low concentration, $<10^{-5}$ M. Indication for depletion of ions with a high coefficient k and for surface activity effects.. 71
III. Physical background and significance of coefficients k and equation 3-4. 75
a. Properties of the Iribarne ion evaporation equation. 75
b. Ion evaporation and solvent evaporation. 82
c. Competitive ion evaporation. 85
d. Charge, radius, concentration and time dependence for droplets evolving towards gas phase ion emission. 88
e. Prediction of the decrease of observed k_A/k_B ratio at low concentrations due to depletion of ions with higher evaporation coefficient. 93
f. Predictions of k_A' / k_B' from theory and experiment:. 96
g. Ion solvation and ion surface activity. 101
h. A possible alternative mechanism for gas phase ion formation. . . 103
3.4 Conclusions. 106
3.5 Appendix Evaluation of depletion effect. 107
3.6 References. 112

4. Complexation of Alkali Cation M^+ to 18-Crown-6. Comparison of Expected Concentrations of M^+ and M^+·18-Crown-6 in Solution with Observed Ion Intensitiesof M^+ and M^+·18-Crown-6 in ESMS. 114
4.1 Introduction. 114
4.2 Experimental. 115
a. Mass-dependent discrimination and ion intensity calibration. . . . 115
b. Gas phase reactions between ion M^+ and crown ethers. 117
4.3 Results and Discussion. 120
a. Complexation of metal ions and cyclic ligands in solution. 120
b. Gas phase reactions of metal ions and macrocyclic ligands. 135
4.4 Conclusions. 141
4.5 References. 142
5. Sampling Efficiency in ESMS. 143
5.1 Introduction. 143
5.2 Experimental. 147
5.3 Results and Discussion. 148
a. Ion intensity dependence on axial distance between ES tip and ion sampling orifice. 148
b. Ion intensity dependence on radial distance between ES tip and the ion sampling orifice. 157
c. Influence of flow rate on the sampling of relative ion intensities. . 161
5.4 Conclusions. 161
5.5 References. 164

LIST OF FIGURES

PAGE

Figure 2-1 Schematic diagram of electrospray device 21

Figure 2-2 Two plots of measured conductivity σ of solutions of HCl respectively NaCl in solvent, 40% methanol, 60% water by weight versus concentration C of electrolyte, at 23°C 23

Figure 2-3 Logarithmic plot of electrospray current I versus conductivity of HCl and NaCl solutions in solvent 40% methanol, 60% water. 25

Figure 2-4 Logarithmic plot of measured ES current I versus concentration C of electrolytes HCl resp. NaCl in solvent 40% methanol, 60% water. 26

Figure 2-5 Linear plot of measured ES current I versus conductivity of solutions. 29

Figure 2-6 (Upper plot) Total electrospray current I as a function of added analyte concentration. (Lower plot) Changes of mass analyzed ion intensity (counts/s) of analyte ion versus analyte concentration. 34

Figure 3-1 A schematic diagram of TAGA 6000E. 50

Figure 3-2 A special APCI set-up of TAGA 6000E for transmission determination. 52

Figure 3-3 Transmission correction curve for ion intensity measurement on TAGA 6000E. 54

Figure 3-4 Ratio of total current on CB, I_{CB}, to total current fron the tip (ES tip or APCI tip) with CsCl in methanol. 55

Figure 3-5 Results from ES where $[A^+] = [CodH^+] = 10^{-5}$ M and $[B^+] = [NH_4^+]$ is increased as shown. (a) Measured capillary current I. (b) Ion intensities of NH_4^+ and $CodH^+$, corrected for transmission. (c) Predicted linear plot based on equation 3-6 leads to ratio $k_A/k_B = 3.4$. 58

Figure 3-6 Linear plots based on equation 3-6 for ions A^+ as shown. . . . 60

Figure 3-7 Ion Intensities of $[A^+] = 10^{-5}$ M and $[B^+] = [NH_4^+]$ at increasing concentrations. 61

Figure 3-8 (A) Capillary current I. (B) Ion intensity for Cs^+ when $[Cs^+] = 10^{-5}$ M and $[B^+] = [NH_4^+]$ or K^+ is increased. 65

Figure 3-9 (A) Capillary current I. (B) Ion intensity for $MorH^+$ when $[MorH^+] = 10^{-5}$ M and $[B^+] = [NH_4^+]$ or $[Bu_4N^+]$ is increased. 66

Figure 3-10 Ion intensities observed in experiment where $[A^+] = [B^+]$ is increased from 10^{-8} to 10^{-2} M. 68

Figure 3-11 Ion intensities observed in experiment where $[A^+] = [B^+]$ is increased from 10^{-8} to 10^{-2} M. 69

Figure 3-12 Ion intensities observed in experiments where $[A^+] = [B^+]$. . . 70

Figure 3-13 Observed ion intensities from separate experiments where $[A^+]$ is increased from 10^{-8} to 10^{-2} M. 74

Figure 3-14 Schematic representation of initial state (a) and transition state (b) proposed by Iribarne and Thomson (11). Evaporating ion leaves as a cluster $M^+(Sl)_m$ where Sl are solvent molecules. 77

Figure 3-15 Free energy as a function of distance x of $M^+(Sl)_m$ from surface of drop predicted by Iribarne equation. (a) R is used as parameter. (b) ΔG°_{sol} is used as parameter. 79

Figure 3-16 Free energy as a function of distance x of $M^+(Sl)_m$ from surface of drop predicted by Iribarne equation (a) d is used as parameter. (b) N is used as parameter. 81

Figure 3-17 (a) Change of number of charges N with time for a droplet undergoing Iribarne ion evaporation and solvent evaporation. (b) Change of radius of same droplet with time, evaluated with equation 3-17. (c) Change of rate constant, k, with time corresponding to the change of N and R. 86

Figure 3-18 Changes of radius R and charge Q with time of a droplet produced by electrospray which undergoes successive not symmetric droplet fission. 90

Figure 3-19 Changes of radius R, charge Q with time in droplet fissions of parent droplet and offspring droplets. 92

Figure 3-20 Predicted k_A/k_B ratio expected for a given ion evaporation ratio k'_A / k'_B in function of concentration $[A^+] = [B^+]$. 95

Figure 4-1 Structures of crown ethers used in the complexation with metal ions. 116

Figure 4-2 Transmission correction curve for ion intensity measurement on TAGA 6000. 118

Figure 4-3 An illustration of the device for gas phase ion molecule reaction. 119

Figure 4-4 Electrospray mass spectra of alkali metal from methanol solutions: (A) sodium ion and its solvated clusters from 10^{-4} M NaCl methanol solution; (B) sodium and crown ether complex from 10^{-4} M NaCl and 10^{-4} M 18C6 methanol solution. 123

Figure 4-5 Electrospray mass spectra of alkali metal from methanol solutions: (A) potassium ion and its solvated clusters from 10^{-4} M KCl methanol solution; (B) potassium and crown ether complex from 10^{-4} M KCl and 10^{-4} M 18C6 methanol solution. 124

Figure 4-6 Dependence of ion intensities of $K^+ \cdot (Sol)_n$ and $K^+ \cdot 18C6$ on 18C6 concentration. 129

Figure 4-7 Mass spectrum demonstrates the formation of "sandwich" style complex $[K^+ \cdot (18C6)_2]$ (m/z=567) when excess crown ether is present in solution. 130

Figure 4-8 Mass spectra obtained from experiment where M^+ is produced by ES and a given crown ether is vaporized as shown in Figure 4-3. 136

Figure 4-9 Crown ethers 12C4 and 18C6 have gas phase ion-molecule exchange reaction: $M^+ \cdot 18C6 + 12C4 = M^+ \cdot 12C4 + 18C6$. $M^+ \cdot 18C6$ is produced by electrospray and 12C4 in gas phase is produced by vaporizer. 138

Figure 4-10 Electrospray mass spectra of lithium chloride in methanol solution. 140

Figure 5-1 The position of electrospray tip is controlled by moving either supporting rod or x-y manipulator. 1. supporting rod; 2. x-y manipulator. 149

Figure 5-2 The axial distance dependence of ion intensities of Et_4N^+ and $K^+ \cdot (Sol)_n$ at constant voltage. Methanol solution contains 5×10^{-5} M Et_4NBr and 5×10^{-5} M KCl with r=0 mm, F=20 μL/min and constant capillary voltage V=5 kV. 150

Figure 5-3 The change of ES tip distance (L) from opposite electrode on the mass spectrometer shifts the relative ion intensities of $K^+ \cdot H_2O$ and $K^+ \cdot CH_3OH$. Both KCl and Et_4NBr concentrations are $5x10^{-5}$ M. (A) L=2.5 cm; (B) L=4 cm.. 151

Figure 5-4 The axial distance dependence of ion intensities of Et_4N^+ and $K^+ \cdot (Sol)_n$ at constant current. Methanol solution contains $5x10^{-5}$ M Et_4NBr and $5x10^{-5}$ M KCl with r=0 mm and constant ES current 0.2 μA. 153

Figure 5-5 Ion intensities change with axial distance observed by Hiraoka. ES solution is $5x10^{-6}$ M $(CH_3)_4NBr$ and $1x10^{-3}$ M CH_3COOH in $CH_3OH+H_2O+CCl_4$ (8/2/0.5 v/v/v); Flow rate=10 μL/min; Capillary voltage V=3.1 kV. 156

Figure 5-6 Ion intensities change with radial distance observed by Hiraoka. ES solution is $5x10^{-6}$ M $(CH_3)_4NBr$ and $1x10^{-3}$ M CH_3COOH in $CH_3OH+H_2O+CCl_4$ (8/2/0.5 v/v/v); Flow rate=10 μL/min; Capillary voltage V=3.1 kV. (A) L=1 cm; (B) L=1.5 cm.. . . 158

Figure 5-7 The radial distance dependence of ion intensities of Et_4N^+ and $K^+ \cdot (Sol)_n$. Methanol solution contains $5x10^{-5}$ M Et_4NBr and $5x10^{-5}$ M KCl with L=5 cm, F=20 μL/min and V=5 kV. . . . 160

Figure 5-8 The axial distance dependence of ion intensities of Et_4N^+ and $K^+ \cdot (Sol)_n$. Methanol solution contains $5x10^{-5}$ M Et_4NBr and $5x10^{-5}$ M KCl with r=0 mm, F=10 μL/min and V=4 kV. . . . 162

Figure 5-9 The radial distance dependence of ion intensities of Et_4N^+ and $K^+ \cdot (Sol)_n$. Methanol solution contains $5x10^{-5}$ M Et_4NBr and $5x10^{-5}$ M KCl with (A) L=5 cm, F=10 μL/min and V=4 kV and (B) L=1 cm, F=10 μL/min and V=3.1 kV. 163

LIST OF TABLES

PAGE

Table 3-1 Experimentally determined Ratios of Coefficients k 62

Table 3-2 Solvation Free Energies in Water 98

Table 3-3 Deviation of the Observed k_A/k_B from Real Ratio $k'_A(d, \Delta G_{sol, A})/k'_B(d, \Delta G_{sol, B})$ due to Ion Depletion 111

Table 4-1 Sensitivity Comparison between Gas Phase Alkali Ion and Complex Ion 125

Table 4-2 Concentration of Alkali Ion and Complex at Equilibrium in Methanol Solution 126

Table 5-1 Ion Intensity Changes with Axial Distance between ES Capillary and Sampling Orifice 154

LIST OF SYMBOLS

12C4	12-Crown-4
18C6	18-Crown-6
c_p	molar heat capacity
d:	distance of capillary tip to planar counter electrode
dm / dt	rate of droplet mass change
f	fraction of droplet charge that gets converted into gas phase ions
h	Planck constant
k	Boltzmann constant (in equation 3-11)
k (k_A)	sensitivity coefficient (of ion A)
m	mass
p	sampling efficiency
p°	solvent vapor pressure
q	charge
r	radial distance
$r_{c:}$	capillary outer radius
t	time
$\bar{v}$	average thermal velocity
z	number of ion charges
A	relaxation function
Å	angstrom
AC	alternative current
APCI	atmospheric pressure chemical ionization
B_j	electrophoretic function
Bu	n-butyl

C	concentration
CB	cluster breaker
CE	capillary electrophoresis
CI	chemical ionization
CAD	collision activated decomposition
$CocH^+$	protonated cocaine
$CodH^+$	protonated codeine
D	dielectric constant
DC	direct current
$E_{c:}$	imposed electric field in vacuum at capillary tip
Et	ethyl
EI	electron impact ionization
ES	electrospray
ESMS	electrospray mass spectrometry
F	volume factor (V_o/V_f)
F	Coulombic force (in Chapter 5)
FAB	fast atom bombardment
FTICR	Fourier transform-ion cyclotron resonance
FTICRMS	Fourier transform-ion cyclotron resonance mass spectrometer
H	a constant in Hendricks equation
$HerH^+$	protonated heroin
HPLC	high performance liquid chromatography
I	electrospray current
I_{obs}	observed ion intensities
$I(A^+,g)$	gas phase analyte ion current
$I(A^+_{ms})$	mass spectrometrically detected analyte ion intensity

ID	inner diameter
K_s	equilibrium constant
L	ligand (crown ether) (in Chapter 4)
L	axial distance (in Chapter 5)
LC	liquid chromatography
LD	laser desorption ionization
M	mole L^{-1}
M	molar mass of the solvent (in equation 3-15)
MS	mass spectrometer
MW	molecular weight
$MorH^+$	protonated morphine
MALDI	matrix assisted laser desorption ionization
N	elementary charges on a charged droplet
OD	outer diameter
Pen	n-pentyl
R	radius of charged droplet
R_g	gas constant
R_R	Rayleigh fission radius
Q:	flow rate (volume/time)
Sl	solvent molecule
SCIEX	a trade name
SCIEX 6000E	name of a triple quadrupole mass spectrometer
T	temperature
T_m	mass transmission
TS	thermospray
TOF	time-of-flight
Tpy	tripyridine

V_c	capillary voltage
V_f	final volume of charged droplet (before ion evaporation)
V_o	initial volume of charged droplet
Xe	fast xenon atom
α	condensation coefficient
γ:	surface tension of liquid
ε:	permittivity of solvent
ε_o:	permittivity of vacuum
η_0	viscosity
λ_m	molar conductivity
λ_m°	limiting molar conductivity
μ_j	relative ionic strength of the ion species j
ρ	density
ρ	space charge density (in Chapter 5)
σ	electrical conductivity
Γ	ionic strength
$\Delta G^{\neq}$	free energy of the transition state
ΔG^o_{sol}	solvation energy
$\Delta H_{vap}(MeOH)$	molar vaporization enthalpy of methanol

Chapter 1. General Introduction

1.1 Electrospray phenomena

Although electrospray mass spectrometry (ESMS) is still considered to be a new technique in modern mass spectrometry, electrospray has origins which can be traced back to the era of the industrial revolution. The early study of the electrospray phenomena started with the work of pioneers in science such as Bose (1) and Kelvin (2). An interesting early experiment was the Kelvin water-dropper apparatus in which water dripping rate was controlled by electrostatic field. Bailey, in his book *Electrostatic Spraying of Liquids* (3), gave an extensive account of the early activities on electrospray.

Since the beginning of this century, more research work on ES has been conducted. The research interests in electrospray was spurred by the wide application fields that electrospray can find as a method for dispersing fluid. A version of electrospray, ink-jet technology (4), has been developed for printing. There are not only single-jet printers but also sophisticated multicolor ink-jet printers. The high-speed, silent printing capability of a modern ink-jet printer makes it an ideal output device for computer systems. The fact that there are no moving parts in most of the these printers means that they are inherently reliable.

The electrostatic crop spraying may be compared directly with electrostatic printing as identical principles apply. Several crop sprayers have been developed (5). The interest in electrospraying of crops is no doubt due to health and safety legislation and an acute awareness of environmental pollution considerations.

Fundamental study has been conducted on charged droplets. The early work on the observation of an evaporating charged droplet was carried out by a simple adaptation of the Millikan oil drop experiment (6). Later, some new techniques were developed, such as point-to-plane electrostatic precipitator (7, 8), quadrupole (9) and light scattering techniques (10). Recently, differential mobility analyzer and anemometer (11-13) have been used for the characterization of the fine charged droplets from electrospray. The development of methodology of droplet measurement provides strong support for the mechanism study of charged droplet formation. Research work on the mechanism of charged droplet formation was initiated by physicists and engineers, among whom are Zeleny (14), Taylor (15, 16), Vonnegut and Neubauer (17, 18), Hayati, Bailey and Tadros (19, 20). Hendricks and his co-workers (21, 22) studied electrospray because of its possible application in an ion propelled rocket engine. They proposed an electrospray model, which is called the Hendricks Model in this thesis. It will be discussed later that the Hendricks Model gives a relation among the parameters involved in electrospray and gives a special insight into electrospray phenomena.

1.2 Ionization methods widely used in analytical mass spectrometry

Gas phase ions required for mass spectrometric analysis are difficult to produce when the analytes are polar compounds with high molecular weight. Most biochemical analyses involve such large compounds. Conventional methods like electron impact ionization (EI) or chemical ionization (CI) require gaseous analyte molecules but such molecules can

not be produced by evaporation of highly polar and high molecular compounds. Several methods have been introduced, such as fast atom bombardment (FAB), laser desorption ionization (LD) and thermospray (TS), where gaseous analyte ions are created directly from analytes present in the solid or liquid state.

The pioneer work done by Barber and his colleagues (23) made FAB become a widely used ionization method. In FAB, the analyte is dispersed in a liquid matrix on the surface of a metal tip. The liquid matrix can be glycerol or other compounds, which have low melting points and low vapor pressures. The metal tip, with analyte sample on it, is subjected to the bombardment by fast atoms, typically Xe, which are obtained from an electric discharge and converted to atoms by charge-exchange neutralization of an ion beam accelerated to several kilovolts. This technique made accurate molecular weight measurement of peptides possible for the first time. Further development of FAB led to the related method of "continuous flow FAB" (24) which delivers a solution of analyte in matrix to the vacuum system through a probe that achieves a continuously refreshed surface for the bombardment of fast atoms.

The popular MS technique laser desorption is somewhat similar to FAB. In the modern version MALDI, matrix assisted laser desorption ionization, the analyte is in a liquid or solid matrix as in the case of FAB. MALDI was introduced by Karas and Killendamp (25). Karas and Killendamp's work showed that both the wavelength of the photons used and the composition of the matrix that contains the analyte play an important role. With this technique, it has become possible to ionize proteins with molecular weights over 200,000 dalton with little internal excitation energy in the desorbed ion.

Thermospray, developed by Vestal and his colleagues (26) has been widely used in the pharmaceutical industry. Because thermospray is a technique producing gas phase ions directly from analyte solution, it has been applied to the interfacing of LC to MS. In thermospray, the LC effluent is passed through a heated capillary which vaporizes the LC effluent into a superheated mist transported in a supersonic vapor jet. Most of the vaporized solvent and mist is pumped away by an auxiliary vacuum pump after it passes by the aperture to the mass spectrometer. The non-vaporized analyte molecules remain in the droplets of the mist as they diminish in size. The solution used for thermospray contains dissolved electrolyte such as ammonium acetate which leads to NH_4^+ and Ac^- ions in the solution. The droplets formed are observed to be charged (27). Both positive and negative charged droplets are observed. It is assumed that the droplet charging is due to a statistical unbalance of positive and negative ions present in the solution. This unbalance process of charging occurs during the fast droplet formation process (27). Finally, the rapidly evaporating charged droplets lead to formation of gas phase ions. The production of gas phase ions from charged droplets is a process that also occurs in electrospray. The mechanism involved will be discussed later. Thermospray is a good approach to HPLC/MS due to its capability of handling solvent flow rates which is useful in HPLC. It has been found suitable for the analysis of only relatively low molecular weight polar biological compounds.

1.3 Electrospray mass spectrometry

Electrospray mass spectrometry began to attract chemists and biochemists' attention world wide due to the successful work done by Yamashita and Fenn (28) in United States and Aleksandrov et al. (29) in the former Soviet Union. Their work demonstrated that ESMS might be the best technique for the mass analysis of biological compounds with high molecular weight. The idea of using ES dispersion of an analyte solution in a bath gas to produce solute ions for mass analysis originated with Dole et al. in the 1960s (30). Interested in the possibility of determining the molecular weights of polymers, they performed some pioneering experiments in which an acetone-benzene solution of polystyrene macromolecules was electrosprayed into a bath gas of nitrogen in a mass analyzer. They hoped that ES dispersion of a sample solution would result in the production of charged droplets, each of which contains only one charge and one solute molecules that gives rise to a macro-ion. Because the available mass analyzers at that time could not accommodate singly charged ions with molecular weights in his range of interest, 50000 to 500000 dalton, Dole only did ion retardation (31, 32) and ion mobility (33) measurements. However, the importance of Dole's contributions cannot be overstated. His research clearly suggested the facile ionization of macromolecules, the multiple charging phenomenon, as well as many of the instrumental methods currently utilized for ESMS technique. Stimpson and Evans (34) summarized the early activity in ESMS. Current activity of ESMS is focused mainly on the application of the ESMS technique on the analysis of biochemical compounds, which is the opinion expressed by recent review articles (35-39).

The ESMS instrumentation consists of three components, which are the electrospray source where charged droplets form by electrostatic nebulization of analyte solution; the atmosphere-to-vacuum interface where the charged droplets evaporate to produce gas phase ions and gas phase ion-molecule reaction may happen; and the mass spectrometer where mass analysis occurs. The ES source may consist simply of a metal capillary at elevated voltage relative to a counter electrode having an orifice where ions or ion-clusters enter the mass spectrometer entrained in a flow of gas. The solution with flow rate in the range of 1 ~ 20 μL/min delivered typically by a syringe or micropump moves through the silica capillary tubing to the spray tip where it is sprayed. The high DC voltage forms a high electric field at the capillary tip, causes charge accumulation on the liquid surface at the capillary terminus and disrupts the liquid surface, resulting in the formation of highly charged liquid droplets. Positively or negatively charged droplets may be produced depending upon the source voltage bias. Polar solvents such as methanol and/or water are usually electrosprayed. Usually, a concentration range of electrolyte in the range of 10^{-8} ~ 10^{-3} M is required at room temperature for a stable electrospray. Although higher voltage can improve ion detection sensitivity, a much higher voltage will generally cause a corona discharge and preclude analyte-ion detection. The corona discharge can be effectively suppressed by adding an effective electron scavenger such as O_2 (40, 41) or SF_6 (42, 43). The ES liquid nebulization process can be pneumatically assisted using a high-velocity annular flow of gas at the capillary terminus. This method is called "ionspray" (44) and has the advantage of accommodating high flow rate up to 100 μL/min.

At a short distance from the ES source, the nebulized liquid has a nearly monodisperse droplet diameter in the range of 1~2 μm (45, 46). Increased liquid flow rates only result in larger droplets (47), and the total electrospray ion current increases only slightly. Increased electrolyte concentration causes a decrease in the average droplet size.

Heating or ultrasound irradiation of the droplets is useful for manipulating the electrospray process. There is evidence that slight heating allows aqueous solutions to be readily electrosprayed (48, 49), presumably due to decreased viscosity and surface tension. The importance of viscosity and surface tension in the ES process will be discussed in Chapter 2. Irradiation of charged droplets by means of ultrasonic waves (50) also facilitates the electrospray process, particularly in the case of electrospray of aqueous solution. The introduction of the ultrasonic technique into ESMS is expected to attract more attention.

After the charged droplets leave the electrospray tip, they drift in the atmosphere and solvent is evaporated. The droplets undergo several fission processes, yielding smaller and smaller charged droplets. Finally, gas phase analyte ions form from these smaller droplets. The ions can be analyzed by a mass spectrometer. An atmosphere-to-vacuum interface is the common feature of ESMS instrumentation. An important attribute of an ion source operated at atmospheric pressure is the efficiency of sampling and transport of ions into the mass spectrometer. A simple design available in a commercial instrument from SCIEX utilizes an orifice with diameter ~100 μm to a vacuum region which is maintained by a cryopump with high pumping speed. Ions formed by ES drift against a countercurrent flow of dry N_2, which serves to exclude large droplets and aerosol particles and aids desolvation of solvated ions. As the ions pass

through the orifice into the vacuum, further desolvation is accomplished by collisions as the ions are accelerated into a cluster breaker. In Chapter 3, a model of a SCIEX mass spectrometer SCIEX 6000E will be shown, where the configuration of atmosphere-to-vacuum interface is illustrated. Several other instruments can also be found on the market, which have been developed based on differentially pumped interfaces. The capillary inlet-skimmer interface developed by Fenn and his co-workers (51) is applied on the instrument produced by Analytica of Branford (Branford, CT). This interface uses a countercurrent flow of bath gas, which is typically N_2 at a pressure slightly above atmospheric pressure, to sweep away high m/z residual particles and solvent vapor from the mass spectrometer inlet. The glass capillary of this interface is metalized at both ends to establish well defined electric fields. Some fraction of ions is entrained in the gas flow entering the glass capillary. Ions can be transmitted through the capillary with high efficiency. Ions swept by the gas flow through the capillary emerge as a component of a free jet expansion in the first differentially pumped stage. Some fraction of the ions is then transmitted through a skimmer into the mass analyzer.

An atmosphere-to-vacuum interface called a "low pressure ion source" (52) takes advantages of both mentioned commercial interfaces and high pressure ion source in chemical ionization (53). This ion source allows ions formed by electrospray to be drawn through a metal capillary into a chamber at 10~100 torr, where they may react with a separately added gas for the study of ion-molecule reactions. The reaction products are then transmitted through the orifice of a SCIEX quadrupole instrument to be mass analyzed. A low pressure ion source is still at the stage of

preliminary study, but it might be a potential new ion source in the study of gas phase ion-molecule reaction via electrospray.

After the ESMS work on a quadrupole mass spectrometer was reported, successful combination of an ES source with other types of mass spectrometers have been accomplished. The combination of ES with a magnetic sector machine demonstrates low ppm mass accuracy and high mass resolution for small proteins (54, 55). Initial results with a time-of-flight (TOF) instrument has also been reported (56). ESMS work done on an ion trap presents highly encouraging results (57), and the ion trap method shows significant advantage for MS/MS sensitivity in comparison with conventional tandem instruments. If ES is combined with Fourier transform-ion cyclotron resonance mass spectrometer (FTICRMS) (58-59), the potential for structural elucidation of proteins by multi-MS is quite promising. The coupling ES to FTICRMS makes the ESMS technique more powerful for the structural identification of nonvolatile molecules. The combination of ES with FTICR also appears to have potential for obtaining accurate molecular weights from high-resolution spectra.

ESMS produces charged droplets in a way that is much simpler than thermospray, and produces more abundant intact molecular ions. In particular, its feature of multiply charged macromolecules overwhelms other soft ionization techniques in biochemical analysis. Electrospray is a continuous process, which makes it suitable for LC-MS. The versatility of ESMS has resulted in its rapid development. ESMS quickly became commercially available after it was invented, and a large amount of ESMS literature has emerged in recent years. It is now not only an important tool in the structural study of polypeptides, proteins and carbohydrates but also a powerful apparatus in the combination of liquid chromatography (LC)

and capillary electrophoresis (CE) separations with mass spectrometric analysis of organic compounds, especially peptides and proteins (60).

Although there were many research articles on ESMS available in the literature when I began my Ph.D program, most of the work described the applications of the method and explored the parameters that lead to improved performance. Little work dealing with the mechanism was available. The understanding of the ESMS mechanism was incomplete and out of pace with the rapid expansion in ESMS activity at that time. The lack of understanding of the mechanism may be expected to slow down the progress of ESMS. This thesis presents an investigation of the mechanism of ESMS.

Three important, mutually related topics are considered: the mechanism of charged droplet formation, the process of charged droplet evolution towards small highly charged droplets, and the gas phase ion formation from these droplets. The principal method in my study was the determination of mass analysed ion intensities of different analytes and the dependence of these intensities on the concentration of the analytes in the electrosprayed solution. These results were combined with available information in the literature on the electrospray mechanism and on the properties of small charged droplets. The combination of all the above information has provided, I believe, a useful synthesis leading to an advance in the understanding of the mechanism involved in ESMS.

1.4 References

1. Bose, G.M., *Recherches sur la cause et sur la veritable theorie de l'electricite*, Wittenberg (1745)
2. Kelvin Lord (Thompson W.), *Proc. Roy. Soc. (London)* **16** 67 (1867)
3. Bailey, A.G., *Electrostatic Spraying of Liquids*, Research Studies Press, Ltd, Taunton, Somerset, England (1988)
4. Kampheoefner, F.J., *IEEE Trans.*, **19** 584 (1972)
5. Law, S.E.; Lane, M.D., *IEEE Trans.*, IA-I8, 673 (1982)
6. Doyle, A.; Moffett, D.R. and Vonnegut, B., *J. Colloid Sci.*, **19** 136 (1964)
7. Cheng, Y.; Yeh, H. and Kanapilly, G.M., *J Am. Ind. Hygiene Asso.*, **42** 605 (1981)
8. Morrow, P.E.; Mercer, T.T., *J Am. Ind. Hygiene Asso.*, January-February, 8 (1964)
9. Philip, M.A.; Gelbard, F.; Arnold; S., *J. Colloid and Interface Sci.*, **91** 507 (1983)
10. Taflin, D.C.; Zhang, S.H.; Allen, T; Davis, E.J., *J AIChE*, **34** 1310 (1988)
11. Horton, K.D.; Mitchell, J.P.; Nichols, A.L., *J Aerosol Sci.*, **19** 1009 (1988)
12. Roth, C.; Berlauer, U.; Heyder, J., *J Aerosol Sci* , **20** 547 (1989)
13. Gomez, A; Tang, K., *Procedings of the 5th International Conference on Liquid Atomization and Spray Systems*, 86 (1991)
14. Zeleny, J., *J. Phys. Rev.*, **10** 1 (1917)
15. Taylor, G.I., *Proc. Roy. Soc. A*, **280** 383 (1964)

16. Taylor, G.I., *Proc. Roy. Soc. A*, **313** 453 (1969)

17. Vonnegut, B.; Neubauer, R.L., *J. Colloid Sci.*, **7** 616 (1952)

18. Vonnegut, B.; Neubauer, R.L., *J. Colloid Sci.*, **8** 551 (1953)

19. Hayati, I.; Bailey, A.I.; Tadros, TH. F. *J. Colloid Interface Sci.*, **117** (1) 205 (1987)

20. Hayati, I.; Bailey, A.I.; Tadros, TH. F. *J. Colloid Interface Sci.*, **117** (1) 222 (1987)

21. Hendricks, C.D. in *Electrostatics and Its Applications*, Chapter 4, A.D. Moore (Editor), Wiley-Interscience, New York (1973)

22. Pfeifer, R.J.; Hendricks, C.D. *J. AIAA* **6** 496 (1968)

23. Barber, M.; Bordoli, R.S.; Sedgwick, R.D.; Tyler, A.N. *J. Am. Soc. Chem. Commun.*, 325 (1981)

24. Caprioli, R.M.; Fan, T.; Cottrele, J.S. *Anal. Chem.* **58** 2949 (1986)

25. Karas, M.; Killenkamp, F. *Anal. Chem.* **60** 2299 (1988)

26. Blakley, C.R.; McAdams, M.J.; Vestal, M.L. *J. Chromatogr.* **158** 264 (1978)

27. Arpino, P.; *Mass Spectr. Rev.* **9** 631 (1990)

28. Yamashita, M.; Fenn, J.B. *J. Phys. Chem.* **88** 4671 (1984)

29. Aleksandrov, M.L.; Gall, L.N.; Krastov, V.N.; Nikolaev,V.I.; Pavlenko, V.A.; Shkurov, V.A. Dokl. *Akad. Nauk. SSSR* **277** 379 (1984)

30. Dole, M.; Mack, L.L.; Hines, R.L.; Mobley, R.C.; Ferguson, L.P.; Alice, M.B., *J Chem. Phys.*, **49** 2240 (1968)

31. Mack, L.L.; Kralik, P.; Phueda, A; Dole, M., *J Chem. Phys.*, **52** 4977 (1970)

32. Clegg, G.A.; Dole, A., *Biopolymers*, **10** 821 (1971)

33. Gieniec, J.; Mack, L.L.; Nakamae, K.; Gupta, C.; Dole, M., *Biomed. Mass Spec.*, **11** 259 (1984)

34. Stimpson, B.P.; Evan, C.A., *J. Electrostatics*, **5** 411

35. Fenn, J.; Mann, M.; Meng, C.K.; Wong, S.F.; Whitehouse, C.M., *Science*, **246** 64 (1989)

36. Bruins, A.P., *Mass Spec. Rev.*, **10** 53 (1991)

37. Mann, M. Org. Mass Spect. **25** 575 (1990)

38. Chait, B.; Kent, S.B.H., *Science*, **257** 1885 (1992)

39. Smith, R.D.; Loo, J.A.; Loo, R.R.O.; Busman, M.; C.J.; Udseth, H.R., *Mass Spec. Rev.*, **10** 359 (1991)

40. Yamashita, M.; Fenn, J.B. *J. Phys. Chem.* **88** 4671 (1984)

41. Ikonomou, M.G.; Blades, A.T.; Kebarle, P., *Anal. Chem.*, **63** 1989 (1991)

42. Ikonomou, M.G.; Blades, A.T.; Kebarle, *J. Am. Soc. Mass Spectrom.*, **2** 497 (1991)

43. Wampler III, F.M.; Blades, A.T.; Kebarle, P., *J. Am. Soc. Mass Spectrom.*, **4** 289 (1993)

44. Covey, T.R.; Huang, E.C.; Henion, J.D., *Anal. Chem.*, **63** 1193 (1991)

45. Gomez, A; Tang, K., *Physics of Fluids* (in print)

46. Vestal, M.L.; Allen, M.H., *Proceedings of the 39th ASMS Conference on Mass Spectrometry and Allied Topics*, Nashville, TN, 445 (1991)

47. Fernandez de la Mora, J.; Rosell-Llopart, J., *Proceedings of the 39th ASMS Conference on Mass Spectrometry and Allied Topics* , Nashville, TN, 441 (1991)

48. Allen, M.; Lewis, I.A.S., US Patent 4, 999, 493, (1991)

49. Ikonomou, M.G.; Blades, A.T.; Kebarle, P., US Patent (pending)

50. Whitehouse, C.M.; Anderin, B.; Banks, F.; Quinn, J.; Shen, S., *Proceedings of the 41th ASMS Conference on Mass Spectrometry and Allied Topics* , San Francisco, CA, (1993)

51. Fenn, J.; Mann, M.; Meng, C.K.; Wong, S.F.; Whitehouse, C.M., *Mass Spec. Rev.*, **9** 37 (1990)

52. Ikonomou, M.G.; Kebarle, P., *Int. J. Mass Spec. & Ion Processes,* **117** 293 (1992)

53. Kebarle, P., in T*echniques for the Study of Ion-Molecule Reactions*, Editor: Farrar, J.M.; Saunders Jr., W., 221 (1988)

54. Meng, C.K.; McEwen, C.N.; Larsen, B.S., *Rapid Commun. Mass Spect.*, **4** 147 (1990)

55. Dobberstein, P.; Giessmann, U.; Schroeder, E., *Proceedings of the 39th ASMS Conference on Mass Spectrometry and Allied Topics* , Nashville, TN, 238 (1991)

56. Boyle, J.G.; Whitehouse, C.M.; Fenn, J., *Rapid Commun. Mass Spect.*, **5** 400 (1991)

57. Van Berkel, G.J.; Glish, G.L.; McLuckey, S.A., *Anal. Chem.*, **62** 1284 (1990)

58. Henry, K.D.; Williams, E.R.; Wang, B.H.; McLafferty, F.W.; Shabanowitz, J.; Hunt, D.F., *Proc. Natl. Acad. Sci. USA*, **86** 9075 (1989)

59. Henry, K.D.; McLafferty, F.W., *Org. Mass Spect.*, **25** 490 (1990)

60. Smith, R.D.; Loo, J.A.; Edmonds, C.G.; Barinaga, C.J.; Udseth, H.R. *Anal. Chem.* **62** 882 (1990)

Chapter 2. Effect of the Conductivity of the Electrosprayed Solution on the Electrospray Current. Factors Determining Analyte Sensitivity in Electrospray Mass Spectrometry*

2.1 Introduction

Electrospray mass spectrometry (ESMS) is a new technique of extraordinary potential (1-3). The exciting applications of this technique have created also a great deal of interest in the mechanism by which the gas phase ions required for the mass spectrometric analysis are produced. The two main stages in the mechanism are the production of charged droplets and the production of gas phase ions from the charged droplets. Since the second stage depends on the first, it seems logical to examine the charged droplet formation first and this approach has been taken in the mechanistic work on ESMS (4-8).

The experimental work discussued in this chapter, which examines the dependence of the total current I produced by electrospray on the electrical conductivity σ of the solution, is connected directly with the charged droplet formation process. However, because the conductivity depends on the concentration of the ions in solution including that of the analyte ions, the findings also set the stage for a partial examination of the second stage, - the production of gas phase ions from the charged droplets and in particular the dependence of the gas phase analyte ion current on the concentration of analyte ions and other electrolyte ions in the electrosprayed solution.

---

* A version of this chapter has been published: L. Tang; P. Kebarle, *Anal. Chem.*, 63, 2709 (1991)

The formation of charged droplets in the electrospray process has been subject to intensive studies which predate the mass spectrometric applications. These studies were driven by a number of important technical applications of electrospray (9). This intensive effort has produced much valuable information; however, a complete understanding has not been achieved and complete equations relating the pertinent variables, are not yet available.

A number of authors (9-12) agree that the charging of the droplets is electrophoretic. Electrophoretic charging means that the external electric field induces a partial separation of positive from negative electrolyte ions which are present in the solution (i.e. "preformed" ions in the mass spectrometric nomenclature). Thus, when the capillary is of positive polarity, the liquid surface at the capillary tip becomes enriched with positive ions. This excess charge induces an instability of the surface which ultimately leads to a dispersal of the liquid into a fine mist of positively charged droplets. The charge of the droplets is due to an excess of positive electrolyte ions over the negative counter ions. The electrophoretic mechanism is of special importance to the mass spectrometrist since it indicates that the gas phase ions detected by the mass spectrometer will be due to electrolyte ions present in the solution (4-8).

Recently, it has been shown (8), in support of the electrophoretic mechanism, that the electrospray process may be viewed as an electrolysis cell of a special kind. When the metal capillary is at a positive potential, an electrochemical oxidation reaction occurs at the metal-liquid interface at the capillary tip. This oxidation either removes negative ions from the solution converting the charge to electrons transferred to the metal or produces positive ions in the solution from metal atoms of the capillary

material. Thus, the reaction: $Zn_{(s)} = Zn^{++}_{(aq)} + 2e$ was identified when the capillary tip was made of Zn metal and $Fe_{(s)} = Fe^{++} + 2e$, when the tip was of the usual material - stainless steel. The rate of positive charge formation due to dissolution of the metal ions was found equal to I, the measured electrospray current (8). An electrochemical reduction reaction is expected to occur at the negative counter electrode and so, the electrospray device may be viewed as an electrolysis cell which exhibits a special feature, i.e. part of the transport of charge is achieved through the gas phase via charged droplets and gas phase ions.

Experimentally it is found that the charged droplet emission current I is dependent on the presence of ionized electrolytes in the solvent to be electrosprayed. No spray is observed with totally deionized solutions. The threshold conductivity σ, where the spray is still intermittent, occurs (6) for methanol containing dissolved electrolytes at a $\sigma \approx 10^{-7}\ \Omega^{-1}\ cm^{-1}$. For electrolytes like the alkali halides, the above σ corresponds to a total electrolyte concentration of $\sim 10^{-6}$ M (M = mole L^{-1}) (13).

As the conductivity is increased above the threshold, the ES current I increases and becomes stable. I is found to follow approximately a power law with the conductivity as shown in equation 2-1, where H is a constant.

$$I = H\,\sigma^{n} \qquad (2\text{-}1)$$
$$n \approx 0.2 - 0.4$$

Such a dependence was reported by Pfeifer and Hendricks (10) for glycerol solutions and was observed also for methanol solutions in previous work from this laboratory (6). For other measurements see (9, 11, 12).

When strong electrolytes like the alkali halides or strong acids like HCl are used at low concentrations $C < 10^{-3}$ M in a solvent like methanol,

they are fully dissociated and ion-pairing effects are minimal. In this case equation 2-2 holds approximately,

$$\sigma \approx \lambda_m^{\circ} C \tag{2-2}$$

where λ_m° is the limiting molar conductivity, corresponding to the molar conductivity λ_m at infinite dilution. Since ES is usually performed in this low concentration range, one can combine equation 2-1 and 2-2 to obtain equation 2-3.

$$I \approx H(\lambda_m^{\circ} C)^n \tag{2-3}$$

The dependence of the electrospray current I on the conductivity has not been fully characterized and the functional form, equation 2-1, does not appear to be fully accepted in the literature. Another important point that has not been proven is the effect of the λ_m° of given electrolytes on the current I. Thus, according to equation 2-3, when two methanol solutions, each containing the same concentration C of two different electrolytes x and y, are electrosprayed, the current ratio measured should be given by,

$$\frac{I_x}{I_y} = \left(\frac{\lambda_m^{\circ}(x)}{\lambda_m^{\circ}(y)} \right)^n \tag{2-4}$$

Most measurements have been performed with alkali halides, for which λ_m° changes very little (13), $\lambda_m^{\circ} \approx 100 \pm 20\ \Omega^{-1}\ cm^2\ mol^{-1}$. These small changes, combined with the facts that the exponent n is small, the electrospray currents I are not perfectly stable and the ES conditions are not perfectly reproducible, makes verification of equation 2-4 difficult.

Only electrolytes with a large λ_m° difference can be expected to lead

to verifiable current differences. The obvious solution of this problem is to choose a strong acid like HCl as one of the electrolytes making use of the well known high mobility and thus also high conductivity of the hydrogen ion. Thus $\lambda^{\circ}_{m}(H^{+}) = 350$ while $\lambda^{\circ}(Na^{+}) = 50\ \Omega^{-1}\ cm^{2}\ mol^{-1}$ in water. ES of water solutions is difficult since high capillary voltages are required (8,11) and these may lead to a corona discharges which will make an unknown contributioned to the measured current (8).

ES of methanol-water solutions are easier to spray. The molar conductivity λ°_{m} of HCl and other electrolytes such as NaCl in the complete range of methanol-water mixtures has been determined previously by electrochemistry researchers (14). For the present ES experiments we chose the composition 40% by weight methanol. In this solvent the conductivity difference is still quite large, $\lambda^{\circ}_{m}(HCl) = 190$ versus $\lambda^{\circ}_{m}(NaCl) = 58\ \Omega^{-1}\ cm^{2}\ mol^{-1}$ (14).

As will be seen in Results and Discussion, section (a), the present measurements confirm the dependence of Ion λ°_{m} predicted by equation 2-4.

Pfeifer and Hendricks (10) have derived a theoretical equation which relates I to the parameters: capillary voltage and dimensions, flow rate, surface tension and conductivity of solvent. This equation defines the constants H and n in equation 2-1. In section (b) the present measurements of I were used for an examination of the degree of agreement between the experimentally measured and the theoretically predicted current.

The final section (c), utilizes the observed relationship between electrolyte concentration and ES current to make a quantitative prediction for the effect of concentration of the analyte and of electrolytes, such as impurities, on the sensitivity for mass spectrometric detection of the

analyte.

2.2 Experimental

a. Total ion current measurement

The arrangement used for measurement of the total current I is shown in Figure 2-1. It was shown in earlier work from this group that the positive current leaving the capillary tip is equal to the positive current arriving at the plane electrode (6). The current to the plane electrode, which was at ground potential, was measured in the present experiments.

The 40% methanol-water solvent used in the present work requires a capillary voltage V_c of 5000 V for a stable ES spray. This voltage is higher than what is ordinarily used with methanol solutions ($V_c \approx 4000$ V). Therefore tests were made for the possible presence of a simultaneous corona discharge. These experiments were performed with our SCIEX API TAGA 6000E instrument, modified for ES, see references 4 and 8. The tests showed that the electrospray current I was the same in the absence and presence of discharge-suppressing SF_6 gas. This result means that no measurable discharge was occurring in the absence of SF_6 (8). The mass spectrometrically detected ions, when a NaCl containing solution was electrosprayed, were mostly Na^+ adducts to the solvent molecules. Significantly, the intensities of discharge indicating ions, i. e. protonated solvent molecules, were very low. This finding also supports that the absence of an electric discharge (8).

The stainless steel ES capillary had a diameter 0.004" ID and 0.010" OD. The distance from capillary tip to the planar counter electrode was 4 cm. All experiments were performed with a solvent flow

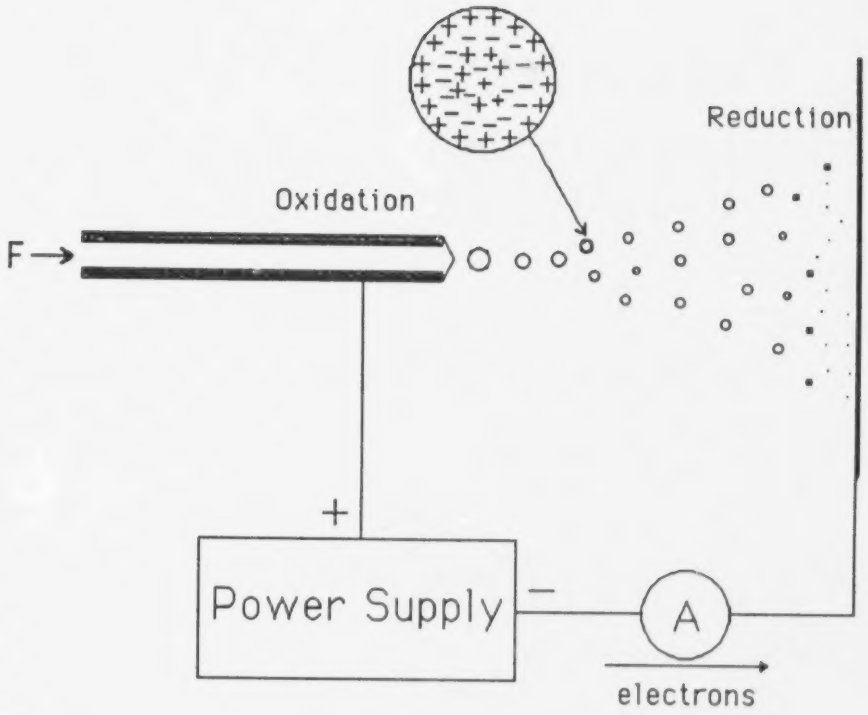

Figure 2-1 Schematic diagram of electrospray device. Capillary tip and droplets are highly magnified. Electrospray (ES) current A was measured with electrometer at ground potential. The operation of ES as an electrolysis cell is indicated by oxidation and reduction labels in figure.

20 μL/min.

b. Electrolyte solutions and conductivity measurements

Analytical grade methanol was fractionally distilled. Its conductivity after distillation was $1 \times 10^{-7}\ \Omega^{-1}\ cm^{-1}$. The water used was deionized to a somewhat lower conductivity. The concentration of HCl in 40%, by weight, methanol was calibrated by titration as suggested by Johnson and Funk (15). Analytical grade NaCl was dissolved directly in the solvent. All experiments were made with freshly prepared solutions stored in Pyrex vessels under an argon atmosphere.

The conductance measurements were performed with a YSI model 31 conductivity bridge and a YSI 3402 dip cell.

2.3 Results and Discussion

a. Electrospray current. Dependence on conductivity of solution, limiting molar conductivity and concentration of electrolyte

The measured conductivities of solutions of NaCl and HCl, dissolved in 40% methanol-water solvent, are shown in Figure 2-2 plotted versus the concentration of the respective electrolyte. The data in the linear plot shown in 2A illustrate that in the concentration range 10^{-4}M to 10^{-2}M, the conductivity σ is very close to being proportional to the electrolyte concentration as assumed in equation 2-2. The slopes of the linear plots, Figure 2-2A, are 55 $\Omega^{-1}\ cm^2\ mol^{-1}$ (NaCl) and 160 $\Omega^{-1}\ cm^2\ mol^{-1}$ (HCl). These values are close to the λ_o values obtained by the more accurate and extensive measurements of Shedlovsky and Longsworth (14). λ_o(NaCl) =

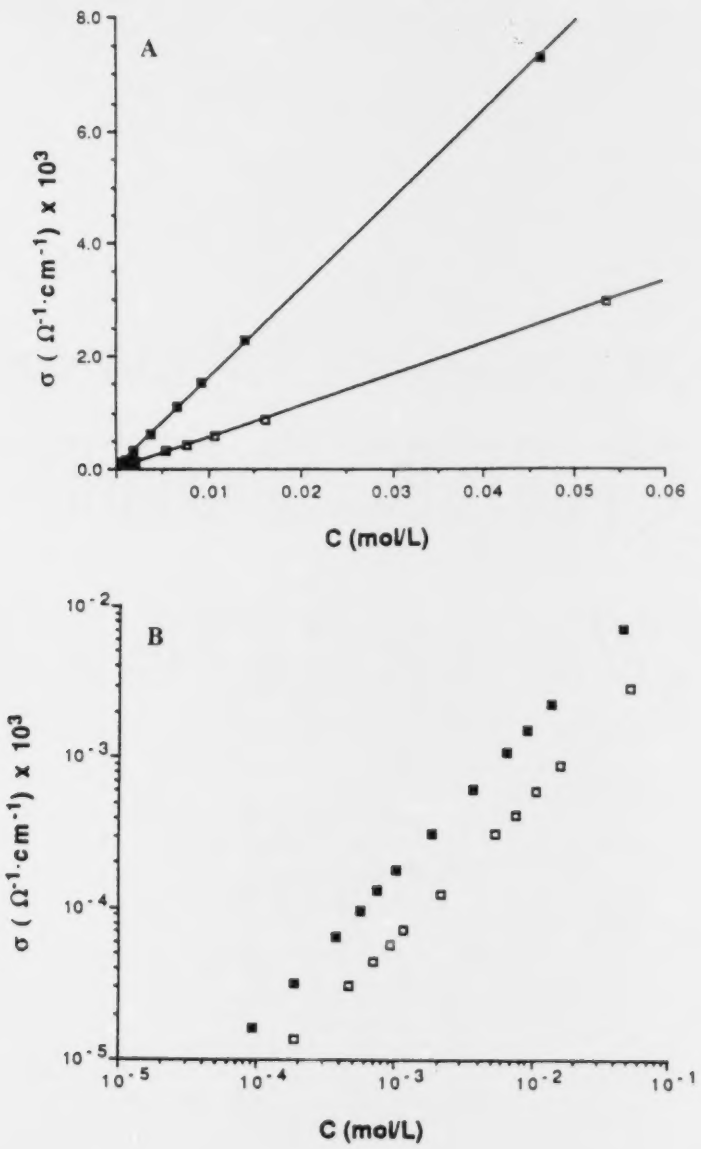

Figure 2-2 A. Plot of measured conductivity σ of solutions of HCl and NaCl respectively in solvent, 40% methanol, 60% water by weight versus concentration C of electrolyte, at 23°C.
Linear plots indicate that equation. 2-2 holds in concentration range used. ■ HCl, ❐ NaCl.
B. Same data is in Figure 2-2A, but plotted as log σ versus log C.

58 and $\lambda_o(HCl) = 190\ \Omega^{-1}\ cm^2\ mol^{-1}$. The present data when plotted according to the Kohlrausch equation; $\lambda = \lambda_o - A\sqrt{C}$, led to λ_o values which are in closer agreement with the literature results (14). However, the point here is not to determine accurate λ_o values, but to show that equation 2-2 holds quite well in the concentration range of interest in ES and that the solutions used and the measured conductivities in this work are close to those expected from more specialized determinations.

The measured electrospray currents I with the above solutions are given in Figures 2-3 and 2-4. The current I plotted versus the conductivity σ is shown in Figure 2-3 for NaCl and HCl solutions. The experimental points for I versus σ for NaCl and HCl are seen to fall essentially on the same line. The straight line obtained in the log I versus log σ plot used provides a confirmation of equation 2-1. The slope of the plot is equal to 0.22 and can be equated to the exponent n in equation 2-1.

$$n \approx 0.22 \quad \text{(verified for NaCl and HCl solutions)} \qquad (2\text{-}5)$$

Since the linear plot in Figure 2-2A provided a confirmation of equation 2-2 for the systems used here, it follows that equation 2-3 which follows from equation 2-1 and equation 2-2, is also verified by the plots in Figures 2-2 and 2-3.

The measured log currents I for NaCl and HCl solutions plotted versus the log electrolyte concentration are shown in Figure 2-4. Two distinct straight lines with approximately the same slope are obtained in the log I vs log C plots used. The HCl line is displaced towards higher currents as expected from equation 2-3. The difference: $\log I_{HCl} - \log I_{NaCl}$ is found to be equal to 0.11. According to equation 2-3 the relationship, equation 2-6, should hold.

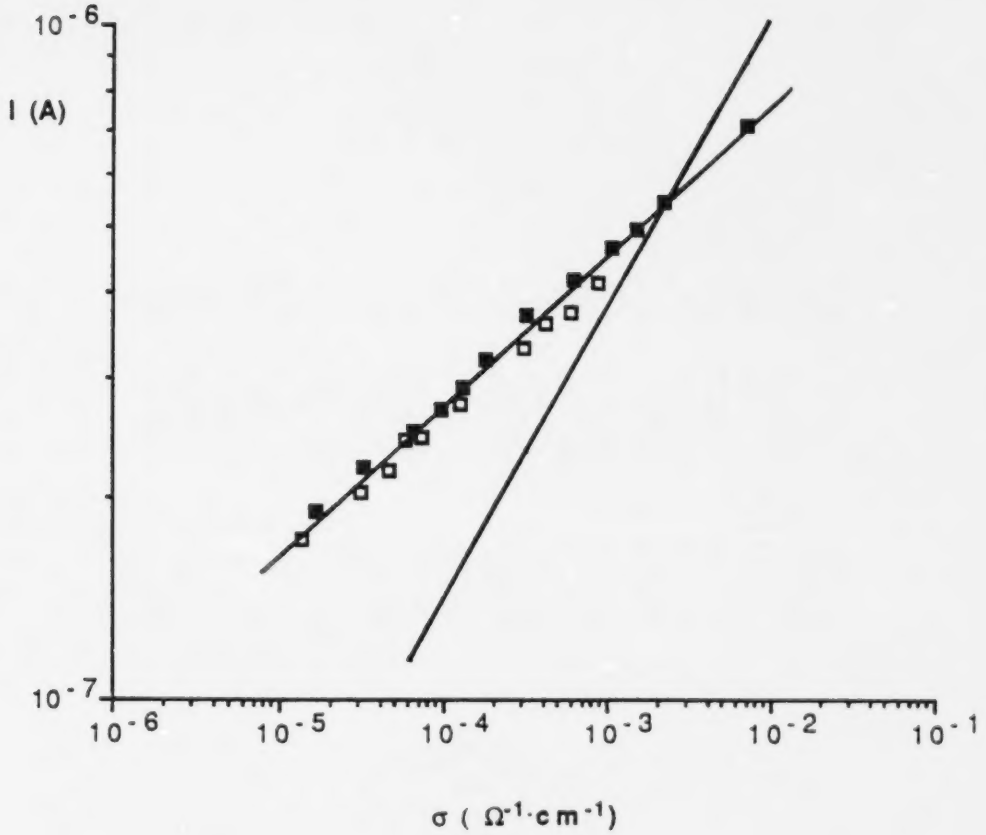

Figure 2-3 Logarithmic plot of electrospray current I versus conductivity of HCl and NaCl solutions in solvent 40% methanol, 60% water. The observation that currents I from NaCl and HCl fall on the same line confirms equation 2-3. Slope of present plot provides n = 0.22 for exponent n of equation 2-3 (R=0.98 in linear regression). ■ HCl, ❐ NaCl. Solid line with higher slope represents current I calculated with Hendricks expression, see equation 2-7.

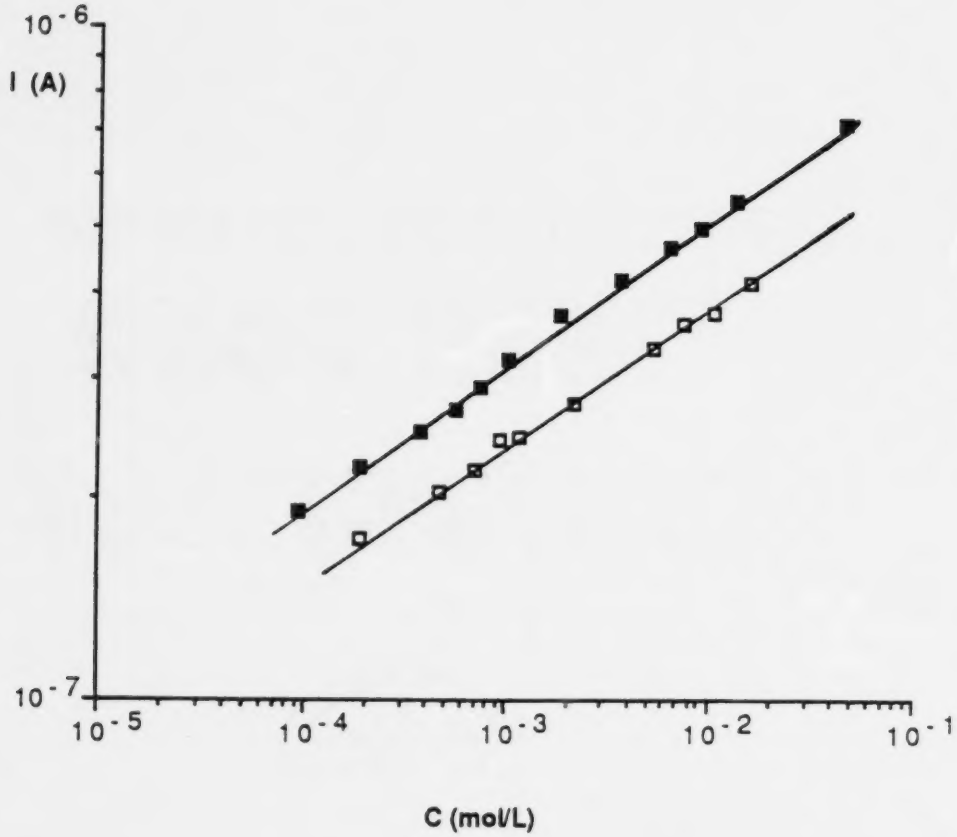

Figure 2-4 Logarithmic plot of measured ES current I versus concentration C of electrolytes HCl resp. NaCl in solvent 40% methanol, 60% water. Plots in Figure 2-3 and present figure confirm equation 2-3. ■ HCl, ❐ NaCl

$$\log I_{HCl} - \log I_{NaCl} = n(\log \lambda_m^{\circ}(HCl) - \log \lambda_m^{\circ}(NaCl) \qquad (2\text{-}6)$$

using $n \approx 0.22$, see equation 2-5, and the log I difference of 0.11, one obtains from equation 2-6

$$\frac{\lambda_m^{\circ}(HCl)}{\lambda_m^{\circ}(NaCl)} \approx 3.2$$

This result is close to the ratio of 3 obtained from the conductivities measured in this work, see Figure 2-2 and the ratio of 3.3 obtained with the literature values (14).

Thus, the approximate equation 2-3 is fully confirmed by the plots in Figures 2-2 to 2-4.

b. Comparison with the Hendricks equation for the electrospray current I

In spite of considerable attention to the theoretical problem that the electrospray nebulization represents, there appear to be only two treatments (10, 11) which provide equations that predict the electrospray current I. The first treatment, that of Pfeifer and Hendricks (10) leads to the expression shown in equation 2-7. The treatment by D.P.H. Smith (11) is probably more realistic (6), but it does not provide a complete equation which explicitly predicts the functional dependence on the conductivity.

$$I = \left(\frac{4\pi}{\varepsilon}\right)^{3/7} (9\gamma)^{2/7} \varepsilon_o^{\,5/7} Q^{4/7} (\sigma E_c)^{3/7} \qquad (2\text{-}7)$$

ε_o: permittivity of vacuum

ε: permittivity of solvent

Q: flow rate (volume/time)

σ: conductivity of solution

γ: surface tension of liquid

E_c: imposed electric field in vacuum at capillary tip

E_c can be evaluated from the capillary voltage V_c applied to the capillary tip, with the use of the approximate equation 2-8, used by Hendricks (10) and Smith (11).

$$E_c = \frac{2\,V_c}{r_c \ln(4\,d/r_c)} \qquad (2\text{-}8)$$

r_c: capillary outer radius

d: distance of capillary tip to planar counter electrode

Therefore, it is possible to evaluate the current I predicted by equation 2-7 for the experimental parameters used in the present work:
$Q = 20\ \mu L/min$, $\gamma = 3.4 \times 10^{-2}\ N\ m^{-1}$ for 40% w/w methanol water (16), $\varepsilon_o = 8.8 \times 10^{-12}\ C^2\ N^{-1}\ m^{-2}$, $r_c = 1.27 \times 10^{-4}$ m; $d = 4 \times 10^{-2}$ m, $V_c = 5000$ V, $E_c = 1.1 \times 10^7\ V\ m^{-1}$ from equation 2-8.

The current I evaluated with these parameters for a range of conductivities is shown in Figure 2-3 and 2-5 together with the experimentally determined I. The experimental data for NaCl and HCl which were used for the plots in Figures 2-3 to 2-4 are used also in Figure 2-5. The agreement between the experimental and theoretical currents is fair. This was to be expected from the experimental plot in Figure 2-3 which gave an $n \approx 0.22$, while the predicted n by equation 2-7 is $n = 3/7 = 0.43$. The largest deviation occurs at low conductivities, i.e. below $10^{-4}\ \Omega^{-1}\ cm^{-1}$. This conductivity corresponds to concentrations below 10^{-3} M. Even in this range, the deviation is not large. Thus at $\sigma = 10^{-5}\ \Omega^{-1}\ cm^{-1}$ the current predicted by equation 2-7 is smaller by only a factor

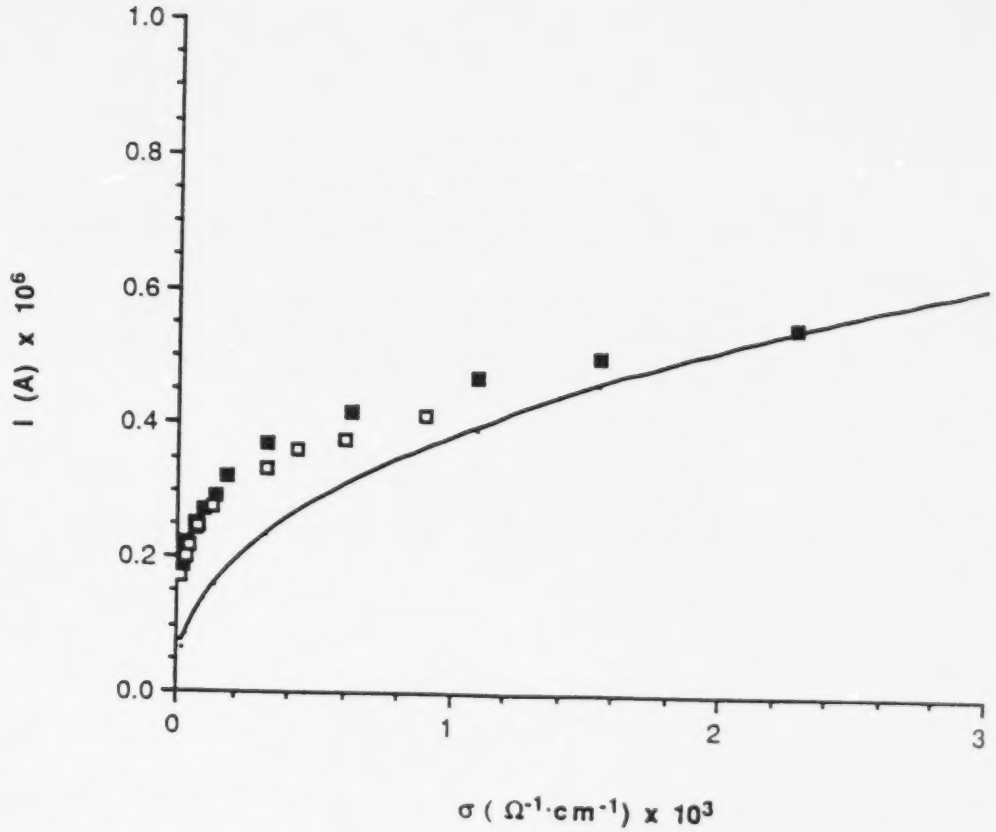

Figure 2-5 Linear plot of measured ES current I versus conductivity of solutions. Solid line represents calculated current predicted by the Hendricks [10] equation 2-7.

of 3 relative to the experimental I. Considering the complexities of the electrospray nebulization process (9-12) even an agreement within a factor of 10 between theoretical predictions and experiment might be considered a considerable success for the theory, when an equation like 2-7 is involved which has no adjustable parameters.

The experimentally observed exponent n for the concentration dependence appears to depend also on the type of capillary tip used. The earlier work in references 7 and 17 where a wider outer diameter capillary was used, produced electrospray currents I which depended on the conductivity with an exponent n which was higher, 0.37-0.42, and thus closer to the n = 0.43 predicted by equation 2-7.

The dependence of I on the flow rate Q of the solution was also examined and found to depend on an exponent close to the 4/7 power predicted by equation 2-7 in the earlier work.

The partial success of the Hendricks equation 2-7 need not mean that the assumptions used for the derivation are correct. However, the equation obviously makes some useful predictions.

Since the imposed external field E_c is very high, one might be concerned that the low field conductivities determined in the present work and used in the equations may not apply. This question is briefly examined in the Appendix where it is shown that use of the low field conductivities is justified.

c. Dynamic range of detected analyte ion intensity in ESMS

The preceding experimental and theoretical information shows that the electrospray current I and thus also the product between the average charge on the droplets and the rate of droplet emission is a function of the

conductivity of the solution. However, the functional dependence is weak, i.e. I changes with the conductivity, see equation 2-3, 2-4 and 2-7, taken to the $n \approx 0.3$ power.

Furthermore, because the limiting molar conductivities λ°_{m} for most electrolytes are within ~30% of each other, one might expect that the relative concentrations of the electrolytes in the charged droplets formed at the capillary tip will be very similar to those in the solution subjected to electrospray. By this we mean that no significant enrichment (fractionation) of one ionic species over another is expected for the initially formed droplets.

The assumption of no fractionation of ionic species must be qualified with regard to any new electrolyte species produced by the electrospray process. As shown in the work of Blades et al.(7), new ions, such as Fe^{++} can be produced by an electrolytic oxidation at the stainless steel capillary tip, when the capillary potential is positive. It is these ions that provide the charge balance for the extra positive charge on the droplets. However, at normal electrospray currents, $I \sim 5 \times 10^{-7}$ A, the concentration of these ions is in the 10^{-6} M range (7) and thus considerably lower than the typical impurity electrolyte concentration and very much lower than the concentration of electrolyte buffers that would be present in any liquid chromatography (LC) effluent. Thus, even though the electrosprayed droplets may contain one ionic species that was initially not present in the electrosprayed solution, the concentration of that species will be low (10^{-6} M) and of little significance unless the solvent used was deliberately deionized.

While the selectivity for one ionic species over another for the transfer of ions from the bulk solution to the droplets may be expected to

be very low, the same need not be the case in the transfer of ions from the droplets to the gas phase. Thus, assuming that the Iribarne ion evaporation model (18) is the principle mechanism for the ion transfer to the gas phase, one may conceive of ionic species whose ion evaporation free energies might be especially low and lead to much higher ion evaporation rates.

To obtain a simple model, we propose that the ion evaporation rate from the droplets is proportional to the ion concentration in the droplet. Singling out analyte ions A^+ and lumping all other electrolyte ions as external electrolytes E^+, one can assume equation 2-9 to provide a prediction for the gas phase analyte ion current $I(A^+,g)$ in the vicinity of the planar counter electrode, see Figure 2-1.

$$I(A^+,g) = f\frac{k_A[A^+]}{k_E[E^+] + k_A[A^+]}I \qquad (2\text{-}9)$$

I is the total current, see equations 2-1, 2-3 and 2-7, and $I(A^+,g)$ is the current due to gas phase ions generated by escape of analyte ions from the droplets. k_A and k_E are rate constants which express the rate of transfer of ions from the droplets to the gas phase, $[A^+]$ and $[E^+]$ are the respective electrolyte concentrations in the droplets. The proportionality constant f represents the fraction of droplet charge that gets converted into gas phase ions.

Since $I(A^+,g)$ could not be determined in the present experiment and since the interest is in the mass spectrometrically detected analyte ion intensity $I(A^+_{ms})$, we assume a proportionality,

$$I(A^+,ms) = p\ I(A^+,g)$$

where p is a proportionality constant expressing the "sampling efficiency"

of the system, and obtain

$$I_{(A^+,ms)} = pf \frac{k_A[A^+]}{k_A[A^+] + k_E[E^+]} I \qquad (2\text{-}10)$$

The predictions of equation 2-10 are compared in Figure 2-6 with previously reported experimental results from ESMS on cocaine hydrochloride solutions (6). Shown in Figure 2-6 is the measured total ES ion current I as well as the mass analyzed current I (A^+, ms) due to the analyte A^+ where A^+ is protonated cocaine. Also shown is the calculated I (A^+, ms) obtained with equation 2-10. This curve was obtained with the simplest assumption $k_{A^+} = k_{E^+}$. It was also assumed that the bulk solution concentrations can be substituted in equation 2-10. The presence of external electrolyte E was due to impurities in the solvent used. Conductivity determinations and mass spectrometric analysis of the ES produced ions with the pure solvent, had shown that the impurities E^+ were mostly NH_4X and NaX electrolytes with a total concentration of ~5 x 10^{-6} M and this value was used in equation 2-10. Since the factor pf in equation 2-10 is not known at this stage, the calculated A^+ intensities were obtained by adjusting pf to obtain agreement with the measured A^+ intensity at one experimental point, $[A^+] = 10^{-7}$ M.

Two regions in the analyte A^+ intensity curve can be recognized in Figure 2-6. The first is the important linear region of constant analyte sensitivity. It occurs where the external electrolyte concentration $[E^+]$ is much larger than the analyte concentration $[A^+]$. Under these conditions equation 2-10 reduces to

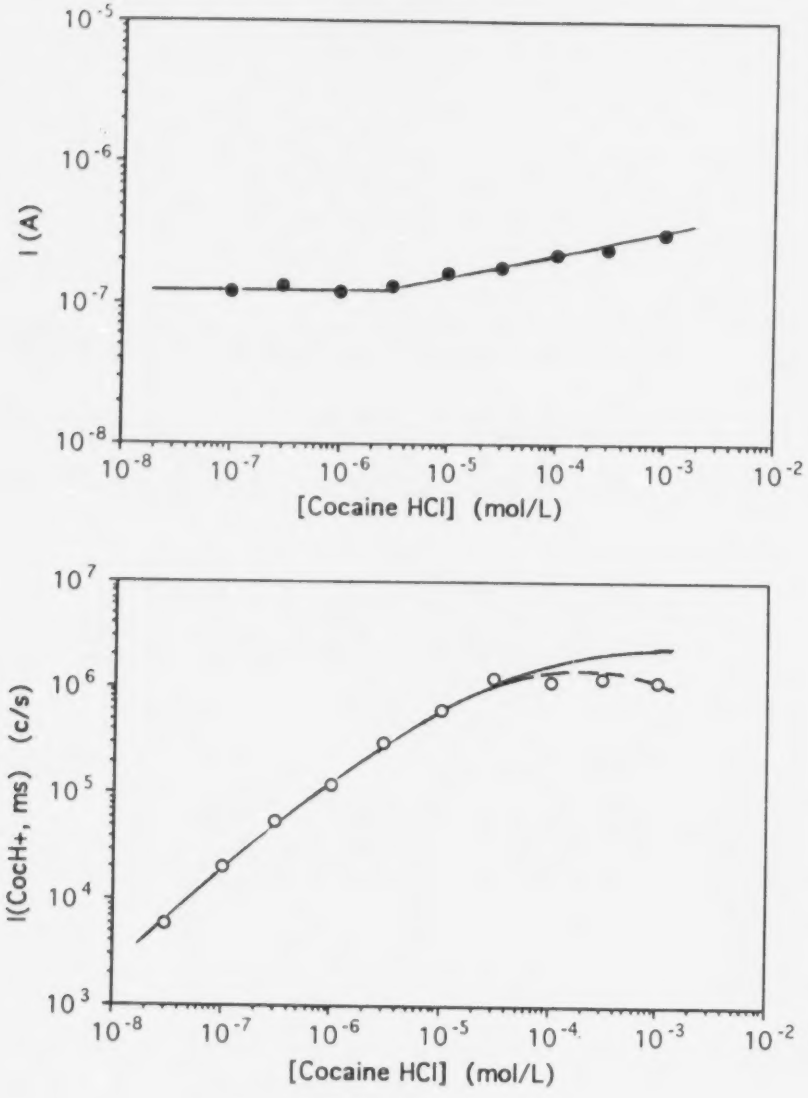

Figure 2-6 (Upper plot) Total electrospray current I as a function of added analyte concentration.

(Lower plot) Changes of mass analyzed ion intensity (counts/s) of analyte ion versus analyte concentration. Solid line: predictions of equation 2-10. ○: experimental points.

$$I(A^+,ms) = \frac{pf\,k_A[A^+]}{k_E[E^+]}\,I \qquad (2\text{-}11)$$

Furthermore since $[E^+]$ is constant and E^+ is the dominant electrolyte, also I is constant, see Figure 2-6. Therefore, $I(A^+, ms)$ is proportional to the only variable, $[A^+]$.

In the second region, where $[A^+] >> [E^+]$, equation 2-10 assumes the limiting form:

$$I(A^+, ms) \approx pfI = pf\,H(\lambda_m^{\circ})^n\,[A^+]^n \qquad n \approx 0.2 \qquad (2\text{-}12)$$

where the last equality involves use of equation 2-3, with A being the dominant electrolyte. $I(A^+, ms)$ increases very slowly in this region, see Figure 2-6, due to the slow increase of I with electrolyte concentration.

Above $[A^+] = 10^{-3}$ M, it is observed that the experimental points begin to deviate significantly from the calculated curve. The downward deviation indicates that either p or f or both decrease in this region. A decrease of the ion sampling efficiency p with increase of I may be expected particularly for conditions where the system is space charge dominated, see for example Sunner (19). However, the increase of I is small. Furthermore, evidence will be presented in next chapter that space charge effects become important only for $I > 10^{-6}$ A, i.e. currents considerably higher than those occurring in the present experiments.

A more probable cause for the downward experimental trend of $I(A^+, ms)$ is the decrease at high concentrations of the fraction f of charge evaporating from the droplets. It is known, that when the electrolyte concentration is increased at constant flow rate, there is an initial decrease followed by an increase of droplet radius (12). Unfortunately, quantitative

data for flow rates and solvents used in ES mass spectrometry are not available. In the experiments with methanol solution at flow rates of ~20 μL/min it is generally observed that the counter electrode remains dry for electrolyte concentrations up to ~10^{-3} M but becomes wet at higher concentrations. Obviously this change indicates incomplete droplet evaporation presumably due to an increase of droplet size with concentration in this range. Therefore, a decrease of f in this range could well be expected from these results.

Activity coefficients of both electrolytes (A^+ and E^+) may vary dramatically when the concentration of A^+ is in the high concentration range. If one takes into account the solvent evaporation of charged droplet, which is necessary for the ion emission (see Chapter 3), the difference between the activity coefficients of both electrolytes would be bigger. However, the activity coefficients can not be predicted due to the lack of reliable solvent evaporation data. The use of concentration instead of activity will result in the deviation.

A totally different reason for the deviation observed in Figure 2-6 should be considered also. As is evident from equation 2-11, which gives the limiting condition at low $[A^+]$, the assumption $k_A = k_E$, taken together with the fitting procedure to one experimental point, amounts to lumping the real k_A/k_E ratio into the fitted pf product, i.e. the fitted product actually corresponds to: pf k_A/k_E. This fitted constant is not suitable for the regime of high $[A^+]$ where equation 2-12 applies, since in this region the fitting constant is only pf. For instance, assuming that the actual ratio is $k_A/k_E > 1$, which is a general case for two different ion species, the fitted constant at low $[A^+]$ will be too high for the high $[A^+]$ regime, i.e. the predicted A^+ intensity will be higher than the measured one.

The experimental A^+ intensity in Figure 2-6 is seen to actually decrease at the highest concentrations. The decrease would not be expected on the basis of the fitting constant argument and this suggests that a decrease of f at high concentrations is the most likely cause. However, the above discussion illustrates the fact that much more extensive measurements, involving a variety of pairs of A^+ and E^+ at different concentration regimes, should be performed in order to examine the range of validity of equation 2-10. Such work will be shown in Chapter 3.

The prediction of equation 2-10 for the situation where $[A^+]$ is kept constant and $[E^+]$ increases is for a decrease of the measured $A^+_{m,s}$ intensity. A degree of quantitative agreement is also observed and such data will be presented in section 3 as part of an extensive investigation dealing with the validity and limitations of equation 2-10. For the present, equation 2-10 could be considered as a promising but probably oversimplified approach to deal with the prediction of dynamic region of ion intensity in mass analysis.

2.4 Conclusions

The electrospray current I is a function of the conductivity σ of the electrosprayed solution and thus also a function of the concentration C and the nature of the electrolyte via the molar conductivity λ°_m. However, because λ°_m changes by no more than a factor of 3 for the vast majority of electrolytes, and the functional dependence $(\lambda^\circ_m)^n$, where $n \approx 0.2\text{-}0.4$ is weak, changes of I for different electrolytes at the same concentration are minimal and hard to detect. The changes of I show also a weak dependence, C^n, on the concentration of the electrolyte. However, the

practical concentration range increase, from 10^{-6} to 10^{-2} M, is very large and therefore the total change of I by a factor of $10^{4n} \approx 15$ is significant.

For the relative transfer rates of ions from the droplets to the gas phase one expects a proportional dependence on the relative concentrations of the ions in the droplets. This proportionality can be expressed by equation 2-10. The predictions of equation 2-10 are found to be in good agreement with the experimental data. In particular, equation 2-10 predicts a constant sensitivity for analyte at concentrations below about 10^{-5} M and a decreasing sensitivity above this value, which depends on the impurity level in the solution. It also predicts that the presence of electrolytes other than the analyte always leads to a decrease of the analyte sensitivity.

2.5 Appendix

Conductivity at high electric fields

Although the electric field E_c at the capillary tip in vacuo is very high, the electric field in the liquid at the tip need not be high. Apart from the reduction of E_c in the solvent by the ratio of the permittivities $\varepsilon/\varepsilon_o = D$, where D is the dielectric constant of the solvent, the redistribution of electrolyte charges under the influence of the field, i.e. charge relaxation in the solution, may reduce the field to a very small value (9-12). Nevertheless, it is still of interest to know the dependence of the conductivity on the field. For example in the derivation of the Hendricks equation it is assumed (10) that each charged droplet removes the local charge, thus restoring the electrical field to its original high field value. Therefore, substitution of the low field conductivity in the Hendricks equation 2-7 may be inappropriate.

It is possible to show that the change of the conductivity with changing field will be small. Since the electrolytes used are strong, only the first Wien effect (20) due to the destruction of the "ion atmosphere" by the field (in modern terms, the reduction of ion pairing) will be important. Equation 2-11, developed by Onsager and Kim (21), provides predictions for the change of the equivalent conductivity λ_j of ionic species j with the field.

$$\lambda_j = \lambda_j^0 - 5.9420 \times 10^6 \frac{|z_1 z_2|}{(DT)^{3/2}} A \lambda_j^0 \Gamma^{1/2} - \frac{43.744 |z_1 z_2|}{(|z_1| + |z_2|)\eta_0 (DT)^{1/2}} B_j \Gamma^{1/2} \qquad (2\text{-}11)$$

where λ_j^0: limiting equivalent conductivity of j-ion

$|z_1|$ and $|z_2|$: number of charges of ions j and counterions.

η_0: viscosity of solution [1.6×10^{-2} poise] (14a)

D: dielectric constant of the solution [60] (14a)

T: temperature of the solution [296°K]

A: relaxation function

B_j: electrophoretic function

Γ: ionic strength, $\Gamma = 2C$ (mole/L) for present, electrolyte

At the low concentrations used in the present ES work, i.e. $C \leq 10^{-2}$ M, the functions A and B_j are given (21) by,

$$A = \frac{1}{2a} \tag{2-12}$$

$$B_j = \frac{2\sqrt{\mu_j}}{2(1 - \mu_j)} + a^{-1} \log a \tag{2-13}$$

where a is defined by,

$$a = 1.63 \times 10^{-6} \left(|z_1| + |z_2| \right) \sqrt{\frac{D}{T}} \frac{E}{\sqrt{\Gamma}} \tag{2-14}$$

where E is the field strength in V/cm.

Substituting in equation 2-14 the values that apply for the present conditions, $z_1 = z_2 = 1$, $E = 1.103 \times 10^{-5}$ V/cm, for $V_c = 5000$ V, $\Gamma = 2C$ where C is concentration in mole/L, and the values for D and T given in square brackets under equation 2-11, one obtains,

$$a = 0.1146 \times \frac{1}{\sqrt{C}} \tag{2-15}$$

μ_j in equation 2-13 stands for the relative ionic strength of the ion species j which for the present 1:1 electrolytes leads to $\mu_j = 1/2$.

Equation 2-12 and 2-13 can now be evaluated and substituted into equation 2-11. The other numerical data required for equation 2-11 are given in square brackets beside each symbol, see definition of symbols under equation 2-11. Substitution of these values into equation 2-11 allows the evaluation of this expression. The high field molar conductivity due to the positive and negative counter ion will be,

$$\lambda_m = \lambda_+ + \lambda_-$$

Evaluating λ_+ and λ_- with equation 2-11 and adding the result one obtains,

$$\lambda_m(5\text{ kv}) = (1\text{-}15.491C)\lambda_m^0 - 2\left[27.353 + 253.16\sqrt{C}\,\log\left(\frac{0.1146}{\sqrt{C}}\right)\right]\sqrt{C} \qquad (2\text{-}16)$$

The equivalent limiting molar conductivity λ_m° now stands for the sum: $\lambda_+^\circ + \lambda_-^\circ$ of the positive and negative ion present in the 1:1 electrolyte.

Since, for the low concentration range used, the low field molar conductivity is essentially equal to the limiting molar conductivity λ_m°, subtracting λ_m° from the expression in equation 2-16 one obtains the difference between the high and low field molar conductivity which in this concentration range is equal to the difference between the high and low field conductivity of the electrolyte;

$$\lambda_m(5\text{ kv}) - \lambda_m^\circ = [\sigma(5\text{ kv}) - \sigma]/C = \Delta\sigma/C \qquad (2\text{-}17)$$

The left side of equation 2-17 can be evaluated from equation 2-16 and the known λ_m° for the given electrolyte. $\Delta\sigma$ increases with concentration of the electrolyte. For the highest concentration, C = 10^{-2} M used in the present experiments, $\Delta\sigma$ is found to correspond to an increase of 9% of the low field conductivity for NaCl and 2% for HCl. These are very modest changes which will have no effect on the magnitude of I evaluated with the Hendricks equation 2-7. The result of the $\Delta\sigma$ calculations could have been anticipated from the fact that the "ion atmosphere" becomes significant only at concentrations above 10^{-1} M, for 1:1 electrolytes.

2.6 References

1. Whitehouse, C.M.; Dreyer, R.N.; Yamashita, M.; Fenn, J.B. *Anal. Chem.*, **57**, 675, (1985); Wong, S.F.; Meng, C.K.; Fenn, J.B. *J. Phys. Chem.*, **92**, 546, (1988); Fenn, J.B.; Mann, M., Meng, C.K., Wong, S.F. *Mass Spectrometry Reviews*, 9, 37, (1990); Fenn, J.B.; Mann, M., Meng, C.K.; Wong, S.F.; Whitehouse, C. *Science*, **246**, 64, (1989)
2. Bruins, A.P.; Covey, T.R.; Henion, J.D. *Anal. Chem.*, **59**, 2642, (1987); Covey, T.R.; Bonner, R.F.; Shushan, B.I.; Henion, J.D. *Rapid Commun. Mass Spectrom.*, **2**, 249, (1988); Huang, E.C.; Henion, J.D. *J. Am. Soc. Mass Spectrom.*, **1**, 158, (1990).
3. Olivares, J.A.; Nguyen, J.A.; Yonker, C.R.; Smith, R.D. *Anal. Chem.*, **59**, 1230, (1987); Smith, R.D.; Olivares, J.A.; Nguyen, N.T.; Udseth, H.R. *Anal. Chem.*, **60**, 436, (1988); Udseth, H.R.; Loo, J.A.; Smith, R.D. *Anal. Chem.*, **60**, 1948, (1988).
4. Ikonomou, M.G.; Blades, A.T.; Kebarle, P. *Anal. Chem.*, **62**, 957, (1990).
5. Juhasz, P.; Ikonomou, M.G.; Blades, A.T.; Kebarle, P. in "Methods and Mechanisms for Producing Ions from Large Molecules" Standing, K.E.; Ens, W. Eds. *Plenum Press* (1991).
6. Ikonomou, M.G.; Blades, A.T.; Kebarle, P. *Anal. Chem.*, **63,** 1989, (1991)
7. Blades, A.T.; Ikonomou, M.G.; Kebarle, P. *Anal. Chem.*, **63**, 2109, (1991).
8. Ikonomou, M.G.; Blades, A.T.; Kebarle, P. *J. Am. Soc. Mass Spectrom,* **2**, 497,(1991)

9. Bailey, A.G. "Electrostatic Spraying of Liquids" John Wiley, N.Y. (1988)
10. Pfeifer, R.J.; Hendricks, C.D. *AIAA Journal,* **6**, 496, (1968)
11. Smith, D.P.H. *IEEE Trans. Ind. Appl.,*.**IA-22**, 527, (1986)
12. Hayati, I.; Bailey, A.I.; Tadros, T.F. *J. Colloid and Interface Science,* **117**, 205, (1987); ibid 222.
13. Landolt, Börnstein, "Zahlenwerte und Funktionen" **II 7**, p. 366, 533, 651, Springer Verlag, Berlin. (1960)
14. (a) Shedlovsky, T.; Kay, R.L. *J. Phys. Chem.,* **60**, 151, (1956) (b) Longsworth, L.G.; MacInnes, D.A. *J. Phys. Chem.,* **43**, 239, (1939)
15. Johnson, J.B.; Funk, G.L. *Anal. Chem.*, **27**, 1464, (1955)
16. Handbook of Chemistry and Physics, 59 edition *CRC Press*, (1978)
17. Blades, A.T.; Jayaweera, P.; Ikonomou, M.G.; Kebarle, P. *J. Chem. Phys.*, **92**, 5900, (1990); *Int. J. of Mass Spectrometry and Ion Processes*, **102**, 251, (1990)
18. Iribarne, J.V.; Thomson, B.A. *J. Chem. Phys.*, **64**, 2287, (1976)
19. Busman, M.; Sunner, J.; Vogel, C.R. *J. Am. Soc. Mass Spectrom.*, **2**, 1, (1991)
20. Wien, *M. Annal. Physik.*, **83**, 327, (1927); **85**, 759, (1928)
21. Onsager, L.; Kim, S.K. *J. Phys. Chem.*, **61**, 198, (1957)

Chapter 3. Dependence of Ion Intensity in Electrospray Mass Spectrometry on the Concentration of the Analytes in the Electrosprayed Solution*

3.1 Introduction

On the basis of previous work (1-7) it has become clear that electrospray is a method by which ions present in solution, i.e. ions due to an electrolyte, are transferred to the gas phase. The presence of the very high electric field at the capillary tip leads to a partial separation of positive from negative ions present in the solution. For convenience we will in all subsequent discussions assume that the capillary is of positive polarity. At this polarity, the liquid near the meniscus becomes enriched in positive ions. The effect of the field on this positive charge leads to a destabilization of the meniscus, the formation of a liquid cone and the emission of charged droplets whose charge is due to an excess of positive electrolyte ions over the negative counter ions. The negative ions remaining in the solution are either electrolytically discharged on the wall of the capillary or electrolytically provided by positive counter ions by formation of positive ions from the capillary wall. Therefore, the electrospray process can be likened to an electrolysis cell of a special kind where oxidation occurs at the capillary anode and the positive current is carried away by the charged droplets (7).

In the present work we will examine how the analyte ion signal detected with the mass spectrometer depends on the concentration of the

---

* Part of this chapter has been submitted for publication: P. Kebarle, L. Tang; *Anal. Chem.* (accepted)

analyte ion in the solution and also how this signal is affected by the presence of other electrolytes. Other electrolytes are practically always present either as impurities in the solvent, as other coanalytes and particularly as buffers required in chromatographic separation or capillary electrophoresis.

The ions in the gas phase are originated from the excess charges on the droplets. Therefore, the current I leaving the ES capillary is a measure of the rate at which excess positive electrolyte ions leave the capillary. This current is easily measured and is found to depend on the conductivity σ of the solution (8). There is a minimum (threshold) conductivity below which there is no ES. The threshold occurs at $\sigma \approx 10^{-7}$ Ω^{-1} cm^{-1} (methanol) (6), which corresponds to a concentration of ~10^{-6} M (M = mole/L) of electrolytes like NaCl or NH_4Cl (7, 8). As the conductivity is increased above this value, the current I leaving the capillary increases and becomes stable. I is only a very weak function of the conductivity (4, 6, 8):

$$I = H\sigma^n \qquad n \approx 0.2\text{-}0.3 \tag{3-1}$$

H is a constant which can be determined experimentally. A derivation of equation 3-1 in which H is given a functional dependence on experimental parameters such as electric field at the tip, radius of the capillary, surface tension of the solvent, flow rate etc. has been obtained (4).

When strong electrolytes are used at concentrations not exceeding 10^{-2} M, the conductivity σ follows the relationship

$$\sigma = \lambda_m^0 C \tag{3-2}$$

where C is the concentration of the electrolyte and λ_m is the limiting molar

conductivity of the given electrolyte. Therefore, the current I depends on both the concentration and the nature of the electrolyte (8).

$$I = H\sigma^n = H\lambda_m^{\circ\,n}C^n \qquad (3\text{-}3)$$

$$n \approx 0.2\text{-}0.3$$

However, the changes of λ_m from one electrolyte to the other are generally not large. Due to the small value of n in equation 3-1, in practice, the changes of I with the nature of electrolyte are very small. Equation 3-1 is obeyed over the concentration range: $C = 10^{-5}$ M to $C = 10^{-3}$ M. At higher concentrations the current levels off and even decreases slowly with concentration (6, 8).

When two electrolytes such as A^+X^- and B^+Y^- are present in the solution, both A^+ and B^+ ions will be present amongst the excess positive ions that constitute the charges of the droplets. However, because of the very weak dependence of I on the total electrolyte concentration, see equation 3-3, addition of BY to AX will not materially increase the current, i.e. the total excess charge. On the other hand B^+ will compete with A^+ amongst the excess charges on the droplets. This means that the amount of gas phase ions A^+ produced from the charged droplets will decrease as BY is added to the solution.

On the basis of the above consideration, we proposed (8) the relationship:

$$I_{(A^+ ms)} = pf\frac{k_A[A^+]}{k_A[A^+] + k_B[B^+]}I = \frac{pf[A^+]}{[A^+] + k_B/k_A[B^+]}I \qquad (3\text{-}4)$$

$$I_{(A^+ ms)} = pI_{(A^+, g)} \qquad (3\text{-}5)$$

$I_{(A^+ ms)}$ is the mass spectrometrically detected ion current of A^+. p is a constant expressing the efficiency of the mass spectrometer for sampling the gas phase ions, see equation 3-5, and f is the efficiency of conversion of droplet charge to gas phase ions. $[A^+]$ and $[B^+]$ are the concentrations of the ions in the electrosprayed solution, which will be abbreviated as [A] and [B] in the following discussion. $I_{(A^+ ms)}$ depends on the ratio, k_A/k_B and not on the individual values of k_A and k_B. The ratio expresses a "fractionation" factor in the ES conversion of ions in solution to ions in the gas phase. The nature of the phenomena responsible for that ratio will be considered in the Results and Discussion section.

In the previous work (8) it was shown that equation 3-4 provided a good fit of limited, available experimental data. It was pointed out (8) that an examination involving a much wider variety of AX and BY partners as well as a greater change of relative concentrations of A^+ and B^+ would be required to establish the range over which equation 3-4 is applicable. The present work provides such experimental data and an examination of the validity of equation 3-4. Because the possible choice of concentrations is extremely wide, the comparisons were restricted to three types of experiments:

(a) [AX] was kept constant and [BY] was increased.

(b) [AX] = [BX] were increased simultaneously.

(c) [AX] was increased without BY being present.

Since the mass analysis was obtained with a quadrupole mass spectrometer and quadrupoles have strongly mass dependent ion transmission, all mass analyzed ion currents I(ms) were corrected for the mass dependent transmission. The method used to obtain the transmission is given in the Experimental part which includes also other details about the

apparatus and methodology of the measurements.

The experimental results obtained have significance for the practicing ES mass spectrometrist. For example, they show that the suppression of a desired analyte ion by a buffer depends not only on the concentration but also on the nature of the buffer. Buffer cations with high coefficients, k, lead to strong suppression of the analyte and should be avoided.

In trying to correlate the observed relative values of the coefficients k with properties of the ionic species, such as surface activity and ion solvation, one has to consider not only models for the escape of gas phase ions from the charged droplets but also the fission processes through which the very small droplets are formed which lead ultimately to ions. The solvent evaporation rates from the droplets are also of great importance. In the treatment presented in the Discussion, we try to combine all these elements to present a relatively complete account.

3.2 Experimental

The instrument used was the SCIEX TAGA 6000E triple quadrupole atmospheric pressure mass spectrometer fitted with an electropsray interface, see Figure 3-1. The stainless steel electrospray capillary tip was 0.1 mm i.d. and 0.25 mm o.d. The capillary tip was ~4 cm from the opposing electrode (the interface plate) and at +4.35 kV relative to the interface plate. Gas phase ions produced by the electrospray in the 1 atmosphere plenum chamber [1] are accelerated towards a 4 mm orifice in the interface chamber [4]. The interface chamber contains dry N_2 gas at 1 atmosphere. The ions, M^+, have solvent molecules attached to them, i.e.

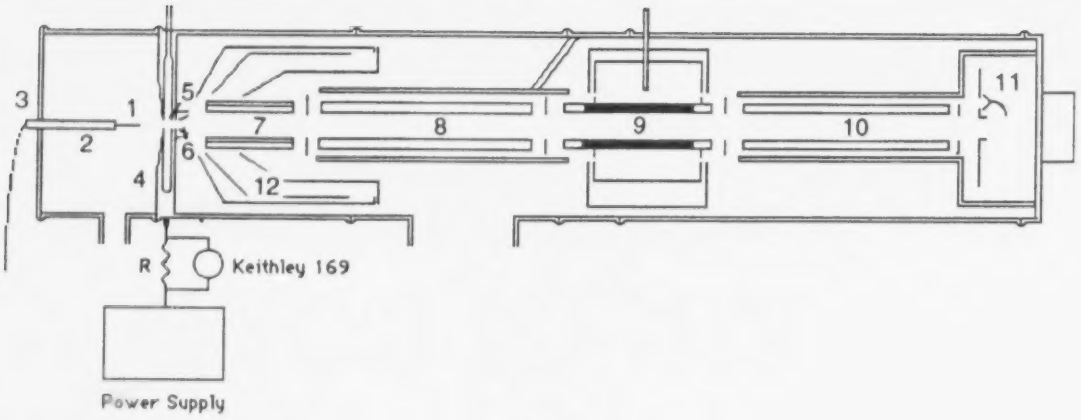

Figure 3-1 A schematic diagram of TAGA 6000E.

1. ES capillary tip (i.d. = 0.1 mm, o.d. = 0.25 mm) in plenum chamber at 1 atmosphere air pressure, 5 kV;
2. supporting rod;
3. front plate with jig which allows x, y, z motion of capillary;
4. interface plate (650 volts);
5. orifice to vacuum (100 μm diameter, 55 V)
6. cluster breaker CB (33 volts);
7. quadrupole 0 (30 volts);
8. quadrupole 1 (28 volts);
9. quadrupole 2 (20 volts);
10. quadrupole 3 (28 volts);
11. electron multiplier (-3.4 kV);
12. cryosurface at temperature ~20 K.

they are ion-solvent molecule clusters $M^+(CH_3OH)_n$. When they enter the dry N_2 chamber some of their solvent molecules are lost and other get replaced by H_2O due to residual H_2O in the N_2 gas. The gas phase ions drift, under the influence of the electric field in the interface chamber, to the aperture [5] where a sample of air and ions enters the vacuum of the mass analysis section. When the orifice [5] is at 55 V and the first electrode CB [6] is at 33 V, the ions are accelerated relative to the neutral gas beam in the space between the orifice and CB. The collisions of the ions with the gas lead to partial or complete cluster breakup so that the original $M^+(CH_3OH)_n$ ions are detected as M^+.

The rods in quadrupole 0 are made of wire mesh and operated in the AC mode only. It guides the ions while the gas molecules fly to the cryo-surfaces [12] where they are frozen, i.e. cryopumped. For our work no collision activated decomposition (CAD) was necessary. Therefore, in the present experiments quadrupole 1 was used for the mass analysis and quadrupole 2 and 3 were operated in the AC mode only. The ion detection was obtained with an electron multiplier [10] and the intensity was measured with an ion counting device.

Determinations of the mass dependent transmission were obtained with use of the corona discharge atmospheric pressure ionization (APCI) mode of the TAGA (9, 10). Ten different amines B were chosen for this purpose. When protonated by APCI these become BH^+. The masses of the bases were chosen so as to cover evenly the mass range to be calibrated. The typical assembly for this experiment is shown in Figure 3-2. A constant, low concentration of amine solution in a solvent was injected into a heated tube where the solution evaporated into the APCI source. Hexane

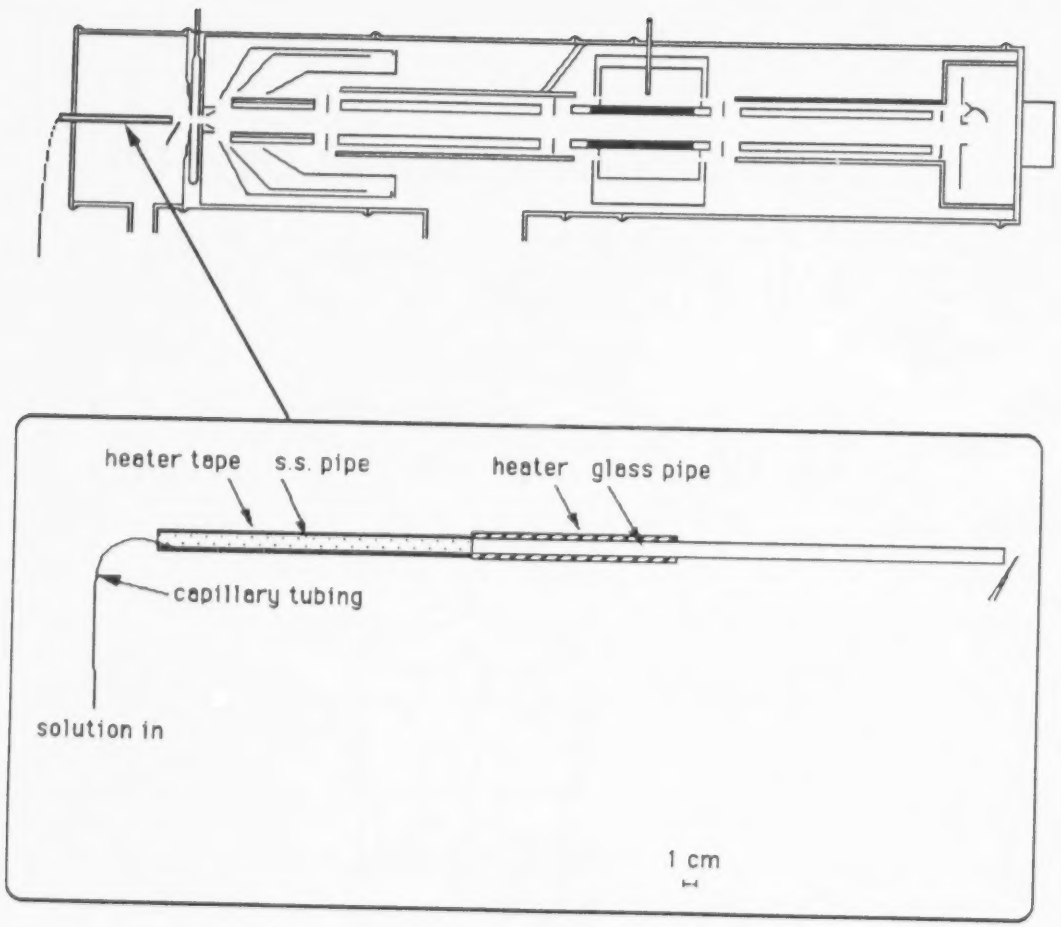

Figure 3-2 A special APCI set-up of TAGA 6000E for transmission determination.

(b.p 68.3 - 68.8 ^{o}C) was used as solvent for its low proton affinity, low boiling point and good solvent properties for amines. A 10^{-4} M concentration and 15 µl/min were used for each amine and were found to produce a stable amine BH^+ ion signal. Keeping APCI current constant as 2 µA, we could measure the ion intensity of each protonated amine signal. Because the generated B pressures are the same, the observed BH^+ signal should be the same in the absence of mass discrimination (9, 10). The measured relative BH^+ intensities are shown in Figure 3-3. They correspond to the relative transmissions at the given m/z.

The highest transmission was assigned as $T_m = 1$. To correct the observed ion intensities, I_{obs}, for mass dependent transmission, one has to divide I_{obs} by T_m for the given mass. Since T_m changes by more than a factor of 10 over the mass range that was used, errors in the corrected relative ion intensities are expected to increase with the mass difference of the two ions that are compared. For larger mass differences errors as large as a factor of two can not be excluded.

For the subsequent interpretation of the data, it is desirable to know the values of p and f which appear in equation 3-4. The product pf is easily determined. In general, the two mass analyzed ion intensities I_A and I_B dominate the mass spectrum. The total mass analyzed ion current corrected for transmission is thus $I_A + I_B$. The capillary ES current I is also measured and one obtains: $pf = (I_A + I_B)/I$. Generally for a typical I of 0.3 µA, the product was found to be $pf \approx 1 \times 10^{-6}$.

A determination of f, the fraction of droplet charge that is converted to gas phase ions, is much more difficult and would require specialized apparatus. A rough estimate, $f \approx 0.3$, was obtained in Figure 3-4 by measuring the total current, I_{CB}, reaching the first electrode, CB, located

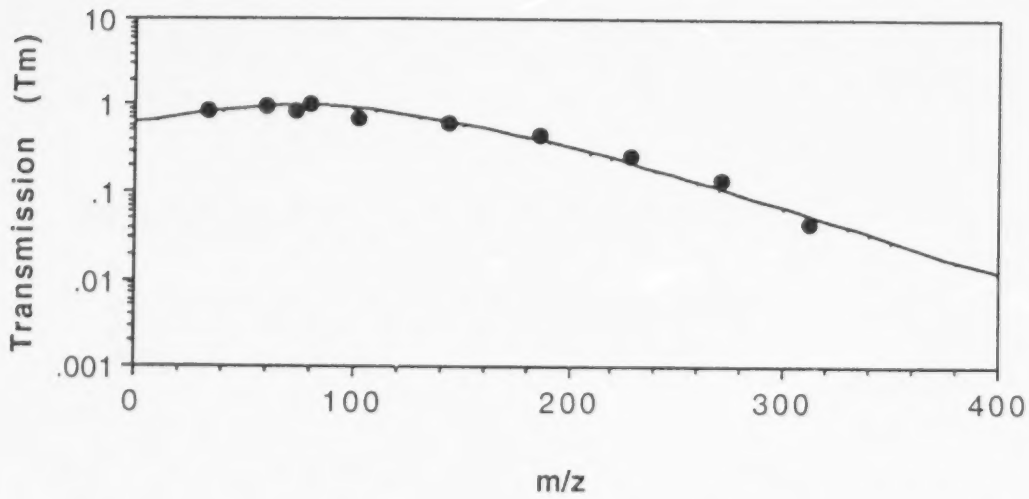

Figure 3-3 Experimental ion transmission curve which provides correction for mass dependent transmission of quadrupole used. The m/z with highest transmission T_m is given the value $T_m = 1$. Points shown are obtained from ion intensity measurements obtained with atmospheric pressure ionization using a technique described previously (9). Ten protonated amine ions are: $CH_3NH_3^+$ (m/z=33), i-$PrNH_3^+$ (m/z=60), n-$BuNH_3^+$ (m/z=74), PyH^+ (m/z=80), $Et_3NH_2^+$ (m/z=102), $Pr_3NH_2^+$ (m/z=144), $Bu_3NH_2^+$ (m/z=186), $Pe_3NH_2^+$ (m/z=228), $Hx_3NH_2^+$ (m/z=271) and $Hp_3NH_2^+$ (m/z=312)

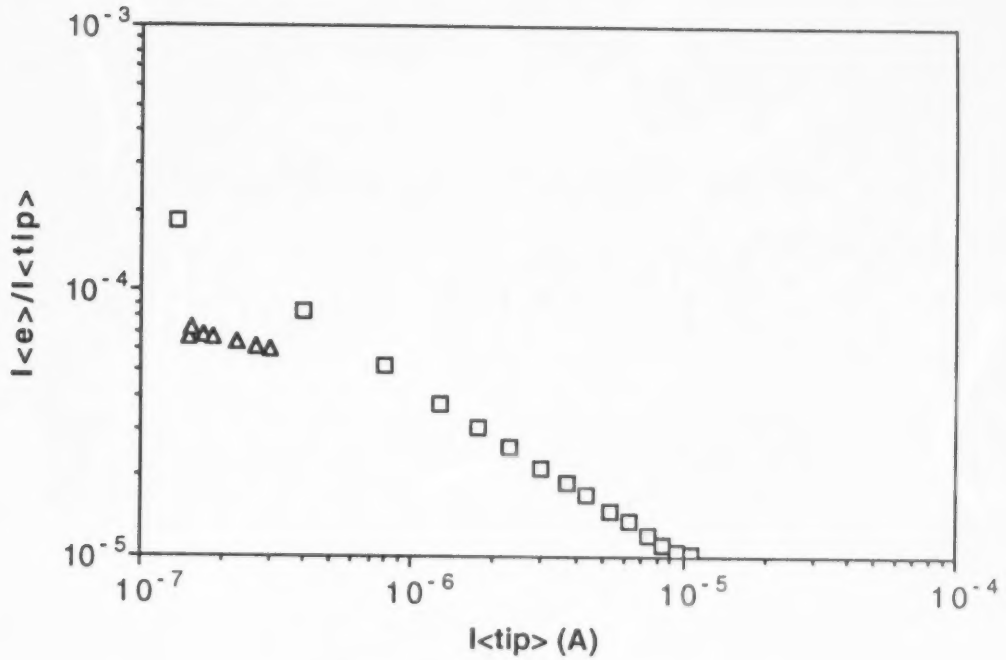

Figure 3-4 Ratio of total current on CB, I_{CB}, to total current fron the tip (ES tip or APCI tip), I_{tip}; ❑: APCI with room air; ▲: ES with CsCl in methanol.

in the vacuum of the mass analysis section. The electrode CB was closed off by spot welding a bit of metal foil to it. First, I_{CB} was obtained for an APCI electric discharge operated at atmospheric pressure with a total current, I = 0.1 μA. Then, I_{CB} was determined with an ES capillary placed in the same position as the API needle and electrospray current I = 0.1 μA. The ratios $I_{CB}/I = 2 \times 10^{-4}$ (API) and 0.7×10^{-4} (ES) were determined. Since APCI produces gas phase ions while ES initially produces charged droplets and later gas phase ions, the ratio: ES/API = 0.35, may be taken to give the yield of gas phase ions from the droplet charge in ES, if it is assumed that space charge effects, geometry and other conditions for the API and ES were the same. This assumption is probably not warranted and therefore, the estimate of the yield is very uncertain. However it may be taken to indicate that f is in the range: 0.5-0.1.

The flow rate of electrosprayed solution was 20 μL/min. Reagent grade methanol from the same bottle was used in all experiments. This methanol had a conductivity of $10^{-6}\Omega^{-1}$/cm which corresponds to an impurity level of NaCl or NH_4Cl of ~1.3×10^{-5} M. In previous work attempts were made to work with completely electrolyte free methanol solvent. It was found that the conductivity of such methanol increased rapidly on storage after purification. In order to obtain reproducible experiments, we chose to work with the reagent grade methanol which had a constant electrolyte impurity level.

3.3 Results and Discussion

I. Behavior when electrolytes are at higher, 10^{-5}-10^{-3} M, concentrations

a. Experiments where the analyte ion concentration is constant and a second electrolyte, B^+, is present in increasing concentrations

A series of experimental measurements were made in which the concentration of one of the compounds in solution was constant, $[A^+] = 10^{-5}$ M, and a second electrolyte $B^+ = NH_4^+$, was increased stepwise from 10^{-5} to 10^{-3} M. Used as A^+ were: Cs^+, $MorH^+$, $CodH^+$, $CocH^+$, $HerH^+$, $Ni^{++}(Tpy)_2$, $(Bu)_4N^+$, where Mor, Cod, Coc, Her, stand for the alkaloids morphine, codeine, cocaine, heroin, Tpy for tripyridine and Bu for n-butyl.

A typical result is shown in Figure 3-5 for $A^+ = CodH^+$. The top plot (a) in the figure gives the capillary current I. As pointed out in the Introduction, this current changes very slowly with electrolyte concentration, see equation 3-1. Thus, an increase of concentration by a factor of 50 increases the current by only a factor of 2. The relationship given in equation 3-1 predicts a straight line for the current I where a log plot is used and this is in agreement with the experimental result in Figure 3-5a.

The plot in Figure 3-5b gives the experimentally observed mass analyzed ion currents corrected for transmission efficiency. Addition of NH_4^+ decreases the ion intensity of $CodH^+$ as predicted by equation 3-4. The lines drawn through the experimental points are predicted changes calculated with equation 3-4. To obtain the parameter pf and k_B/k_A

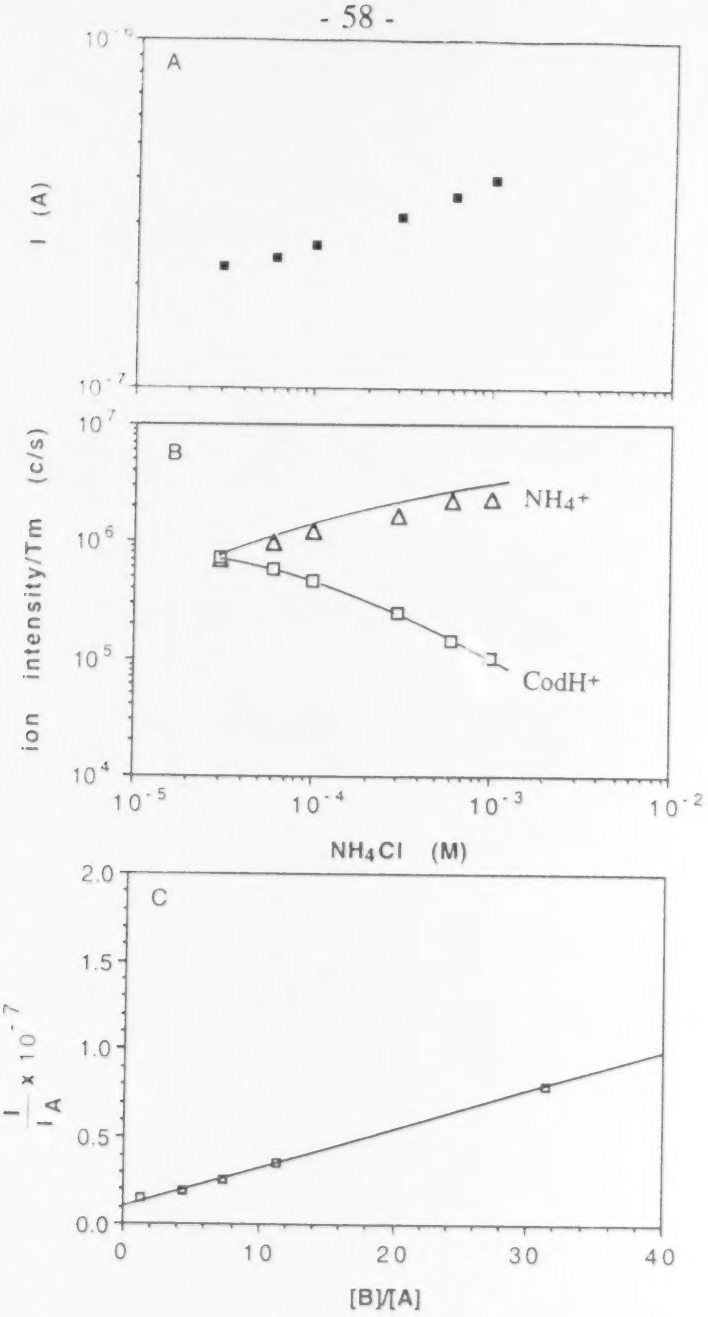

Figure 3-5 Results from ES where $[A^+] = [CodH^+] = 10^{-5}$ M and $[B^+] = [NH_4^+]$is increased as shown. (a) Measured capillary current I. (b) Ion intensities of NH_4^+ Δ and $CodH^+$ □, corrected for transmission. Curves shown as solid lines are a calculated fit using equation 3-4. (c) Predicted linear plot based on equation 3-6 leads to ratio $k_A/k_B = 3.4$.

required for the fit, a rearranged form of equation 3-4 was used.

$$\frac{I}{I_A} = \frac{1}{pf} + \frac{1}{pf}\frac{k_B}{k_A}\frac{[B^+]}{[A^+]} \qquad (3\text{-}6)$$

I_A is the mass analyzed current of A^+, corrected for mass dependent transmission and converted from counts per second to amperes. Equation 3-6 predicts a straight line when I/I_A is plotted versus the solution concentrations ratio [B] / [A]. The predicted intercept is 1/pf and the slope is: $k_B/(k_A\ pf)$. The experimental plot shown in Figure 3-5c demonstrates that a good straight line relationship is observed. The intercept provides; $pf = 1.2 \times 10^{-6}$ and the slope $k_B / k_A = k_{NH_4^+} / k_{CodH^+} = 0.29$. These two parameters were used to obtain the predicted intensities in Figure 3-5b. For this system the agreement between the predictions of equation 3-4 and the experimental results can be considered as very good.

Similarly good agreement was observed for other AX electrolytes with $B^+ = NH_4^+$ in analogous plots as in Figure 3-5. A summary of these results is given in Figures 3-6 and 3-7. Figure 3-6 gives the plots obtained with the linearized form, equation 3-6, while Figure 3-7 gives the observed and predicted I_A as in Figure 3-5b but for all AX electrolytes used. The k_B / k_A ratios obtained are summarized in Table 3-1.

The pf values were found to be relatively close to each other and in the range: 1.2×10^{-6} and 2.5×10^{-6}. Considering the difficulties of the extrapolations to the intercept, see Figure 3-5c and Figure 3-6, the differences probably reflect experimental scatter rather than real trends. These pf values are in agreement with a $pf = 10^{-6}$ obtained with a more direct method, see Experimental section. An estimate of $f \approx 0.3$, refer to Experimental section, leads to $p \approx 3 \times 10^{-6}$. The very small p is mostly a

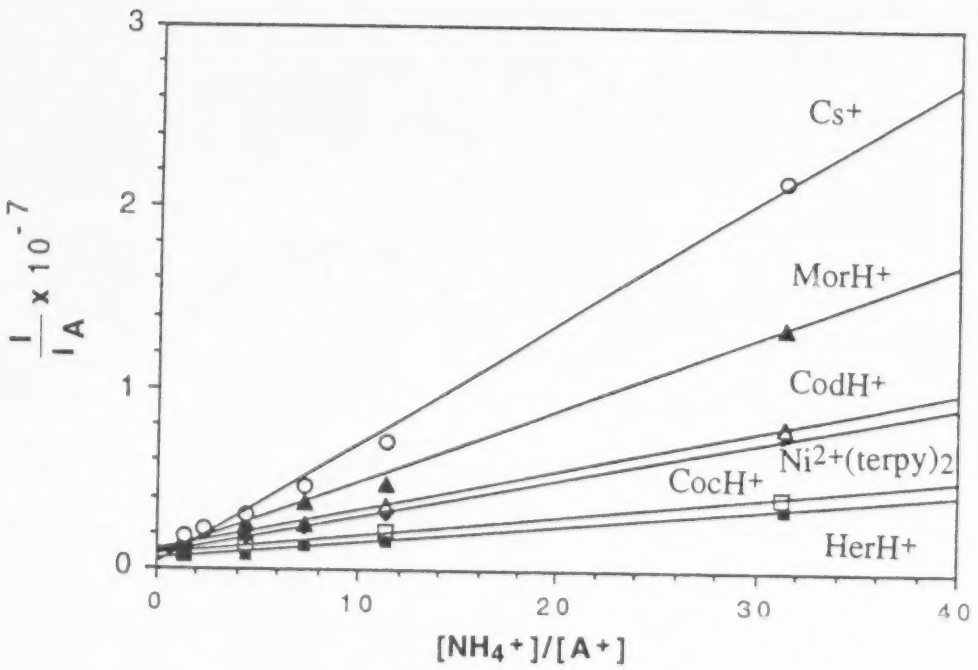

Figure 3-6 Linear plots based on equation 3-6, see Figure 3-5c, but for ions A^+ as shown.

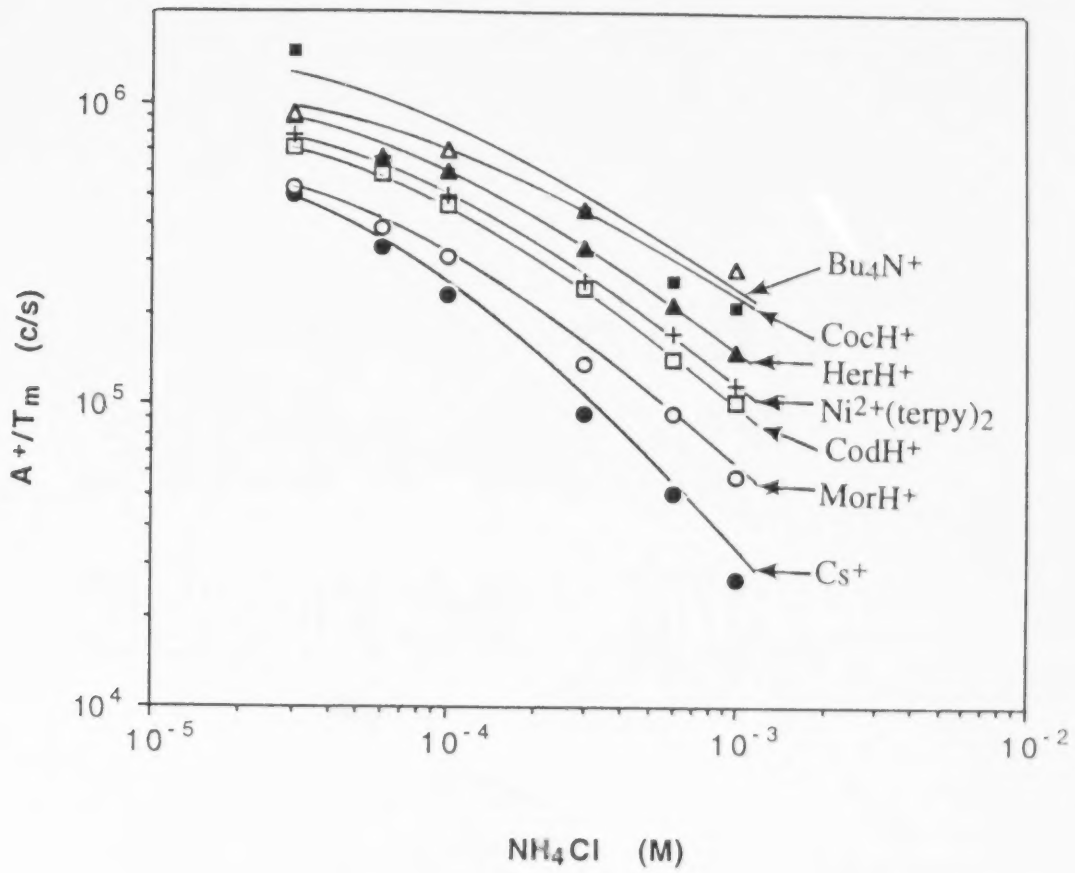

Figure 3-7 Ion intensities of A^+ (10^{-5} M) and with increasing concentration of B^+ (NH_4^+). Solid line curves are intensities of A^+ calculated with equation 3-4 and coefficients k from Table 3-1. ■ Bu_4N^+, Δ $CocH^+$, ▲ $HerH^+$, + $Ni^{2+}(Terpy)_2$, ❑ $CodH^+$, ○ $MorH^+$, ● Cs^+.

Table 3-1. Experimentally determined Ratios of Coefficients k[a]

Ion	m/z	T_m	k[c]	k[d]	ion	m/z	T_m	k[d]
Cs^+	133	0.6	1	1	Et_4N^+	130	0.72	(3)[g]
Li^+	e	e	–	1.6	Pr_4N^+	186	0.38	(5)[g]
Na^+	23	0.75	–	1.6	Pen_4N^+	298	0.064	(16)[g]
K^+	39	0.90	–	1.0	$C_7NH_3^+$	115	0.83	8
NH_4^+	18	0.72	1.1	1.3	$C_{11}NH_3^+$	171	0.46	8
$MorH^+$	286	0.08	2.1	(2.1)[f]				
$CodH^+$	300	0.065	3.8	(3.8)[f]				
$HerH^+$	370	0.019	5.5	–				
$CocH^+$	304	0.06	8.3	(8.3)[f]				
$Ni^{2+}(Tpy)_2$	262	0.72	4.9	–				
Bu_4N^+	242	0.17	9.1	8.0(16)[f]				

a. The coefficients are defined in equation 3-4. All coefficients relative to $k_{Cs^+} = 1$. These coefficients are valid only at concentrations above 10^{-5} M.

b. T_m mass dependent ion transmission, see Figure 3-3.

c. From plots using equation 3-6 where $B^+ = NH_4^+$, see Figures 3-5 to 3-7.

d. Coefficients k obtained with $[A^+] = [B^+]$ experiments at high concentrations. Numbers without brackets measured for $B^+ = Cs^+$. For numbers in brackets A^+ and B^+ are identified in footnotes.

e. For Li^+ also clusters $Li(H_2O)^+$, $Li(H_2O)_2^+$, $LiCH_3OH^+$, $LiCH_3OH.H_2O$ and $Li^+(CH_3OH)_2$ were observed. k given refers to total intensity of all Li^+ ions corrected for respective transmission.

f. Coefficients based k values for $MorH^+$, $CodH^+$ and $CocH^+$ as in left

column. Ratios from plots Figure 3-10: on $Bu_4N^+/CocH^+ = 2$, $Bu_4N^+/CodH^+ = 5$, $Bu_4N^+/MorH^+ = 10$, lead to a high value for $Bu_4N^+ \approx 16$ when combined with above coefficients.

g. Coefficients based on ratios from Figure 3-11 and $Bu_4N^+ = 8$. These coefficients could be twice as high assuming that $Bu_4N = 16$, see footnote f.

consequence of the small orifice, 100 μm in diameter, which separates the atmospheric and vacuum region in the TAGA instrument.

It is clear from Figure 3-7 that the decrease of I_A is dependent on the nature of A. Thus Cs^+ experiences the largest decrease and $(Bu)_4N^+$ the smallest. At $[NH_4^+] = 10^{-3}$ M, the decrease of Cs^+ is 10 times larger than that for $(Bu)_4N^+$. The extent of decrease is dependent on the k_B / k_A ratio; the bigger the ratio, the bigger the decrease of analyte ion intensity, thus $k_B / k_A = 1.1$ for Cs^+ and 0.1 for $(Bu)_4N^+$, see Table 3-1.

Instead of working with the k_A / k_B ratios it is convenient to assign an arbitrary value to one of the constants and then evaluate the other relative to that value. We have assigned a normalization value k = 1 for Cs^+. The resulting other normalized values are given in Table 3-1.

A^+ and B^+ in equation 3-4 can be interchanged and it is of interest to examine the validity of the equation for B different from NH_4^+.

On the basis of equation 3-1 one expects that replacing NH_4^+ ($k \approx 1$) with potassium, K^+ ($k \approx 1$), will lead to decreases in I_A^+ with increase of [B] which are very close to those observed for $B^+ = NH_4^+$. The plots shown in Figure 3-8 for $A^+ = Cs^+$, $B^+ = K^+$ and $A^+ = Cs^+$, $B^+ = NH_4^+$ exhibit a nearly identical decrease of A^+ in agreement with the near equal k values for NH_4^+ and K^+.

A more interesting case is the replacement of NH_4^+ with an ion such as Bu_4N^+ with much larger k ($k \approx 10$). In this case a much larger decrease of the A^+ intensity with increasing concentration of $[Bu_4N^+]$ is predicted by equation 3-4. Experiments where $A = MorH^+$, shown in Figure 3-9, demonstrate that this prediction is upheld. At the highest concentration of $[B] = 10^{-3}$ M, the $MorH^+$ intensity with $B = Bu_4N^+$ is close to 50 times smaller than that with $B = NH_4^+$.

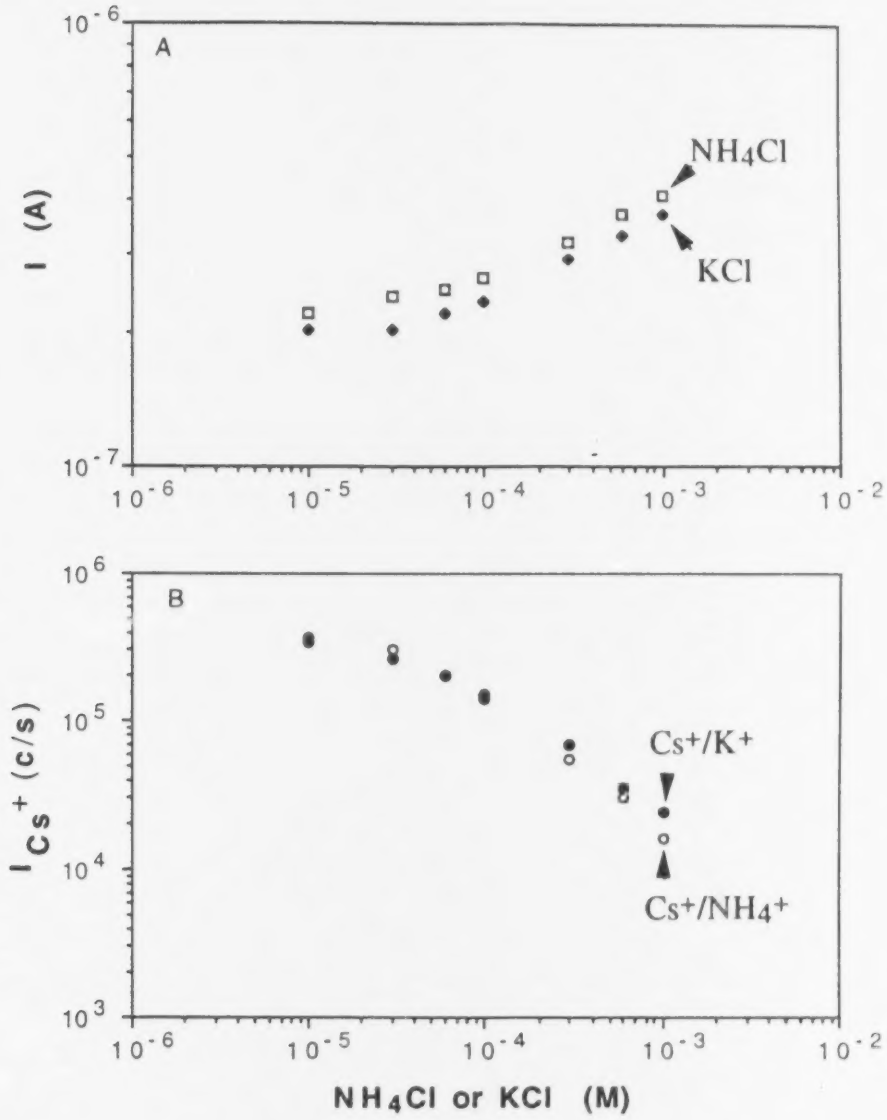

Figure 3-8 (A) Capillary current I. (B) Ion intensity for Cs^+ when $[Cs^+] = 10^{-5}$ M and $[B^+] = [NH_4^+]$ is increased ○, or $[B^+] = K^+$ is increased ● in separate experiments. Ions K^+ and NH_4^+ which have close to same coefficient k, Table 3-1, have the same effect in decreasing ion intensity of Cs^+.

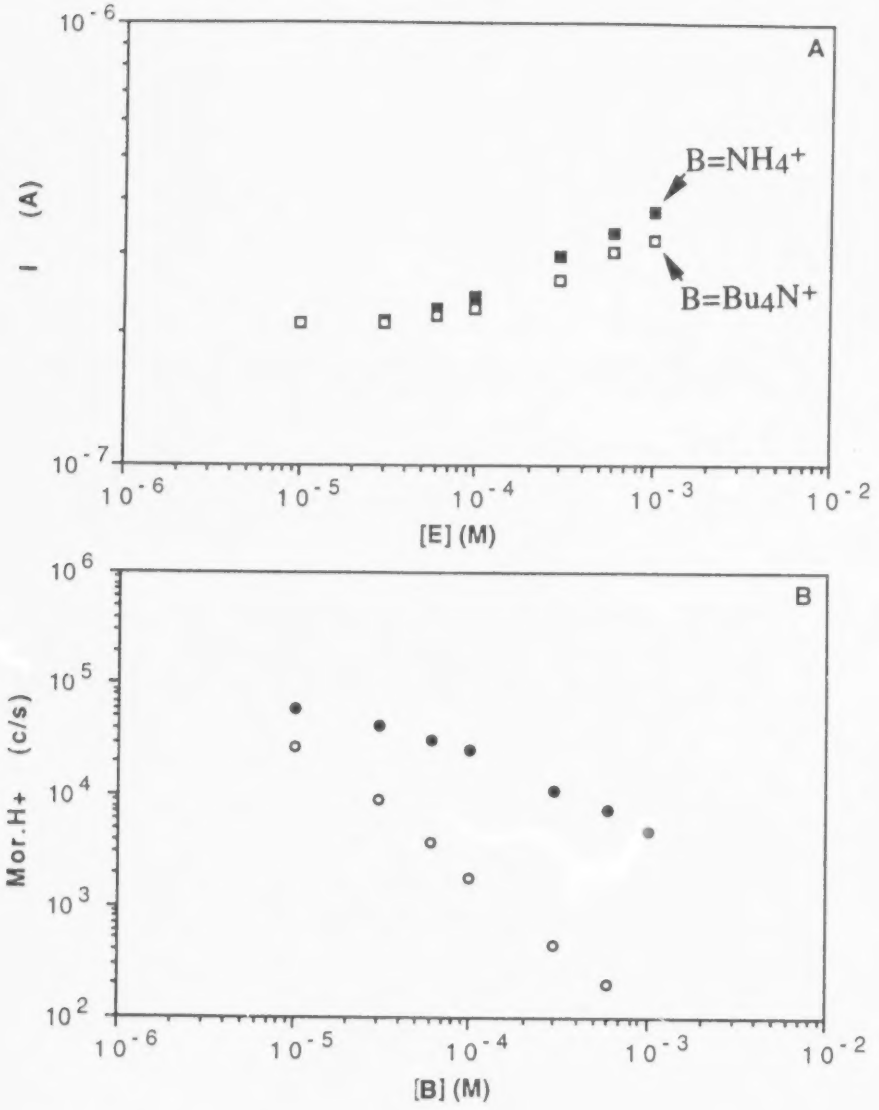

Figure 3-9 (A) Capillary current I. (B) Ion intensity for MorH+ when [MorH+] = 10^{-5} M and [B+] = [NH_4^+] is increased ●, or [Bu_4N^+] is increased ○, in separate experiments. Data show that B+ = Bu_4N^+ with high, k = 9, coefficient leads to much higher suppression of MorH+ intensity than B+=NH_4^+ whose k = 1.

The results in Figure 3-8 and 3-9 illustrate that by choosing buffer cations with low sensitivity coefficients, k, one can minimize the adverse effect of the buffer on the sensitivity of the analyte. This effect was also observed on codeine, heroin and cocaine.

b. Experiments where concentration is increased and [A] = [B]

An alternative method of evaluating the k_A / k_B ratio is to use the I_A / I_B ratio whose concentration dependence predicted by equation 3-4 is given by

$$\frac{I_A}{I_B} = \frac{k_A[A]}{k_B[B]} \qquad (3\text{-}7)$$

Shown in Figures 3-10 to 3-12 are results where the concentrations of two electrolytes AX and BY, are kept equal [AX] = [BY] and increased from 10^{-8} to 10^{-3} M.

For the logarithmic plots shown, a constant ratio I_A/I_B corresponds to a constant distance: $\log I_A - \log I_B$. Because [A] = [B], a constant k_A/k_B requires a constant vertical distance in the intensity plots. This is observed at high concentrations $C > 10^{-5}$ M. At low concentrations, the two logI curves exhibit a different behavior which is considered in subsequent sections. The k_A/k_B ratio obtained from the high concentration region are given in Table 3-1. The coefficients are expressed relative to $k_{Cs} = 1$.

A comparison of the k values given in Table 3-1 obtained from the plots, Figures 3-5 to 3-8 and the $[A^+] = [B^+]$ results in Figures 3-10 to 3-12, shows that the data are in fair agreement and indicate the same trends. Differences between the two sets of data are to be expected. The

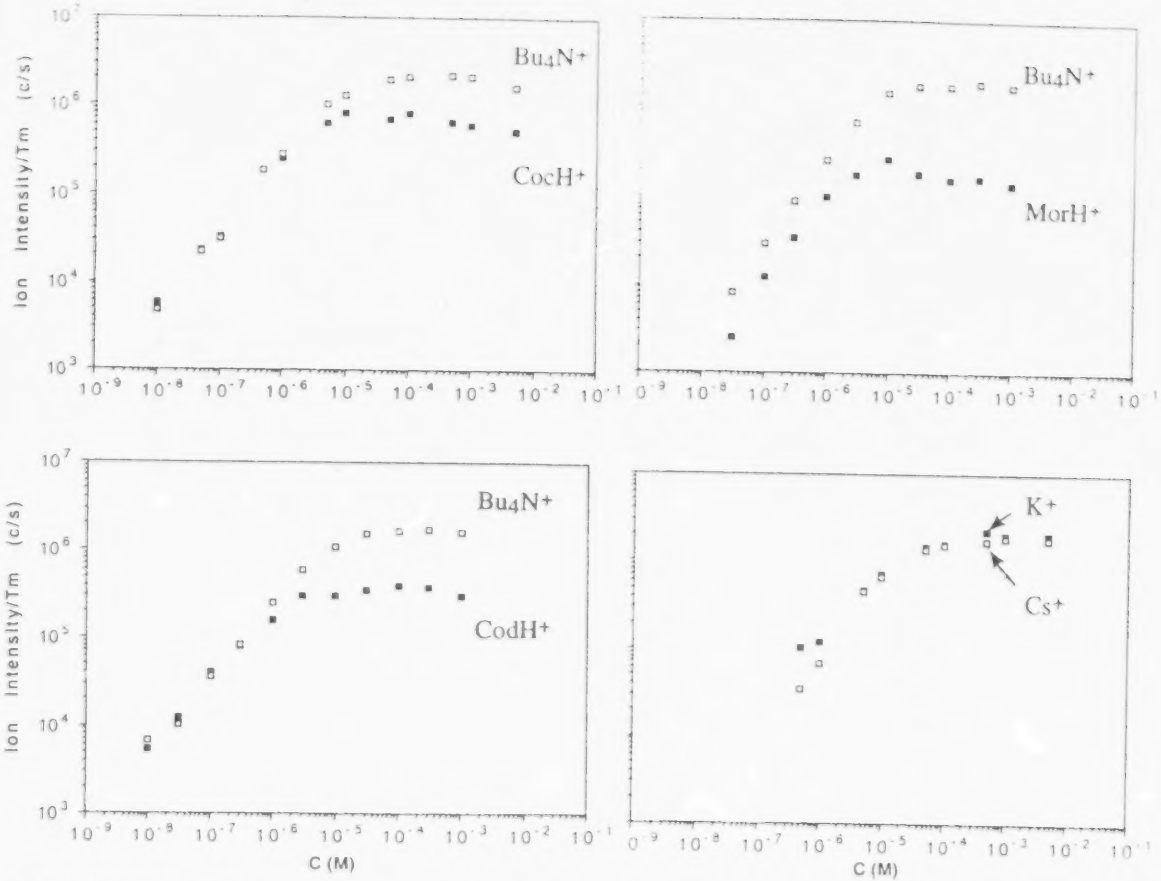

Figure 3-10 Ion intensities observed in experiment where $[A^+] = [B^+]$ is increased from 10^{-8} to 10^{-2} M. I_A/I_B ratio is different at high and at low concentrations and this means that significance of k_A/k_B ratio is different at high and low concentrations.

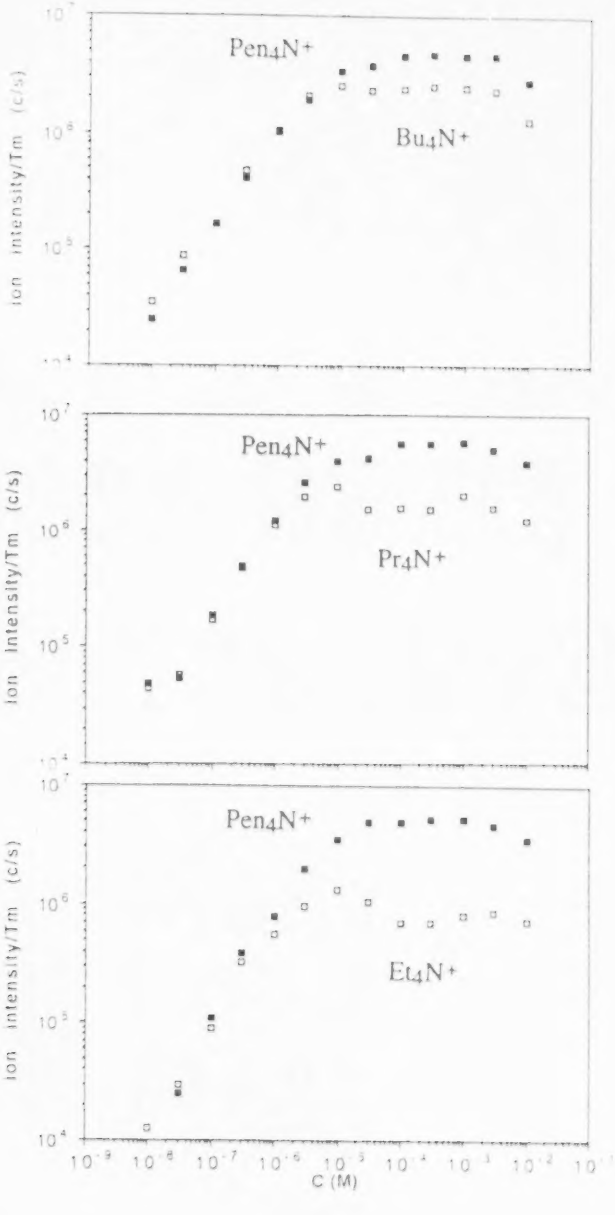

Figure 3-11 Ion intensities observed in experiment where $[A^+] = [B^+]$ is increased from 10^{-8} to 10^{-2} M. I_A/I_B ratio is different at high and at low concentrations and this means that significance of k_A/k_B ratio is different at high and low concentrations.

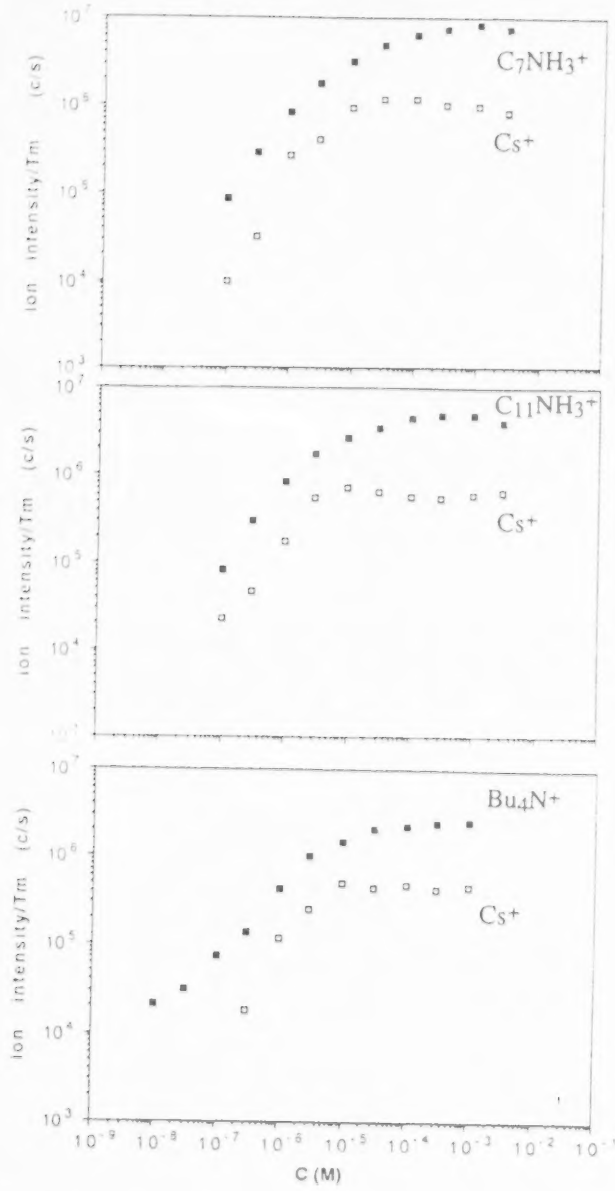

Figure 3-12 Ion intensities observed in experiments where $[A^+] = [B^+]$. In Figures 3-10 and 3-11, the intensity ratio approaches $I_A/I_B \approx 1$ at low concentrations. In present figure $I_A > I_B$ even at low concentrations.

plots, Figure 3-3 and 3-5 to 3-8, were obtained for $[A^+] = 10^{-5}$ M. This is a concentration that is at the low edge of the high concentration region. Therefore, these data are partly affected by phenomena which become important in the low concentration region, see next section.

The coefficients in Table 3-1 have their lowest values, $k \approx 1$, for the alkali and NH_4^+ cations. The tertiary ammonium ions, $MorH^+$ to $CocH^+$, have intermediate values and the quaternary ammonium ions like Bu_4N^+ have high values. The highest value $k \approx 16$ is observed for Pen_4N^+. An examination of the relationship between the structure and properties of the cations and their observed k values will be given in a later section.

II. Behavior when electrolytes are at low concentration, $<10^{-5}$ M. Indication for depletion of ions with a high coefficient k and for surface activity effects.

The low concentration region 10^{-8}-10^{-5} M of the equal concentration plots [A] = [B], see Figures 3-10 to 3-12 exhibits very different behavior from the high concentration region 10^{-5}-10^{-3} M discussed in the preceding section. There are two important differences: (a) The ion intensities I_A and I_B experience a large decrease as [A] = [B] is decreased below 10^{-5} M; (b) The ratio $I_A : I_B$ gradually decreases and becomes close to unity, Figures 3-10 to 3-11, as the concentration is decreased much below 10^{-5} M.

The cause for the decrease of the intensities I_A and I_B, as [A] = [B] are decreased, was explained in Chapter 2. Due to the presence of an electrolyte impurity in the pure methanol used which is equivalent to 1.3×10^{-5} M NH_4Cl or NaCl = C, see Experimental, we have actually a three component system where the dominant electrolyte is the impurity

electrolyte C whose concentration is constant. Therefore as [A] and [B] are decreased below 10^{-5} M, the presence of C becomes more and more important and since the C ions compete in the conversion process to gas phase ions, they lead to a decrease in the observed I_A and I_B. This type of behavior is analogous to that observed in section Ia and is in accord with equation 3-4 which can be extended in order to include a third electrolyte

$$I_A = \frac{k_A [A]}{k_A [A] + k_B [B] + k_C [C]} \, pf \, I \qquad (3\text{-}8)$$

Under conditions where [C] >> [A] = [B] equation 3-8 reduces to

$$I_A = \frac{k_A [A]}{k_C [C]} \, pf \, I \qquad (3\text{-}9)$$

and since pf, I and k_C [C] are constant, I_A becomes proportional to [A]. This equation predicts a linear region with a slope ≈1 for the logarithmic plots in the low [A] = [B] regions and such a region is observed in Figures 3-10 and 3-11. However, equation 3-9 and the ratio of I_A / I_B derived from it

$$I_A / I_B = \frac{k_A [A]}{k_B [B]} = \frac{k_A}{k_B} \qquad \text{when } [A] = [B] \qquad (3\text{-}10)$$

can not be valid because it predicts that $I_A \neq I_B$ since in general $k_A \neq k_B$, yet the observation is that the two ion currents become the same at low concentrations, see Figures 3-10 and 3-11.

The reasons for the failure of the equations are explored in the next section. It is shown there that the unipolar (+) ions on the surface of the droplets from which ion evaporation is assumed to occur (11) dominate over the charge paired electrolyte ions in the bulk of the droplet. Under

these conditions of no resupply of the surface by ions from the bulk, a depletion of the surface ions A^+ with the higher ion evaporation coefficient, k_A, occurs which reduces the ratio, I_A / I_B, of the gas phase ion products.

The ion intensities I_A and I_B where $B^+ = Cs^+$ shown in Figure 3-12, do not become close to equal at very low concentrations. The ions A^+ can be expected to be surface active while Cs^+ is not. Under conditions where the surface ion population exceeds the bulk of droplet ion population, surface enrichment of A^+ due to surface activity will be especially important in leading to higher intensities I_A. As shown in section IIIf, it is probably differences in surface activities that lead to the observation that $k_A > k_B$ at low concentrations.

A somewhat simpler situation, where the same effects can be expected, occurs in experiments where there is only one added electrolyte AX, apart from the constant concentration impurity electrolyte C. In a series of experiments the concentration [AX] was varied over a wide range. Results from such experiments are shown in Figure 3-13 where AX = MorHCl, CodHCl, HerHCl, CocHCl and CsCl. The experimental points at low [A] show considerable scatter. This is unavoidable since absolute intensities I_A are difficult to reproduce exactly in separate electrospray experiments. Also shown in the figure are calculated I_A obtained with equation 3-4. The required parameters k_A, k_B, were taken from the data in Table 3-1 which were obtained from the linearized plots, equation 3-6, involving the same analyte A and the electrolyte, $B = NH_4^+$. Because the impurity C in methanol is mostly NH_4^+X and Na^+X and since the coefficients, k, for NH_4^+ and Na^+ are expected to be very similar, the k from Table 3-1 for $B = NH_4^+$ should be suitable. The current I required

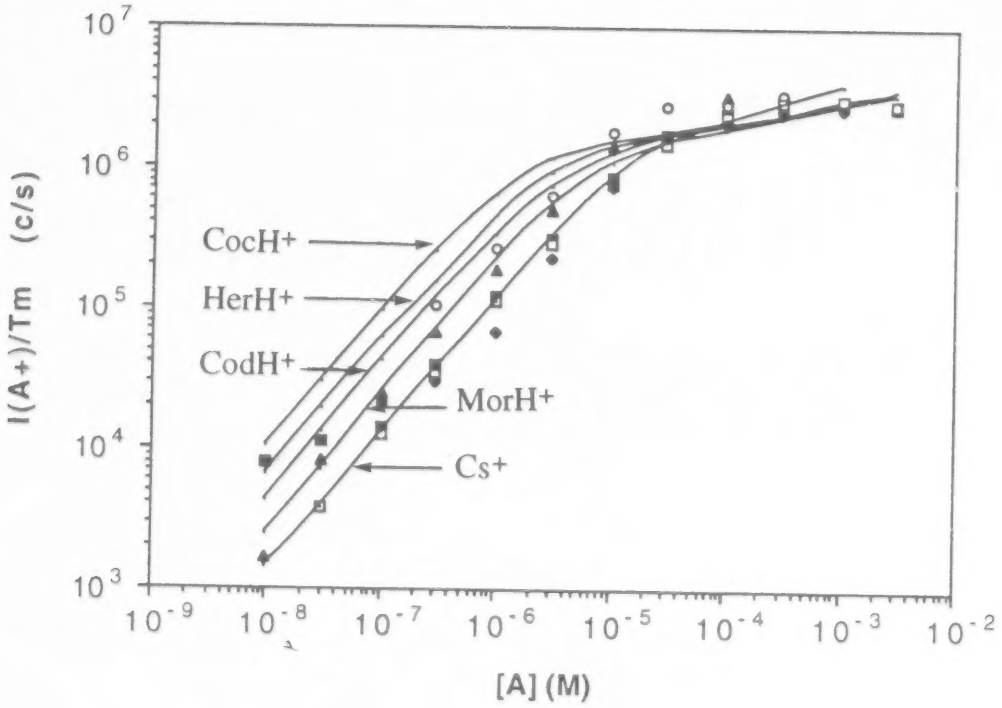

Figure 3-13 Observed ion intensities from separate experiments where [A+] is increased from 10^{-8} to 10^{-2} M. Solid lines are predicted intensities of A+ evaluated with equation 3-4 and coefficients in Table 3-1. Although no B is added, electrolyte impurity in the methanol used must be taken into account. ❑ MorH+, ■ CodH+, ○ HerH+, ▲ CocH+, ◆ Cs+.

for the evaluation of I_A, see equation 3-4, was measured in each experiment. It should be noted that I is constant for [A] 10^{-8}-10^{-6} M for all A since in this region C is the dominant electrolyte. Furthermore, I increases very slowly as [A] surpasses 10^{-5} M and is essentially independent of the nature of A, see equation 3-1 and Figure 3-5a.

The calculated curves in Figure 3-13 show clearly the predicted order of I_A dependent on the magnitude of k_A, Table 3-1, which is $CocH^+ > HerH^+ > CodH^+ > MorH^+ > Cs^+$. Despite the scatter in the experimental data it is very clear that the experimental data do not obey the predicted order and are much more compatible with nearly equal I_A currents at low $[A^+]$. This result is in agreement with the observations presented in Figures 3-10 and 3-11 which involved the simultaneous presence of two analytes [A] = [B] and the failure of equation 3-4 in the present case must be due to the causes already indicated for Figures 3-10 to 3-12.

III. Physical background and significance of coefficients k and equation 3-4

In this section we will examine phenomena concerning the mechanism of gas phase ion production by electrospray and their relationship to the present experimental findings and the significance of equation 3-4.

a. Properties of the Iribarne ion evaporation equation

It will here be assumed that the mechanism of ion evaporation from small highly charged droplets proposed by Iribarne and Thomson (11, 12) is at least qualitatively correct. After an examination of the properties of

this equation, it will be shown that equation 3-4 can be derived from the Iribarne theory and that the coefficients k of equation 3-4 obtained at high concentrations should correspond to the (relative) ion evaporation rate constants of the Iribarne equation, when ions of similar surface activities are involved.

The ion evaporation rate constants of the Iribarne equation

$$k_I = (kT/h)\, e^{-\Delta G^{\neq}/RT} \qquad (3\text{-}11)$$

are based on Transition State Theory and $\Delta G^{\neq}$ stands for the free energy of the transition state where an ion solvent molecule cluster $M^+(Sl)_m$ leaves a small charged droplet. A basic assumption of the Iribarne treatment is that the transition complex occurs late, i.e. at a state where the ion cluster $M^+(Sl)_m$ is fully free of the droplet and at some distance x_m from it. The advantage of this assumption is that the free energy of this state can be evaluated with a closed classical expression:

$$\Delta G^{\neq} = \left(\frac{Ne^2}{4\pi\varepsilon_0(R+x_m)} - \frac{e^2}{16\pi\varepsilon_0 x_m}\right) - \left(\Delta G^{\circ}_{sol} + \frac{Ne^2}{4\pi\varepsilon_0(R-d)}\right) \qquad (3\text{-}12)$$

The terms in the first bracket give the energy of the transition state while the terms in the second bracket, give the energy of the initial state, see Figure 3-14. The zero level for both states is the charged drop and the ion cluster at infinite distance. The first term expresses the electrostatic potential energy due to the repulsion between the ion cluster and the charged droplet which has N elementary charges. The second term expresses the potential due to attraction between the charge of the ion and the polarizable drop. This term is approximated by the electrostatic attraction due to the image force. The third term represents the solvation

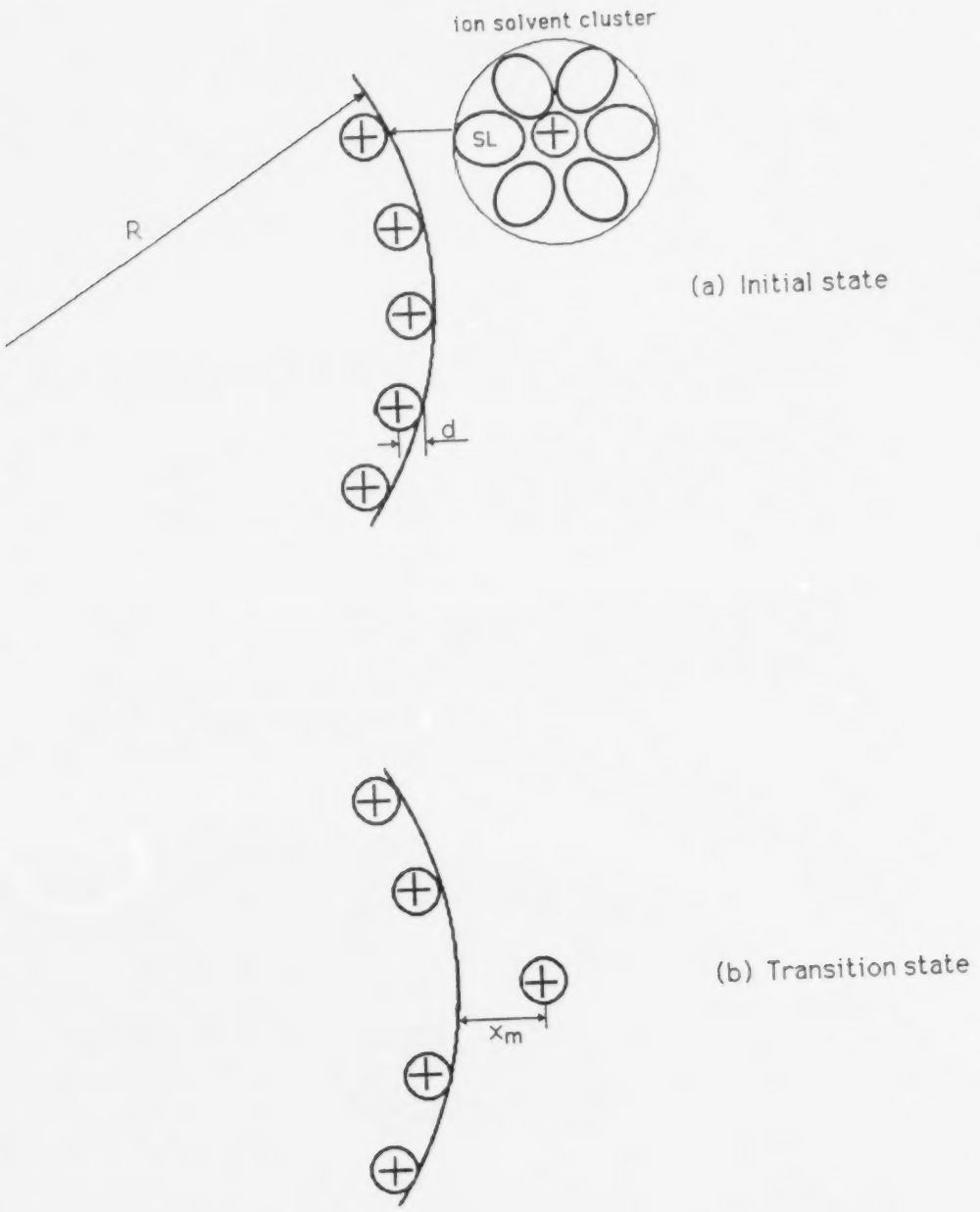

Figure 3-14 Schematic representation of initial state (a) and transition state (b) proposed by Iribarne and Thomson (11). Evaporating ion leaves as a cluster $M^+(Sl)_m$ where Sl are solvent molecules.

energy of the ion cluster $M^+(Sl)_m$ in the neutral drop, while the last term corrects for the fact that the drop is not neutral but has N elementary charges. Thus, $Ne^2 / 4 \pi\varepsilon_0 (R - d)$ corresponds to the electrostatic repulsion energy required to bring the cluster from infinity to a distance d inside the drop, where the ΔG°_{sol} is released.

$\Delta G^{\neq}$ can be obtained by treating the distance x as parameter and finding the value x_m for which $\Delta G^{\neq}$ is maximum. Iribarne and Thomson (11) provide a very useful figure that gives the charge of the droplet N and the radius R for $\Delta G^{\neq}$ = 9 kcal/mol, which leads to the rate constant k = 10^6 s^{-1} at T = 298, see equation 3-11. Iribarne reasoned that ion evaporation would become important only after k_I reaches such large values corresponding to μs lifetimes for ion evaporation. Two curves for, ΔG°_{sol} = –56 kcal/mol and ΔG°_{sol} = –64 kcal/mol were shown.

An additional illustration of results obtained with the Iribarne equation is given in Figure 3-15. The change of $\Delta G^{\neq}$ and k_I for constant ΔG°_{sol} (= –57 kcal/mol) and N (= 70) with the droplet radius treated as a parameter is shown in Figure 3-15a. These results illustrate the extremely rapid change of k_I with R. Thus, for a change from R = 100 Å to 70 Å, k_I increases from 3×10^{-3} s^{-1} to 1.4×10^{13} s^{-1}, i.e. by 16 orders of magnitude! This very strong dependence on the radius of the droplet supports Iribarne's decision to assume that ion evaporation for a given charge N will be completely unimportant relative to Rayleigh fission for conditions where the Rayleigh fission radius R_R is larger than the radius R_I that leads to ion evaporation with $k_I = 10^6$ s^{-1}. Iribarne showed that the ion evaporation condition, $R_I > R_R$, occurs when the droplets become very small, R = 80 Å and N ≈ 70 as typical values.

The results given in Figure 3-15b illustrate the change of $\Delta G^{\neq}$ and k_I

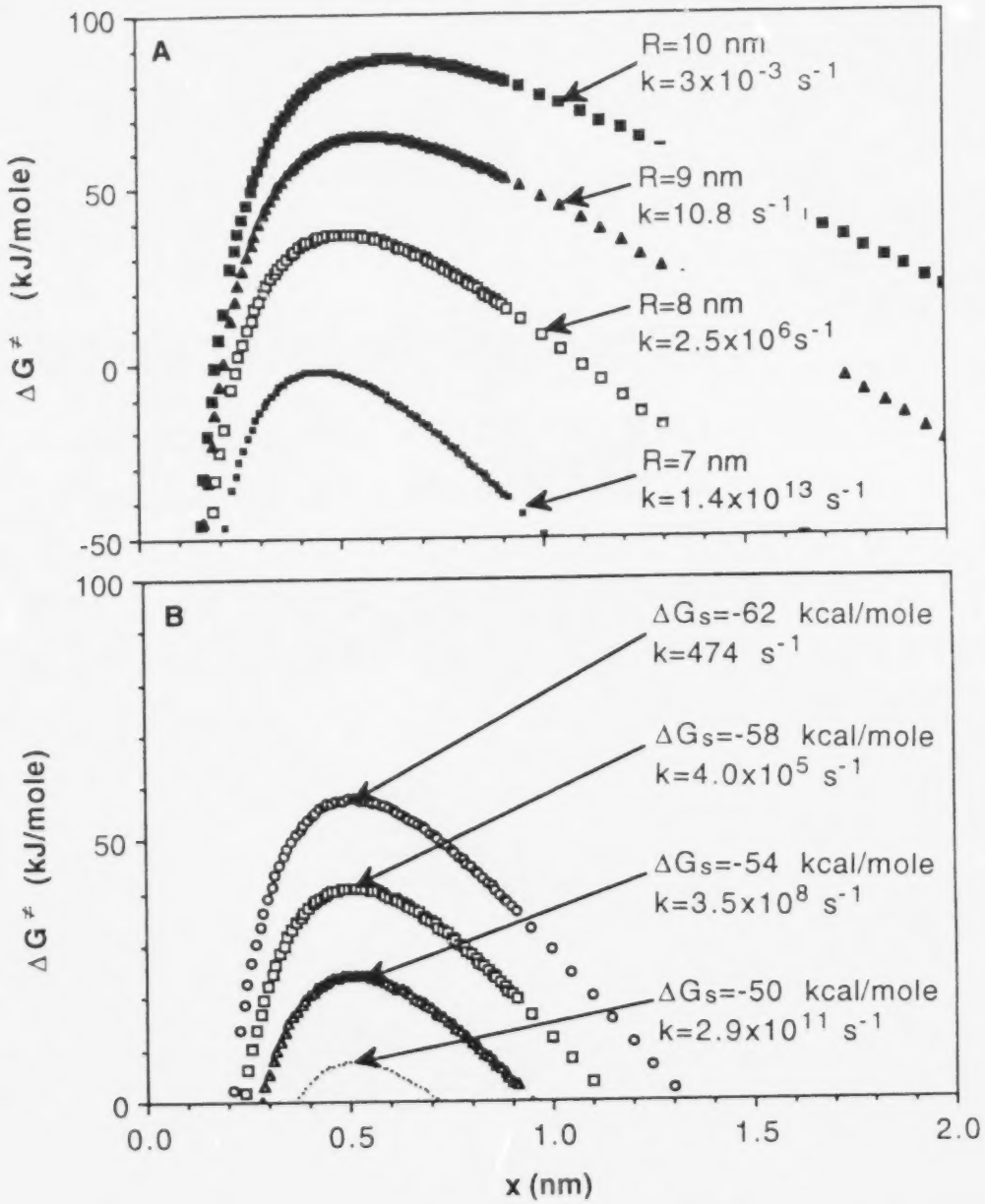

Figure 3-15 Free energy as a function of distance x of $M^+(Sl)_m$ from surface of drop predicted by equation 3-12. N = 70, d = 3.85 Å. (a) R is used as parameter and ΔG°_{sol} = –57 kcal/mol. (b) ΔG°_{sol} is used as parameter for R = 80 Å. Values of k_I obtained at ΔG°_{sol} are given beside each curve.

for constant N and d with ΔG°_{sol} as a variable parameter. It is interesting to note that the distance x_m which corresponds to the transition state remains essentially constant for different ΔG°_{sol}. An examination of equation 3-12 shows that for a constant x_m and constant d, the difference between $\Delta G^{\neq}$ for two given ΔG°_{sol} is given by

$$\Delta\Delta G^{\neq} = \Delta G^{\neq}_{a}(A^{+}) - \Delta G^{\neq}_{b}(B^{+}) = -\left(\Delta G^{o}_{sol}(A^{+}) - \Delta G^{o}_{sol}(B^{+})\right)$$

which means that the rate constant ratio for two different ion species which have different ion cluster solvation energies and the same value for d will be given by

$$\frac{k_{I(A^{+})}}{k_{I(B^{+})}} = e^{\left(\Delta G^{\circ}_{sol}(A^{+}) - \Delta G^{\circ}_{sol}(B^{+})\right)/RT} \qquad (3\text{-}13)$$

The plot shown in Figure 3-16a illustrates the change of $\Delta G^{\neq}_{I}$ and k_I when d is changed at constant R, N, ΔG°_{sol}. It is seen that also in this case x_m remains essentially constant for substantial changes of d. The independence of x_m on d and ΔG°_{sol} allows an important simplification.

$$k_{I,A}(N, R, d_A, \Delta G^{\circ}_{solA}) \approx k(R, N)\, k'_A(d_A, \Delta G^{\circ}_{solA}) \qquad (3\text{-}14a)$$

$$\approx k(R, N)\, k''_A(\Delta G^{\circ}_{solA})\, k'''_A(d) \qquad (3\text{-}14b)$$

Thus, when more than one ion species is present in a droplet, k_I for each species can be factored into a function k(N, R), which represents the droplet state R, N and is independent of the nature of the ion and a constant $k'_A(d_A, \Delta G^{\circ}_{sol}(A))$which expresses the nature of the ion A and is independent of R, N. Furthermore $k'_A(d_A, \Delta G^{\circ}_{solA})$ can also be factored into two independent functions as shown in equation 3-14b. Equation 3-14 is based

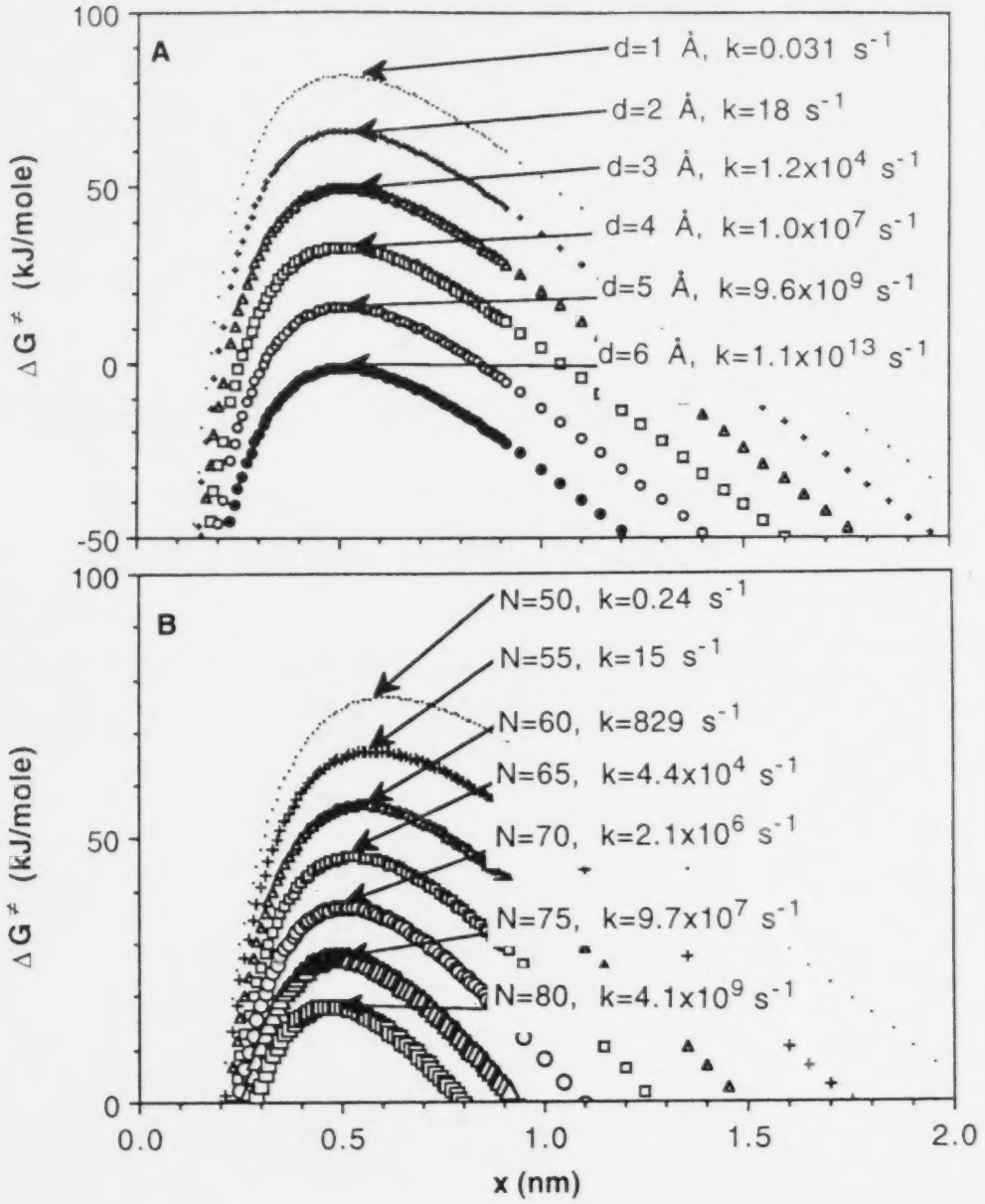

Figure 3-16 Same as Figure 3-15, (a) d is used as parameter while: R = 80 Å, N = 70, ΔG°_{sol} = –57 kcal/mol. (b) N is used as parameter while R = 80 Å, d = 3.85 Å, ΔG°_{sol} = –57 kcal/mol.

on the results given in Figures 3-15 and 3-16 and is valid for the range of parameters covered in these figures.

b. Ion evaporation and solvent evaporation

The results presented in Figure 3-16b illustrate the rapid decrease of the ion evaporation rate constant k_I with decrease of droplet charges N. Thus, the actual ion evaporation rates from a droplet will be controlled also by the solvent evaporation rate which will shrink the droplet and increase k_I. The droplets undergoing ion evaporation are very small and for the volatile solvents normally used, such as methanol and water, the evaporation rate will be under surface, rather than diffusion control (13). This means that the evaporation rate will be controlled by the rate of liquid to vapor conversion at the surface, since the recondensation of evaporated solvent molecules is negligible relative to the surface evaporation.

The rate of evaporation under surface control is expressed by equation 3-15 (13)

$$\frac{dm}{dt} = -\alpha \frac{\bar{v}}{4} 4\pi R^2 \frac{pM}{RgT} \qquad (3\text{-}15)$$

where the dm / dt is the rate of change of droplet mass, $\bar{v}$ is the average thermal velocity of the vapor molecules of the solvent, R is the radius of the droplet, p° is the vapor pressure of the solvent, M the molar mass of the solvent and R_g and T are the gas constant and temperature in K. α is the condensation coefficient equal to the fraction of solvent vapor molecules on collision with the droplet surface condense on the droplet. The value $\alpha = 0.04$ has been determined for water and ethanol (14). We make the assumption that the same value holds also for methanol.

Using the relationship between mass m, density ρ and volume of the

droplet, $m = 4/3\ \pi R^3\rho$, equation 3-15 can be recast in the form

$$\frac{dR}{dt} = -\frac{\alpha\bar{v}}{4\rho}\frac{p^{\circ}M}{R_gT} \qquad (3\text{-}16)$$

which on integration leads to a relationship between the radius R of the droplet and time t,

$$R = R_0 - \frac{\alpha\,\bar{v}\,p^{\circ}M}{4\,\rho\,R_gT}t \qquad (3\text{-}17a)$$

$$R = R_0 - 1.2 \times 10^{-3}\,t \qquad (3\text{-}17b)$$

where the numerical factor of equation 3-17b was evaluated for methanol ($p^{\circ} = 1.66 \times 10^4$ Pa, $M = 0.032$ kg/mol, $\bar{v} = 4.5 \times 10^2$ m/s, $\rho = 0.8 \times 10^3$ kg/m^3, $\alpha = 0.04$, $T = 298$ K). The radius of the droplet at $t = 0$ is R_0.

The temperature T to be used with equation 3-17a is the temperature of the droplet. The temperature of the droplet will be lower than the temperature of the surrounding air because of cooling of the droplet by solvent evaporation. The temperature difference can be evaluated as follows:

$$\frac{\text{collisions/s of drop with gas}}{\text{evaporating solvent molecules/s}} \approx \frac{p_g}{\alpha\,p^{\circ}} \approx 160 \text{ for MeOH}$$

$$p^{o}(\text{MeOH}) \approx 120 \text{ torr} \qquad \alpha = 0.04$$

Heat gained from ambient gas = Heat lost by evaporation

$$p_g\,c_p\,\Delta T = \alpha\,p^{o}\,\Delta H_{vap}(\text{MeOH})$$

where c_p is the molar heat capacity of air and ΔH_{vap}(MeOH) is the molar enthalpy of vaporization of methanol.

$$\Delta T = \frac{\alpha\, p^{\circ}\, \Delta H_{vap}}{p_g\, c_p} = \frac{9000}{7 \times 160} = 8^{\circ}C$$

$c_{p\ air} = 7/2\ R \approx 7$ cal/K mole $\qquad \Delta H_{vap}(MeOH) = 9000$ cal/mole

The assumption was made that every gas molecule assumes the temperature of the droplet on collision (i.e. accommodation coefficient = 1). A smaller accommodation coefficient will lead to higher ΔT. In the subsequent discussion, the temperature of the droplets is assumed to be T = 298 K. This means that the ambient gas in the electrospray was at ~ 298+8 = 316 K.

According to equation 3-17, the time required for the complete evaporation of an R_0 = 100 Å ($\approx 10^{-10}$ m) methanol droplet is t = 8 μs, which is very short relative to the time scale of droplet residence between the ES capillary and the orifice to the mass spectrometer. Thus, once a droplet of Iribarne ion evaporation size is formed, it will evaporate and lead to gas phase ions within a few microseconds.

On the basis of equation 3-17 and the Iribarne rate constants it is possible to evaluate the gas phase ion yield as a function of time. The results shown in Figure 3-17a give the residual charge N on a droplet with N = 70, R_0 = 80 Å at t = 0. The data were obtained with the equation

$$\frac{\Delta N}{\Delta t} = -k_I N \qquad (3\text{-}18)$$

by selecting $\Delta N = -1$. The Δt_1, required for evaporation of the first charge is obtained with the $k_I(N_0, R_0)$ as predicted by the Iribarne equations, see Figures 3-15 and 3-16. Using Δt_1 the new radius for time t = Δt_1 was evaluated with equation 3-17. A new rate constant k_I was evaluated with the Iribarne equation using $N_1 = N_0 - 1$ and the new $R = R_1$.

Then Δt_2 was evaluated with equation 3-18. Proceding in this manner, the data shown in Figure 3-17 were obtained. The change of N with t is shown in Figure 3-17A, the change of R in 3-17B and the change of k with time in 3-17C. The results in Figure 3-17A indicate that about half of the charge N is converted to gas phase ions in ~1 μs. The solvent evaporation during the ion evaporation was found important as shown in Figure 3-17B.

c. Competitive ion evaporation

When the total charge N is due to two different ion species A and B, equation 3-18 can be reformulated with inclusion of equation 3-14a as shown

$$-\frac{\Delta N_A}{\Delta t} = k_{I_A} N \frac{N_A}{N} = k'_{(R,N)} k'_A N \frac{N_A}{N_A + N_B} \qquad (3\text{-}19)$$

where $N_A / (N_A + N_B)$ is the ratio of ions A to total ions N at the surface of the drop. There will be situations where the ratio $N_A / (N_A + N_B)$ will not change (significantly) during the ion evaporation process. This will be the case when the number of ions n_A and n_B in the bulk of the droplet, due to electrolyte in the droplets is very much higher than the number $N_A + N_B$ of ions at the surface. In this case the surface ratio $N_A : N_B$ will be maintained by rapid exchange with ions from the bulk. An approximate time constant for the exchange rate, time for diffusion of the ion to the surface, is given by

$$t_{Diff} \approx \frac{R^2}{\pi D} \qquad (3\text{-}20)$$

where D is the diffusion coefficient of the ion in the given solvent (23).

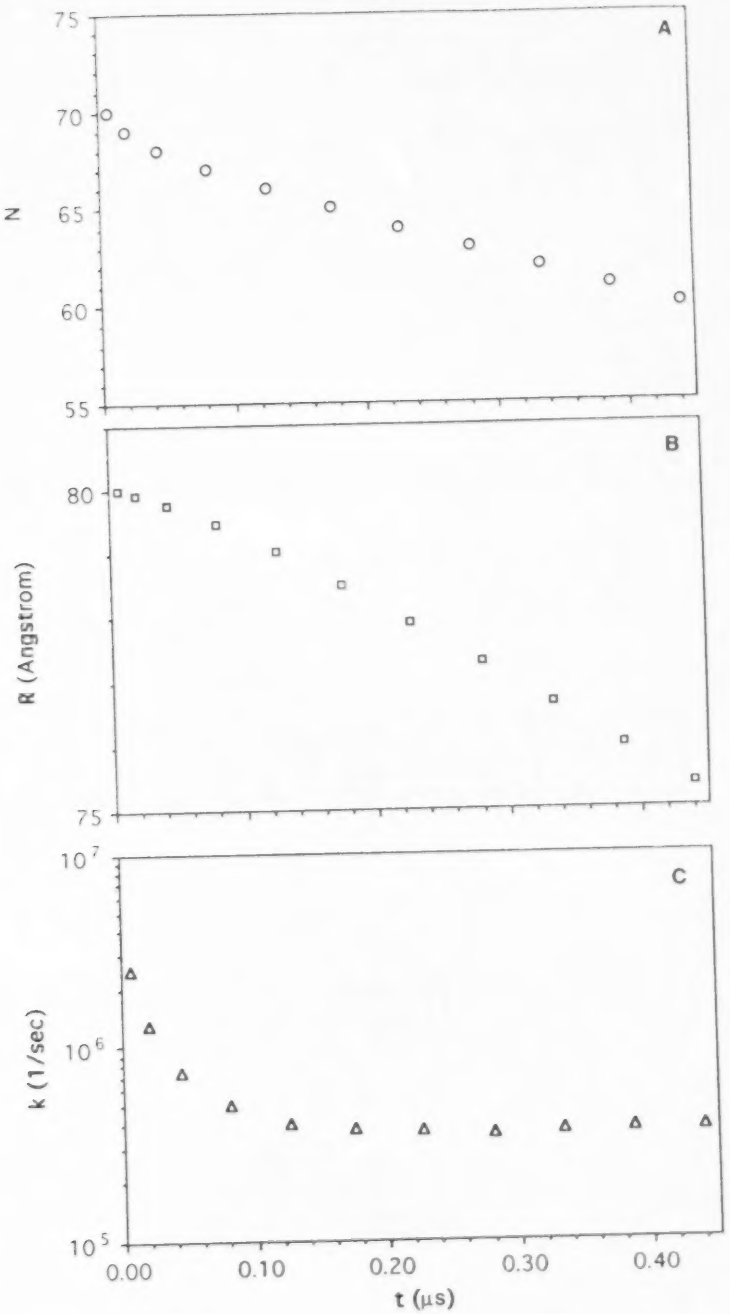

Figure 3-17 (a) Change of number of charges N with time for a droplet undergoing Iribarne ion evaporation and solvent evaporation. Evaluated with equation 3-17 and 3-18 for ΔG°_{sol} = –57 kcal/mol, d = 3.85 Å. Temperature of droplet is T=298 K. Ambient air temperature is ~316 K. (b) Change of radius of same droplet with time, evaluated with equation 317. (c) Change of rate constant, k, with time corresponding to the change of N and R.

Choosing R = 500 Å and a typical diffusion coefficient for alkali ions in water, D = 1.7 x 10^{-5} cm^2 s^{-1} one obtains $t_{Diff} \approx 1$ µs. The time required for smaller droplets will be much shorter. Furthermore, in methanol, the diffusion coefficients are higher. Since the Iribarne droplets are very small, diffusion will be able to maintain an approximately constant N_A / N_B ratio on a submicrosecond time scale. When the ions are not surface active, this ratio will be equal to the concentration ratio c_A / c_B in the bulk of the droplet.

For the condition where, $N_A / (N_A + N_B) = c_A / (c_A + c_B)$, remains constant during the Iribarne droplet evaporation one can obtain the total number of gas phase ions A^+ produced by the droplet by integration of equation 3-19 over a time, t_f, required for the complete evaporation of all ions from the droplet.

$$N_{A,g} = k'_A \frac{c_A}{c_A + c_B} \int_0^{t_f} k(R,N)\, N\, dt \qquad (3\text{-}21)$$

The value of the integral is the same for all ion species since k(R,N) is independent of the chemical nature of the evaporating ions. Assuming that the gas phase ion current $I_{A,g}$ is proportional to $N_{A,g}$ the number of gas phase ions produced in the average drop, the ratio of gas phase ion currents can be obtained with application of equation 3-21 and since the integrals cancel

$$\frac{I_{A,g}}{I_{A,g} + I_{B,g}} = \frac{k'_A c_A}{k'_A c_A + k'_B c_B} \qquad (3\text{-}22)$$

Furthermore, assuming that the droplet bulk ratio c_A / c_B equals the solution concentration ratio,

$$N_A / N_B = c_A / c_B = [A]/[B] \qquad (3\text{-}23)$$

one obtains,

$$\frac{I_{A,g}}{I_{A,g} + I_{B,g}} = \frac{k'_A[A]}{k'_A[A] + k'_B[B]} \qquad (3\text{-}24)$$

Equation 3-24 represents a derivation of the empirical equation 3-4 on the basis of the Iribarne relationships. It will be shown in the next section that the condition in equation 3-23 is valid only at higher electrolyte concentrations, i.e. $[A] = [B] > 5 \times 10^{-5}$ M. For that concentration range, and in the absence of differential surface activity between A and B, the experimental coefficient ratio k_A/k_B is predicted to be identical with the ion evaporation rate constants ratio k'_A/k'_B.

d. Charge, radius, concentration and time dependence for droplets evolving towards gas phase ion emission

An estimate of the charge Q, and radius R of the droplets from the time when they are produced by the electrospray to the point where they become gas phase ion emitters is possible on the basis of recent experimental observations of ES droplets by E.J. Davis et al. (16) and Gomez and Tang (17, 18). Reliable data are available only for droplets larger than 1 μm. The assumptions listed below are closely based on the work of Gomez and Tang (18).

(1) The initial droplets produced by ES, particularly at low flow rates, ~3 μL/minute, have a narrow size and charge per droplet distribution. Typical values are $R_0 = 1.5$ μm and $Q_0 = 8 \times 10^{-15}$C. This Q_0 corresponds to a charge that is ~40% of the charge, Q_R, required to lead to the Rayleigh droplet stability limit (19).

$$Q_R^2 = 64\,\pi^2\,\varepsilon_0\,\gamma R_R^3 \qquad (3\text{-}25a)$$

$$Q_R^2 = 1.25 \times 10^{-10}\,R_R^3 \qquad (3\text{-}25b)$$

where $\varepsilon_0 = 8.8 \times 10^{-12}$ is the permittivity of vacuum and γ is the surface tension. For methanol, $\gamma = 0.0226$ N/m^2, equation 3-25a leads to equation 3-25b.

(2) The droplets shrink due to solvent evaporation while the charge Q remains constant. Due to the decrease of radius, the droplets undergo fission when the radius has shrunk to a value for which Q equals 80% of Q_R. The parent droplet loses 15% of its charge and 2% of its mass producing several smaller, offspring droplets each of which has a radius which is ~10% of the radius of the parent droplet.

(3) Process (2) repeats itself when the parent droplet after radius shrinkage due to evaporation, is again at 80% of the Rayleigh stability limit. In this manner a succession of droplet emissions occur from the gradually shrinking parent droplet.

The graph given in Figure 3-18 illustrates the described process. The change of the parent droplet radius R with time was evaluated with equation 3-17. The radius of the parent droplet $R_0 = 1.5$ μm is small enough such that equation 3-17, which is based on surface controlled evaporation, should apply for solvents as volatile as methanol (13). The change of mass and thus also radius of the parent droplet when fission occurs is very small and therefore just perceptible for the data shown in Figure 3-18. The time required for the first fission is ~460 μs and at this point $R_1 = 0.94$ μm. A second fission occurs after a shorter time ~70 μs and further fissions occur at similar but gradually shortening intervals.

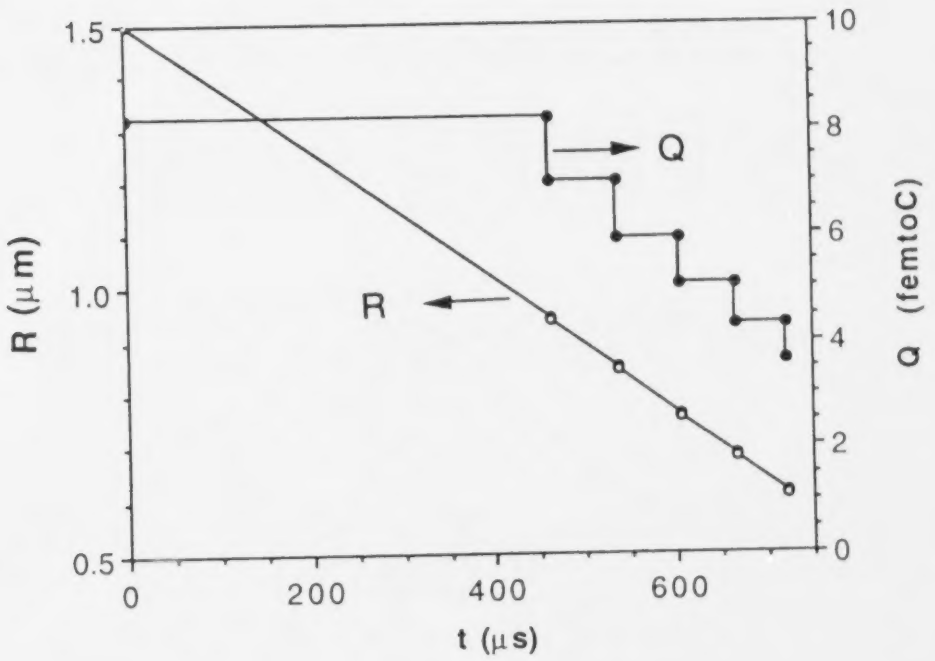

Figure 3-18 Changes of radius R and charge Q with time of a droplet produced by electrospray which undergoes successive not symmetric droplet fission, see Figure 3-19. Fission occurs at 80% of the Rayleigh limit and parent drop loses 2% of its mass and 15% of its charge.

The number n_s and the charge Q_s of the offspring droplets created from the parent droplet at a fission event can be estimated from the assumptions (2); i.e. the parent droplet uses 2% of its mass, 15% of its charge and the offspring droplet radius R_s is 10% of the parent radius R.

Applying conservation of mass where ρ is the density of the solvent

$$n_s \frac{4}{3} \pi R_s^3 \rho = 0.02 \frac{4}{3} \pi R^3 \rho$$

and since $R_s = 0.1\ R$ one obtains

$$n_s \approx 0.02 / (0.1)^3 = 20$$

The charge Q_s of each droplet is given by,

$$Q_s = \frac{0.15}{n_s} Q = 7.5 \times 10^{-3} Q$$

Thus, the first generation of ~20 droplets will have

$$Q_s = 6.12 \times 10^{-17} C \qquad R_s = 0.094\ \mu m$$

$$N_s = 382 \text{ elementary charges.}$$

The Q_s and R_s of second, third, etc. litter of droplets can be evaluated in an analogous manner. In order to obtain an estimate of the process and properties leading to an "average" ion emitting droplet, we select a third generation of offsprings. At this point the parent droplet charge Q is down to 75% of the initial charge Q_0, see Figure 3-18 and 19. We do not select the litter where $Q = 0.5\ Q_0$ because it is likely that a full conversion of the parent droplet to offspring droplets does not occur due to time or other limitations.

The evolution of a third litter offspring droplet to an Iribarne ion emitting droplet is represented schematically in Figure 3-19. The

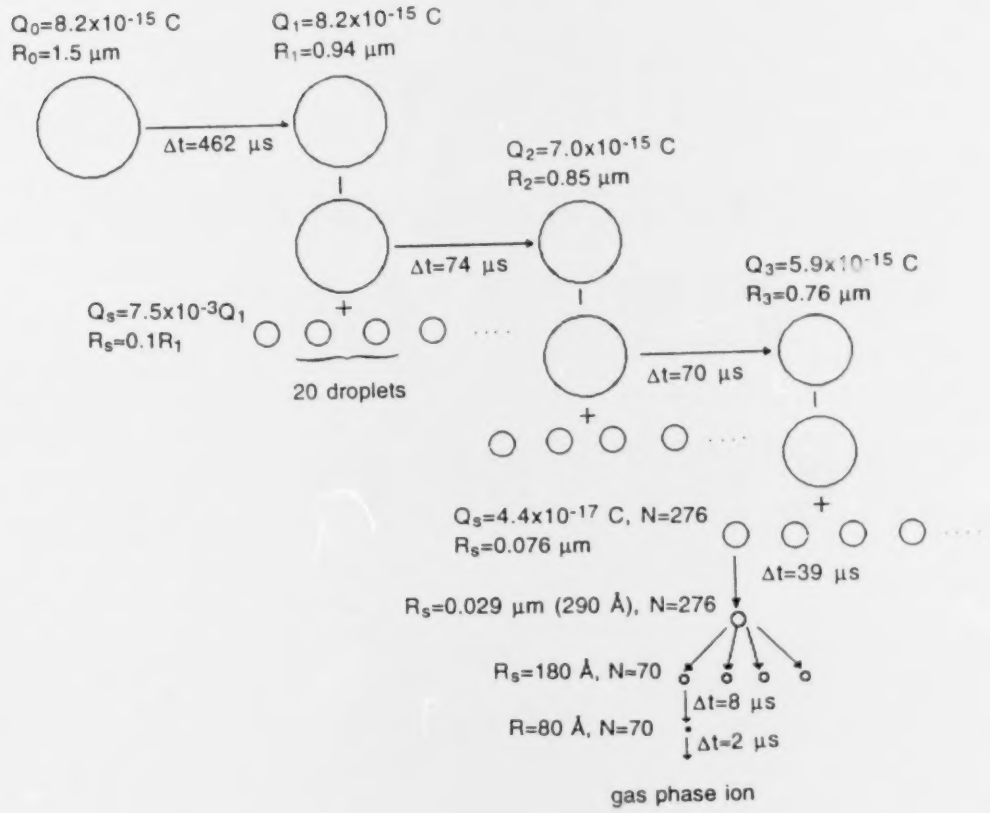

Figure 3-19 Changes of radius R, charge Q with time in droplet fissions of parent droplet and offspring droplets. Required time for solvent evaporation evaluated with equation 3-17. Time for ion evaporation involving Iribarne size droplet, from Figure 3-17.

offspring droplet shrinks through evaporation until it reaches 80% of the Rayleigh limit. At this point its radius is 290 Å and its charge consists of N = 276 elementary charges. The fission of such a small droplet has not been observed. For convenience we assume that the droplet splits into 4 droplets each carrying 1/4 of the charge. Then, each droplet shrinks through evaporation until it reaches the radius typically required for Iribarne ion emission, R = 80 Å for N = 70.

e. Prediction of the decrease of observed k_A/k_B ratio at low concentrations due to depletion of ions with higher evaporation coefficient

An estimate of the concentration of the electrolyte ions in the bulk of the Iribarne droplet can be obtained by assuming that the bulk electrolyte concentration in the offsprings at each fission is equal to the bulk concentration in the parent. With this assumption, because the volume shrinks due to evaporation, the concentration will have increased by the product of the volume ratios: $\left(V_i / V_f\right)_1 \times \left(V_i / V_f\right)_2 \times \left(V_i / V_f\right)_3 = F$ which can be evaluated from the data in Figure 3-18. The result is F = 7.6 x 17.3 x 11 = 1450. This means that the concentration in the Iribarne droplet has increased by a factor of ~1450 relative to the initial concentration. From the known volume V_I of the Iribarne droplet, Figure 3-18, one can evaluate n_M, the total number of paired electrolyte ions in the bulk of the droplet.

$$n_M = [M^+] F V_I L = 1.86 \times 10^6 [M^+] \qquad (3\text{-}26)$$

where $[M^+]$ is the concentration of the electrolyte ions in the electrosprayed solution and L is Avogadros constant. The numerical factor given is for

the droplet of 80 Å radius and $[M^+]$ in moles/L.

For $[M^+] = 10^{-5}$ mol/L the calculated number of bulk ions is $n_M = 18$. Since the number of ions on the surface is N = 70, the solution in the bulk has few additional ions to supply. It is easy to see that at such low initial concentrations the experimentally determined ratio k_A / k_B will be smaller than the theoretical ratio k'_A / k'_B (when $k'_A > k'_B$). To illustrate, we assume [A] = [B] and $k'_A / k'_B \approx \infty$. There will be 35 A and 35 B ions on the surface and 9 A and 9 B ion in the bulk. After all 44 surface and bulk A ions are used up due to the rapid evaporation of A also, 70-44 = 26 B ions will evaporate leading to $k_A / k_B = 44/26 = 1.7$ which is much smaller than $k'_A / k'_B = \infty$. Repeating the same type of calculation for different [A] = [B] concentrations one obtains the results shown in Figure 3-20, see curve $k'_A / k'_B = \infty$. It is possible to evaluate the change of the k_A / k_B with concentration also for other k'_A / k'_B ratios. Two such curves for the ratio 5 and 2 are also shown in Figure 3-20.

These data were evaluated with equation 3-19 using a numerical procedure similar to that used for the data shown in Figure 3-17. Δt for $\Delta N_A = -1$ was obtained for each step, then $\Delta N_A / \Delta N_B$ was evaluated for each Δt. The total A ions available for conversion to gas phase ions was taken as the sum of A ions on surface plus the A ions in the bulk of the droplet. For a complete numerical account see Appendix I.

Representative curves obtained with the experimentally obtained k_A / k_B, see Figures 3-10 and 3-11, are also shown in Figure 3-20. There is considerable correlation between the shapes of the experimental and calculated curves. It should be noted that the data shown in Figures 3-10 an 3-11 involve ions A^+ and B^+ whose surface activities are expected to be similar.

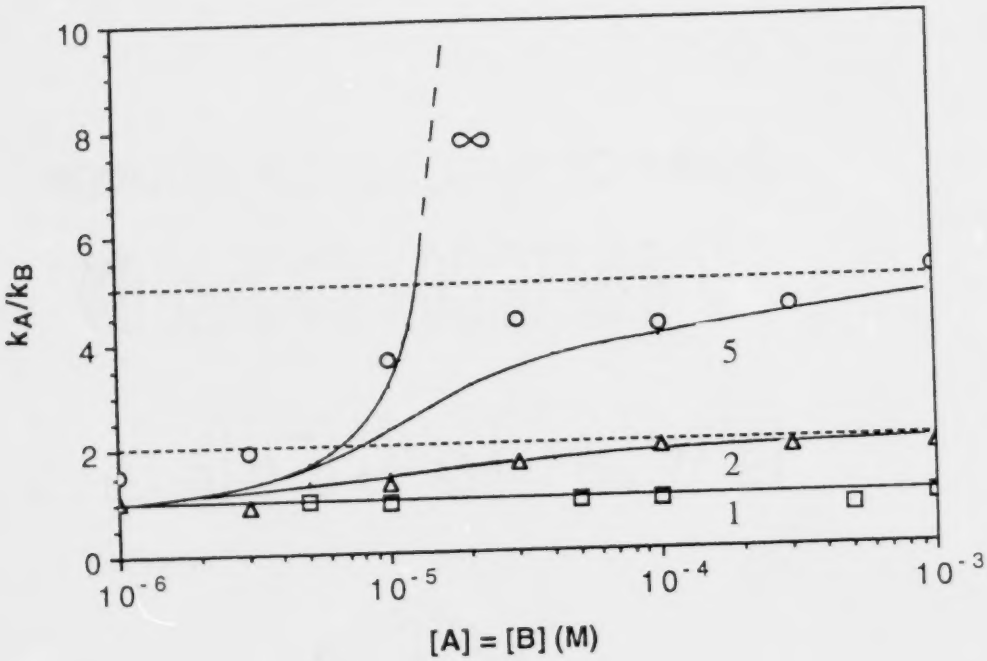

Figure 3-20 Predicted k_A/k_B ratio expected for a given ion evaporation ratio k'_A / k'_B in function of concentration $[A^+] = [B^+]$. Solid curves are predicted k_A / k_B for k'_A / k'_B values shown besides curves. Experimental points are from Figures 3-13 and 3-14 and give k_A / k_B for: $Bu_4N^+/CodH^+$ ○; Pen_4N^+/Bu_4N^+ △; Cs^+/K^+ □. Agreement between predicted and observed k_A/k_B supports proposed depletion mechanism. In calculated curves, A^+ and B^+ are assumed to have equal surface activity.

The agreement between predicted and experimental k_A / k_B in Figure 3-20 supports the depletion of faster evaporating ion interpretation proposed above.

f. Predictions of k'_A / k'_B from theory and experiment:

It was shown in the preceding section that the experimental k_A / k_B ratios obtained at high concentrations should correspond to rate constant k'_A / k'_B ratios for the evaporation of ions from the droplets when A and B have no surface activity or the same surface activity.

For the alkali cations, M^+ (Li^+, Na^+, K^+, Cs^+), the experimental results in Table 3-1 provide $k_A / k_B \approx k'_A / k'_B \approx 1$ which means that the $\Delta G^{\neq}$ for ion evaporation of these ions should be approximately equal, i.e.

$$\Delta\Delta G^{\neq} \approx 0 \qquad \text{for } Li^+ - Cs^+ \tag{3-27}$$

The characteristics of the ions enter $\Delta G^{\neq}$ through the solvation energy ΔG°_{sol} $(M^+(Sl)_m)$ and the distance d, see equations 3-12, 3-14 and Figure 3-15. Assuming that the changes of d are small, equation 3-13 and 3-27 require that the $\Delta\Delta G^{\circ}_{sol}$ be small or close to zero.

$$\Delta\Delta G^{\circ}_{sol}\ (M^+(Sl)_m) \approx 0 \tag{3-28}$$

Fairly accurate estimates for $\Delta\Delta G^{\circ}_{sol}$ $(M^+(H_2O)_m)$, in a small aqueous droplet, can be obtained from the thermodynamic cycle:

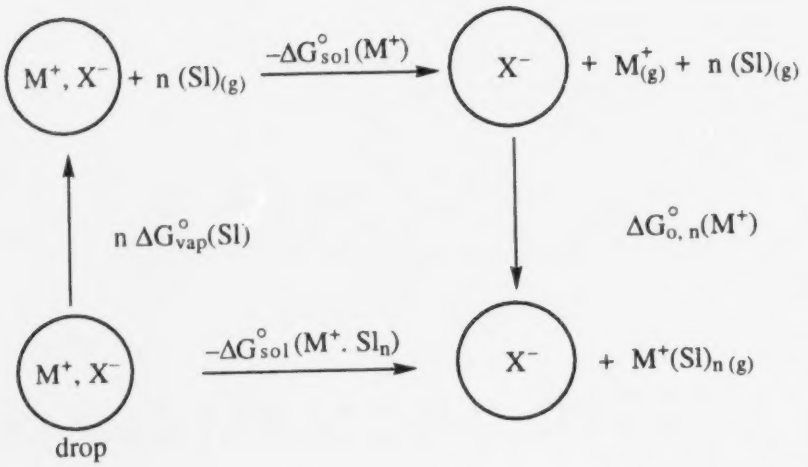

The cycle leads to:

$$\Delta G^{\circ}_{sol}(M^{+}.Sl_n) = \Delta G^{\circ}_{sol}(M^{+}) - \Delta G^{\circ}_{o,n}(M^{+}) - n\Delta G^{\circ}_{vap}(Sl) \qquad (3\text{-}29)$$

Data for the solvation of the naked ion, $\Delta G^{\circ}_{sol}(M^{+})$, and for the solvation of the naked ion by n solvent molecules, $\Delta G^{\circ}_{o,n}(M^{+})$, are available in the literature for Sl = H_2O, (20, 24). The vaporization energy of Sl = water from a small droplet, $\Delta G^{\circ}_{vap}(Sl)$, is also available for water. These data are summarized in Table 3-2. It is found that, $-\Delta G^{\circ}_{sol}(M^{+}(Sl)_n)$ decreases as n increases. A minimum is reached for n = m. These minimum values are given in Table 3-2. With these data we can evaluate the $\Delta\Delta G^{\circ}_{sol}$.

The $\Delta\Delta G^{\circ}_{sol}$ for Na^{+} and Cs^{+} is seen to be:

$$-(\Delta G^{\circ}_{sol}(Na^{+}(H_2O)_m) - \Delta G^{\circ}_{sol}(Cs^{+}(H_2O)_m)) \approx 2.5 \text{ kcal/mole}$$

This difference is very much smaller than the difference of the solvation energy of the naked ions Na^{+} and Cs^{+} which is ~30 kcal/mol. However the $\Delta\Delta G^{\circ}_{sol}$ is still not equal to zero, see equation 3-28. It is not clear whether the disagreement is due to errors in the literature data used (20, 21). The

Table 3-2. Solvation Free Energies in Water

M^+	Li^+	Na^+	K^+	Cs^+	NH_4^+	$(CH_3)_4N^+$	$(C_2H_5)_4N^+$
$-\Delta G^\circ_{sol}(M^+)$[a]	122	98.2	80.6	67.5	81[e]	(54)[f]	(49)[f]
$-\Delta G^\circ_{o,m}(M^+)$[b]	74.4	56.4	36.5	23.5	---	---	---
m[c]	7	7	6	5	---	---	---
$-\Delta G^\circ_{sol}(M^+(H_2O)_m)$[d]	61.2	56.5	55.8	54	55.6[e]	(52)[e]	(48)[f]
$-R_{Ion}$(hydrated)[g]	3.82	3.58	3.3	3.29	3.3	---	---

a. Values in kcal/mol from Desnoyer (20).

b. Values in kcal/mol from Džidić (21).

c. m is the number of H_2O molecules which lead to a minimum in $-\Delta G^\circ_{sol}(M^+(H_2O)_n)$.

d. Evaluated with equation 3-29 and $\Delta G^\circ_{vap}(H_2O)$= 1.95 kcal/mol, where $\Delta G^\circ_{vap}(H_2O) = RT\ln 760/p^\circ_R$ and p°_R is the vapor pressure of H_2O in torr over a droplet with radius R. p°_R was obtained from p°, the vapor pressure over a flat surface with equation $\ln(p^\circ_R/p^\circ) = 2\gamma M/R\rho R_g T$ where γ is the surface tension, M the molar weight and ρ the density of water. R_g is the gas constant (22). p° = 23.8 torr, p°_R = 28 torr at 298 K.

e. Estimate based on near equality: $\Delta G^\circ_{0,5}(K^+) = \Delta G^\circ_{0,4}(NH_4^+)$, Kebarle (23) and value for K^+, see present table.

f. Rough estimates based on data from (23, 24).

g. Radii in Angstrom, from Conway (25)

literature data have expected errors in the ±3 kcal/mol range. Another problem is the use of water rather than methanol, for which the required supporting thermodynamic data are not available. However, the trend of higher $-\Delta G^{\circ}_{sol}(M^{+}(H_2O)_m)$ for the smaller ions in Table 3-2 is so consistent that a result of $\Delta\Delta G_{sol} = 0$ for all the alkali ions appears unlikely.

It is possible that differences in the parameter d might be also involved. d stands for the distance of the surface ion from the surface of the drop, see Figure 3-14. Iribarne assumed that this distance could be approximated by the radius of the ion plus the radius of one water molecule. This would mean that smaller d would have to be used for the smaller ions Li^{+}, Na^{+}. As evident from Figure 3-16a, this would lead to a correction in the wrong direction since smaller d lead to even lower k_I.

It can be argued that the d for the smaller ions should be larger and not smaller. Li^{+}, Na^{+} are much more strongly solvated. Therefore, the electric field that forces the ions towards the surface will not be able to push the more solvated ions as closely to the surface. More suitable for the values of d should be the ionic radii obtained from ion mobility experiments in solution, the so called Stokes or hydrated ion radii (Conway) (25). These radii decrease in the order $Li^{+} \rightarrow Cs^{+}$, see Table 3-2.

The $\Delta G^{\neq}$ for Na^{+} and Cs^{+} was evaluated with the Iribarne equation. using the $\Delta G^{\circ}_{sol}(M^{+}H_2O)_m)$ and d values given in Table 3-2 for a droplet with N = 70 charges and R = 80 Å. The result obtained was: $\Delta G^{\neq}(Na^{+})$ = 9 kcal/mol; $\Delta G^{\neq}(Cs^{+})$ = 7.7 kcal/mol at 298 K and $\Delta\Delta G^{\neq}$ = 1.3 kcal/mol. This value is not equal to zero as required but sufficiently close to be consistent with the Iribarne treatment.

The tetraalkyl ammonium ions (TA) have experimental k values which are much larger than those for the alkali cations, see Table 3-1. This is consistent with expectation on the basis of the Iribarne theory. The solvation energies of the naked TA ions, $-\Delta G^{\circ}_{sol}(TA)$, can be estimated from available literature data (23, 24) and are found to be very much smaller than those for the alkali cations, see Table 3-2. In fact the $-\Delta G^{\circ}_{sol}$ for the naked $(C_5H_{11})_4N^+$ is smaller than the solvation energies for the alkali ion clusters, $\Delta G^{\circ}_{sol}(M^+(Sl)_m)$. The cluster $(C_2H_5)_4N^+(H_2O)_m$ is expected to have an $m \approx 1$, so that $\Delta G^{\circ}_{sol}(C_2H_5)_4N^+) \approx \Delta G^{\circ}_{sol}((C_2H_5)_4N^+(H_2O)_m)$.

The low solvation energies for the TA ions given in Table 3-2 are in line with the observed high k values and with the order $Et_4N^+ < Pr_4N^+ < Bu_4N < Pen_4N$ of the experimental coefficients k in Table 3-1.

The structures of the alkaloids used in the present work are shown below:

Morphine

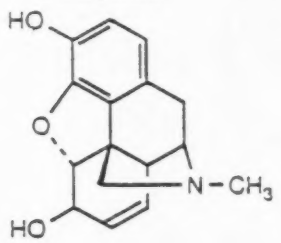

Codeine

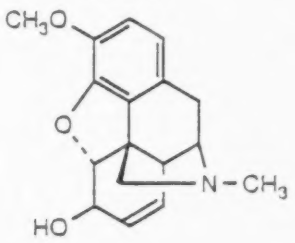

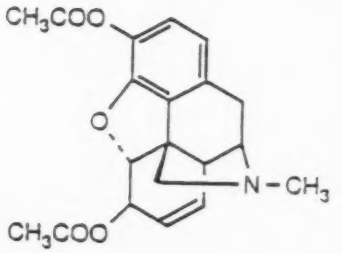

Heroin

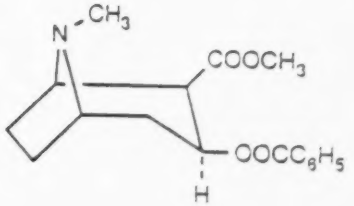

Cocaine

The experimental k values are: Morphine ~2, Codeine ~3.8, Heroin ~5.5, Cocaine ~8, see Table 3-1. Morphine, codeine and heroin are closely related. Morphine has two hydroxyl groups, codeine has one and heroin none. The hydroxyl groups, particularly in the presence of the positive charge on the nitrogen in the protonated compounds, will be somewhat acidic and therefore engage in stronger hydrogen bonding to the methanol or water solvent molecules (26). This will increase the solvation of the ion. Therefore, the observed order of k values for these three compounds follows the order of expected decreasing solvation and is in line with the ion evaporation theory. Although the cocaine structure is very different, this compound is also a tertiary amine. It is also devoid of hydroxyl groups and its high k value is consistent with expected relatively weak solvation.

g. Ion solvation and ion surface activity

It was shown in the preceding section that the magnitudes of experimentally observed coefficients k are, on the whole, consistent with the ion evaporation theory of Iribarne and Thomson. However, so far we have not taken into account the surface activity of the ions. Since surface active ions will have relatively higher concentrations on the surface than in the bulk of the droplet, it may be expected that the experimental k values for such ions will be found to be somewhat higher. Thus, the question may be asked: which is more important, surface activity or ion cluster solvation energies?

Unfortunately, due to the lack of accurate ion cluster solvation energies and of the parameters d, the k' values, see equation 3-14a, can not be predicted quantitatively with the Iribarne equations. Therefore, one has

to resort to qualitative comparisons and with these the difficulty arises that ion cluster solvation energies and surface activities are often closely correlated. Ions with low ion cluster solvation energies for which high k's are expected are generally also of high surface activity. For example, the solvation energies $-\Delta G^{\circ}_{sol}$ for the tetraalkylammonium ions decrease in the order: Me_4N^+, Et_4N^+, Pr_4N^+, see Table 3-2, leading to expected higher k' in that order, but the surface activities also increase in the same order (27).

The k values for the tetraalkylammonium ions are much higher than those for the alkali cations. The cluster solvation energies for these ions are lower than those for the alkali cations, see Table 3-2. However, the surface activities are also much higher.

Fortunately, the previous discussion of the phenomena involved suggests a solution for this dilemma. It was shown in section (e), that as the initial concentration C is decreased, one reaches the condition where the number of unipolar ions on the surface exceeds the number of charge paired ions in the bulk of the ion emitting droplet. This condition holds for $C < 10^{-5}$ M. At such concentrations, the observed gas phase ions reflect directly the surface population of the droplet. In a solution with [A] = [B], the observed k_A / k_B evaluated with equation 3-10 were found to approach the limit $k_A / k_B \approx 1$, for any expected value of the Iribarne constants, k'_A / k'_B, provided that the surface activity of A and B was expected to be equal, see Figure 3-20. The data given in this figure do not include compounds whose surface activities were expected to be very different.

Measured ion intensities I_A, I_B for pairs with expected large surface activity differences: Bu_4N^+/Cs^+, $C_7H_{15}NH_3^+/Cs^+$ and $C_{11}H_{23}NH_3^+/Cs^+$

were shown in Figure 3-12. In all three cases one finds that the observed intensities I_A, I_B do not come together at low concentrations, i.e. the ratio $I_A/I_B = k_A/k_B$ remains quite large, $k_A/k_B \geq 5$, even at the lowest concentrations.

We can conclude that the k_A/k_B ratios observed in the low concentration range $C < 10^{-5}$ M reflect surface activities while those observed in the high concentration range $C = 10^{-3}$-10^{-2} M reflect the ion evaporation constants k'_A / k'_B and also enrichments due to surface activity.

The enrichment of the droplet surface in the more surface active component probably occurs in the evaporation stages of the parent droplets between the Rayleigh instability explosions. As illustrated in Figure 3-18 these evaporation stages are relatively long $t \geq 50$ μs and this should allow the enrichment of the surface with surface active ions.

h. A possible alternative mechanism for gas phase ion formation

In the preceding discussion it was shown that the experimental results are consistent with the Iribarne ion evaporation theory when the surface ion population is corrected for enrichment with ion species which are surface active. However, possibly due to lack of accurate literature data, Table 3-2, a quantitative proof of the Iribarne equation 3-12 could not be obtained.

We consider the relatively narrow range of coefficients k, 1~16, Table 3-1 surprising from the standpoint of the Iribarne theory. A $\Delta G^{\neq}$ difference of only 5 kcal/mol, leads to a $k'_A / k'_B \approx 500$ at 298° K, see equation 3-11. Similarly, the observed selectivity due to surface activity seems too small, since the enrichments of surface active ions could be

expected to be much larger. From the standpoint of electrospray mass spectrometry, the relative lack of selectivity is an advantage. All types of ions are expected to be detectable with ESMS.

It is possible that the relative lack of selectivity is due to a gas phase ions production mechanism that is somewhat different from the Iribarne ion evaporation model as represented by equation 3-12. An alternative is suggested from an examination of the time required for the different processes leading to ion emission. A complex series of solvent evaporation and droplet fissions lasting hundreds of microseconds leads to the Iribarne size droplet. According to the model, ion emission then occurs and requires some 1 μs, see Figure 3-17. However, even if the Iribarne ion emission did not occur, the droplet itself will lose most of its solvent molecules, due to solvent evaporation, in only ~8 μs, see equation 3-17b. This time difference is not very large. Suppose that the Iribarne emission did not occur as predicted, solvent evaporation will then continue until a much more disorderly gas phase ion production occurs which may not follow, equation 3-12, of the model. For this type of ion emission, solvation energy differences, surface effects and the effect of temperature may have a much reduced importance relative to the functionalities predicted by equations 3-11 and 3-12.

One reason why equation 3-12 may not apply is the assumed "late" transition state which occurs after the ion cluster has "broken through" the surface of the droplet. An "early" transition state which occurs just as the cluster disrupts the surface may lead to a higher $\Delta G^{\neq}$. In such a case a higher electric field will be required, i.e. a smaller more highly charged droplet. One would expect a decreased functional dependence on parameters like ΔG°_{sol}. Rayleigh fissions will also remain competitive

down to a smaller radius. The small highly charged offsprings of such fissions may also lead to gas phase ions so rapidly that diffusion is not able to maintain a constant bulk to surface concentration ratio even for high, above 5 x 10^{-5} M, initial concentrations. In this case a resupply with bulk ions will not occur and a depletion effect similar to that observed at low concentrations will reduce the observed k_A/k_B ratios.

As far as the mechanism of gas phase ion formation is concerned, an alternative mechanism first proposed by Dole (28), i.e. single ion in droplet theory (SIDT), can also rationalize most experimental facts in ESMS. The SIDT postulates that the Rayleigh fission of charged droplet continues until the offspring droplet contains one excess ion, which leads to gas phase ion. This theory also expects the selectivity which result in different k_A/k_B ratios in ESMS. Since surface active ions will be enriched on the surface and be the favored charged carriers, they will be favored in the final very small offsprings which are close to the single ion in droplet state. Thus, selectivity for the SIDT is due to differential surface activity.

If the SIDT holds, ion depletion can also be expected at low concentration for two species A^+ and B^+ of very different surface activity because the surface increase on droplet formation is so large that there just are not enough A^+ ions to supply all the surface charges. Large increases of surface to volume occur not only in the initial formation of the droplet but also in the fission process.

Although the SIDT appears very attractive due to the recently observed not symmetric fission of the charged droplets (17, 18), the type of fission for droplets of sizes much below 1 μm is not known yet. Therefore, a clear choice between Ion Evaporation mechanism and SIDT can not be made at this time. One advantage of Ion Evaporation

mechanism over SIDT is that it provides an approach to the quantitative expectation of experimentally detected ion intensity. This is the reason that the experimental data in my research was mainly rationalized on the basis of ion evaporation mechanism.

3.4 Conclusions

(1) Equation 3-4 provides useful predictions, both in the low: 10^{-8} to 5×10^{-6} M, and in the high: 10^{-5} to 10^{-2} M, concentration range. However, the coefficients k have different significance in the two ranges. At low concentration k_A/k_B express relative surface activities of A^+ and B^+. When A^+ and B^+ have equal surface activity, $k_A/k_B = 1$. In this range the unipolar ions on the surface of the ion evaporating droplet dominate over the charge paired electrolyte ions in the drop. At high concentrations, k_A/k_B express the relative ion evaporation rates and relative surface activities.

(2) The relative values k_A/k_B obtained at high concentrations are consistent with predictions of the Iribarne theory. However, a confirmation of the quantitative predictions of the theory could not be obtained due to lack of required literature data. The observed range: 1-20, for the relative values of the coefficients, is smaller than could be expected on the basis of the Iribarne theory and this suggests that the functional dependence, equation 3-12, is not exact.

(3) Solvent evaporation leads to an estimated volume shrinkage which increases the initial concentration $[A^+]$, $[B^+]$ by a factor of ~1500 for change from ES produced drop to ion evaporating droplet.

(4) The formation of the ion evaporating droplets is preceded by a

long (hundreds of μs) and complex process of shrinkage by solvent evaporation and droplet fission. The ion evaporation stage is short - a few μs. Since the solvent evaporation rate is proportional to the vapor pressure of the solvent, equation 3-16, ES with less volatile solvents like water p° = 24 torr relative to methanol: p° = 125 torr at 25°C may lead to higher intensities I_A, I_B if operated above ambient temperature.

(5) The coefficients in Table 3-1 provide a guide to choice for cations in buffers which will lead to the smallest suppression of the intensity of the analyte ion.

(6) In cases where quantitative information is to be obtained by the addition of an internal standard to the solution, the internal standard B^+ should have the same surface activity and the same ion evaporation coefficient as the analyte A^+, as is the case for K^+/Cs^+, Figure 3-10 and Table 3-1. Only in this case will the signal of A^+ be proportional to B^+ over the full concentration range: 10^{-8}-10^{-2} M. In the low concentration range: 10^{-8} - 5 x 10^{-6}, proportionality is maintained even when this requirement is not met.

3.5 Appendix

Evaluation of depletion effect

The depletion of ions from a charged droplet may happen in the low concentration range when one ion species has higher ion evaporation rate constant k. The depletion effect can be evaluated with equations involved in the ion evaporation model.

Ion evaporation from a charged droplet is a first order reaction as described by equation 3-18

$$-\frac{\Delta N}{\Delta t} = k_I N \tag{3-18}$$

Taking a binary system, i.e., two major ions (A and B) in electrospray solution, as the simplest case for the study of depletion effect, one can write a rate law for each ion evaporation process.

$$-\frac{\Delta N_A}{\Delta t_A} = k_A N_A \tag{3-30a}$$

$$-\frac{\Delta N_B}{\Delta t_B} = k_B N_B \tag{3-30b}$$

where $-\Delta N_A/\Delta t_A$ and $-\Delta N_B/\Delta t_B$: rate of ion evaporation for ion A and ion B, respectively;

k_A and k_B: theoretical rate constant of ion A and ion B, respectively;

N_A and N_B: number of ion A and ion B on the surface of a charged droplet.

In equation 3-30, it is assumed that ion evaporation for each ion species is independent of other ions in the droplet. Since rate constant k_I can be factored into two functions k(R, N) and k(d, ΔG_{sol}), as shown in equation 3-14, equation 3-30a can be rewritten in the following form

$$-\frac{\Delta N_A}{\Delta t_A} = k_A N_A$$
$$= k_A(d, \Delta G_{sol,A})\, k(N, R)\, N_A \tag{3-31}$$

Furthermore, diffusion of an ion from the bulk of the droplet to the surface is fast enough to maintain equilibrium of ion population between

surface and bulk solution, see equation 3-20 and relevant discussion. This condition can be expressed with equation 3-32.

$$-\frac{N_A}{N} = \frac{N_A+n_A}{N+n} \tag{3-32}$$

N: total positive ions on the surface of a charged droplet

n: total ions in bulk solution

n_A: number of ion A in bulk solution

Combining equation 3-32 with equation 3-31, one can obtain

$$-\frac{\Delta N_A}{\Delta t_A} = k'_A(d, \Delta G_{sol,A})\, k(N, R)\, N \frac{N_A}{N}$$

$$-\frac{\Delta N_A}{\Delta t_A} = k'_A(d, \Delta G_{sol,A})\, k(N, R)\, N \frac{N_A+n_A}{N+n} \tag{3-33}$$

Similarly, an equation for ion B is obtained as

$$-\frac{\Delta N_B}{\Delta t_B} = k'_B(d, \Delta G_{sol,B})\, k(N, R)\, N \frac{N_B+n_B}{N+n} \tag{3-34}$$

n_B: number of ion B in bulk solution

If $k'_A(d, \Delta G_{sol,A})/k'_B(d, \Delta G_{sol,B})=u$ (constant), the expected experimentally obtained rate constant ratio k_A/k_B at different concentrations can be estimated with following iterative calculation.

As first step (noted in subscript as 1), $\Delta t_{A,1}$ can be calculated for emitting one ion A, i.e., $\Delta N_{A,1}=-1$. Because $\Delta t_{A,1}=\Delta t_{B,1}$, one can obtain $\Delta N_{B,1}$ which is the number of ion B emitted in time $\Delta t_{B,1}$. That is

$$\Delta t_{A,1} = \frac{-\Delta N_{A,1}[N+n]}{k'_A(d, \Delta G_{sol,A})\, k(N, R)\, N\, (N_{A,1}+n_{A,1})}$$

$$= \frac{-\Delta N_{A,1}}{u\, k'_B(d, \Delta G_{sol,B})\, k(N, R)} \times \frac{N+n}{N\,(N_{A,1}+n_{A,1})} \qquad (3\text{-}35)$$

and

$$-\Delta N_{B,1} = \Delta t_{B,1}\, k'_B(d, \Delta G_{sol,B})\, k(N, R)\, N\, \frac{N_{B,1}+n_{B,1}}{N+n}$$

$$= \frac{N_{B,1}+n_{B,1}}{N_{A,1}+n_{A,1}} \times \frac{1}{u} \qquad (3\text{-}36)$$

For the second step (noted in subscript as 2), if $\Delta N_{A,2}$ is taken as -1, one can calculate $\Delta N_{B,2}$. Keeping in mind that $\Delta t_{A,2}=\Delta t_{B,2}$, the following two equations will be obtained.

$$-\Delta t_{A,2} = \frac{N+n-(\Delta N_{A,1}+\Delta N_{B,1})}{\left[N-(\Delta N_{A,1}+\Delta N_{B,1})\right]\left[N_{A,1}+n_{A,1}-\Delta N_{A,1}\right]} \times \frac{-\Delta N_{A,2}}{u\, k'_B(d, \Delta G_{sol,B})\, k(N, R)} \qquad (3\text{-}37)$$

then

$$-\Delta N_{B,2} = \frac{N_{B,1}+n_{B,1}-\Delta N_{B,1}}{N_{A,1}+n_{A,1}-\Delta N_{A,1}} \times \frac{1}{u} \qquad (3\text{-}38)$$

The iteration continues until whole ion evaporation process has to stop:

$$\Sigma(-\Delta N_A)+\Sigma(-\Delta N_B)=N \qquad (3\text{-}39)$$

Thus, the experimental rate constant ratio can be estimated:

$$\frac{k_A}{k_B} = \frac{\Sigma(-\Delta N_A)}{\Sigma(-\Delta N_B)} \qquad (3\text{-}40)$$

The condition set in equation 3-39 reveals the possibility of ion depletion. When [A]=[B] and both are at low concentration range, one ion species would be used up early if it has larger rate constant. If it is supposed

$k'_A(d, \Delta G_{sol, A}) / k'_B(d, \Delta G_{sol, B}) = u >> 1$, B ions can still evaporate after most A ions have evaporated. Therefore, the observed rate constant ratio k_A/k_B will be smaller than the value u. This rationalization would be more visual if the ion evaporation process is calculated with above equation in a typical Iribarne droplet. The results of calculation are shown in Table 3-3. In Table 3-3, it is obvious that depletion effect will exist when the analyte concentration is low such as below 10^{-4} M, which is the range widely used in the ESMS practice. Finally, a mention should be made that ion depletion alleviates the difficulty in ion emission of polar compounds and makes the mass analysis of polar compounds possible in ESMS.

Table 3-3. Deviation of the Observed k_A/k_B from Real Ratio $k'_A(d, \Delta G_{sol, A})/k'_B(d, \Delta G_{sol, B})$ due to Ion Depletion

[C] (M) [a]	n_A [b] (or n_B)	N_A+n_A [c] (or N_B+n_B)	Observed k_A/k_B u=∞	u=5	u=2	u=1
$5x10^{-6}$	9	44	1.69	1.69	1.33	1.0
$1x10^{-5}$	18	53	3.12	2.33	1.50	1.0
$2x10^{-5}$	36	71	∞	3.12	1.59	1.0
$4x10^{-5}$	72	107	∞	3.67	1.69	1.0
$1x10^{-4}$	180	215	∞	4.00	1.80	1.0

a. [C] is the concentration of analyte A (or B) in the bulk solution, [A]=[B];

b. the number of ions in the bulk solution of a typical Iribarne droplet, R=80 Å, N=70;

c. the total available ions of A (or B) in the charged droplet.

3.6 References

1. Bailey, A.G. *"Electrostatic Spraying of Liquids"*, John Wiley and Sons, New York (1988)
2. Hayati, I., Bailey, A.I.; Tadros, T.F. *J. Colloid Interface Science* , **117**, 205, 202 (1987)
3. Smith, D.P.H. *IEEE Trans. Ind. Appl.*, **IA-22**, 527 (1986)
4. Pfeifer, R.J.; Hendricks, C.D. *AIAA J.*, **6**, 496 (1968)
5. Ikonomou, M.G.; Blades, A.T.; Kebarle, P. *Anal. Chem.*, **62**, 957 (1990)
6. Ikonomou, M.G.; Blades, A.T.; Kebarle, P. *Anal. Chem.*, **63**, 1989 (1991)
7. Blades, A.T.; Ikonomou, M.G.; Kebarle, P. *Anal. Chem.*, **63**, 2109 (1991)
8. a. Chapter 2 in this thesis; b. Tang, L.; Kebarle, P. *Anal. Chem.*, **63**, 2709 (1991)
9. Sunner, J.; Nicol, G.; Kebarle, P. *Anal. Chem.*, **60**, 1300 (1988)
10. Ikonomou, M.G. and Kebarle, P. unpublished work.
11. Iribarne, J.V.; Thomson, B.A. *J. Chem. Phys.*, **64**, 2287 (1976)
12. Thomson, B.A.; Iribarne, J.W. *J. Chem. Phys.*, **71**, 4451 (1979)
13. Davies, C.N. Evaporation of Airborn Droplets p. 154 in *Fundamentals of Aerosol Science*, Shaw, D.T. Ed., Wiley Interscience, John Wiley, New York (1978).
14. Pound, G.M. *J. Phys. Chem. Ref. Data*, **1**, 135, (1972)
15. McDaniel, E.W. *"Collision Phenomena in Ionized Gases"* p. 502, John Wiley, New York (1964).
16. Taflin, D.C.; Ward, T.L.; Davis, E.J. *Langmuir*, **5**, 376 (1989);

Davis, E.J. ISA *Transactions*, **26**, 1 (1987)

17. Gomez, A.; Tang, K. *Proceedings of the Fifth Internat. Conf. on Liquid Atomization and Spray Systems* I CLASS-91, Smerjians, H.G. Ed., NIST Special publication 813 Gaithersburgh, MD (1991).
18. Gomez, A; Tang, K. *Physics of Fluids A* (in print).
19. Lord Rayleigh, *Philos. Mag.*, **14**, 184 (1882)
20. Desnoyers, J.E.; Jolicoeur, C. "Hydration Effects and Thermodynamic Properties of Ions" in *"Modern Aspects of Electrochemistry"* Eds. Bockris, J.O.M. and Conway, B.E. **5**, p 20, Plenum Press, N.Y. (1969).
21. Dzidic I.; Kebarle, P. *J. Phys. Chem.*, **74**, 1466 (1970)
22. Glasstone, S. *Textbook of Physical Chemistry*, Second Ed., p. 495, D. Van Nostrand, New York (1946).
23. Kebarle, P. *Annual Reviews of Physical Chemistry*, **28**, 467 (1977)
24. Arnett, E.M.; Jones III, F.M.; Taagepera, M; Henderson, W.G.; Beauchamp, J.L.; Holtz, D.; Taft, R.W. *J. Am. Chem. Soc.*, **94**, 4726 (1972)
25. Conway, B.E. *"Ionic Hydration in Chemistry and Biophysics"*, p. 73, Elsevier Publishing (1981).
26. Davidson, W.R.; Sunner, J.; Kebarle, P. *J. Am. Chem. Soc.*, **101**, 1675 (1979)
27. Tamaki, K. *Bull. Chem. Soc. Japan*, **40**, 38 (1967)
30. Dole, M.; Mack, L.L.; Hines, R.L.; Mobley, R.C.; Ferguson, L.P.; Alice, M.B., *J Chem. Phys.*, **49** 2240 (1968)

Chapter 4. Complexation of Alkali Cation M^+ to 18-Crown-6. Comparison of Expected Concentrations of M^+ and M^+·18-Crown-6 in Solution with Observed Ion Intensities of M^+ and M^+·18-Crown-6 in ESMS

4.1 Introduction

The investigation of the ESMS mechanism has revealed that a charge separation process in electrospray happens at the electrospray tip. This charge separation process is discussed in chapter 2 of this thesis on the basis of the Hendricks model (1). After the charged droplets form, they drift in the atmosphere under the influence of the electric field. The study of the ES mechanism has also revealed that gas phase ions might form via an ion evaporation process, which is the concept first put forward by Iribarne (2). The process of gas phase ion formation was discussed in chapter 3 of this thesis, where it was concluded that gas phase ions are produced by the charged droplets which have already evaporated a large amount of solvent. The work by Gomez and Tang (3) provided experimental data for the droplet shrinkage process, but no direct observation has been made to confirm that the gas phase ions originate from shrunken charged droplets.

To test the assumption that ions in the liquid phase begin to transfer to the gas phase after the charged droplet has evaporated a large amount of solvent, an experiment which takes advantage of reactivity of metal ions with cyclic ligands was devised. The reactions between alkali metal ions and crown ethers have been extensively investigated in both liquid and gas phases (4-18). For instance, equilibrium constants and reaction rate

constants for the reaction: $M^+ + L = M^+L$ in methanol has been determined independently by different researchers (5, 6, 16).

In the present work, crown ethers, mainly 18-crown-6 and 12-crown-4 (Figure 4-1), were used as cyclic ligands to the alkali metal cations. The equilibrium constants for the formation of the metal ligand complex M^+L in methanol have been determined (5-7) and therefore the expected concentrations of M^+, L and M^+L at equilibrium can be evaluated if the initial $[M^+]$ and [L] in the solution are known.

The main purpose of the present work is to attempt to determine the shift of the equilibrium: $M^+ + L = M^+L$ towards the product side caused by the increase of solute concentration due to solvent evaporation from the droplets. The solvent evaporation was discussed in Chapter 3.

4.2 Experimental

a. Mass-dependent discrimination and ion intensity calibration

Because the SCIEX TAGA 6000E used in the work described in chapter 3 was not available at the time of the study described here, my initial experiments were conducted on the quadrupole mass spectrometer SCIEX TAGA 6000, an earlier version of the TAGA 6000E. Some of the later experiments were performed on the TAGA 6000E. Modifications needed to fit ES to the mass spectrometer were discussed in Chapter 3 and reference 19.

In order to compare the ion intensities, a correction must be applied for the mass discrimination introduced by a quadrupole mass spectrometer. The measurement of the mass dependent transmission of the TAGA 6000

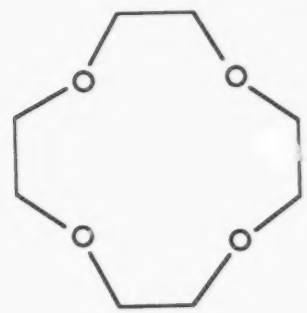

(1) 12-crown-4

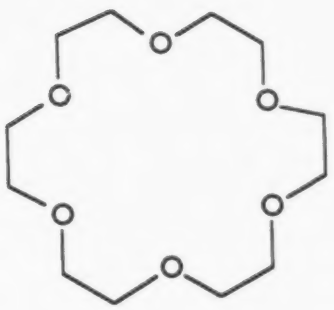

(2) 18-crown-6

Figure 4-1 Structures of crown ethers used in the complexation with metal ions. (1) 12-crown-4, MW=176; (2) 18-crown-6, MW=264.

was obtained with the same procedure as described in Chapter 3 for the TAGA 6000E. The mass dependent transmission plot is shown in Figure 4-2.

b. Gas phase reactions between ion M^+ and crown ethers.

For the reasons explained in Results and Discussion, it was necessary to examine whether a gas phase ion molecule reaction involving alkali metal ion (M^+) and crown ether (L): $M^+ + L = M^+L$, occurs in the electrospray plenum chamber. A special device shown in Figure 4-3 was designed for this purpose. A stainless steel electrospray tip was installed coaxially within a glass tube. The glass tube was mounted in the plenum chamber as shown in the figure. Reactant crown ether dissolved in methanol was injected at a known flow rate into a vaporizer, where it evaporated. The electrospray tip protruded about 1 cm past the glass tube of the vaporizer in order to avoid any electrostatic influence by the glass. The air flow rate through the vaporizer was the same as in the conventional ES experiment, i.e. 0.5 L/sec. The pressure of crown ether can be controlled by either varying the concentration in methanol or the injection flow rate. The solution used for ES contained only the metal halide, M^+X^- salt, and methanol. Under these conditions, gas phase metal ions are produced by ES. The ions can then react with the vaporized crown ether in the gas phase. The reaction products can be detected with the mass spectrometer.

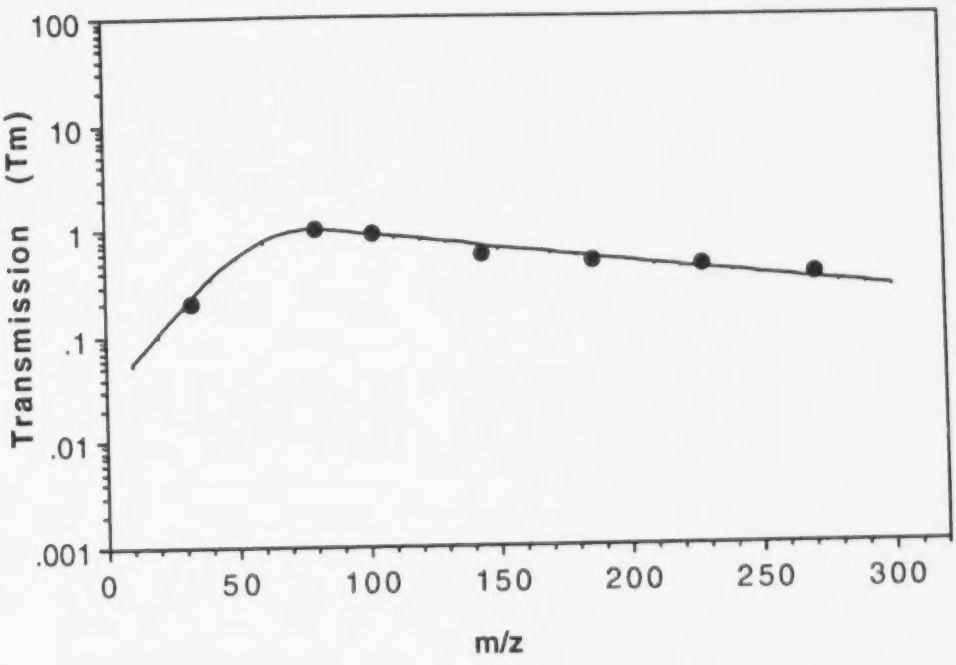

Figure 4-2 Transmission correction curve for ion intensity measurement on TAGA 6000. The seven protonated amine ions are: $CH_3NH_3^+$ (m/z=33), PyH^+ (m/z=80), Et_3NH^+ (m/z=102), Pr_3NH^+ (m/z=144), Bu_3NH^+ (m/z=186), Pe_3NH^+ (m/z=228), and Hx_3NH^+ (m/z=271)

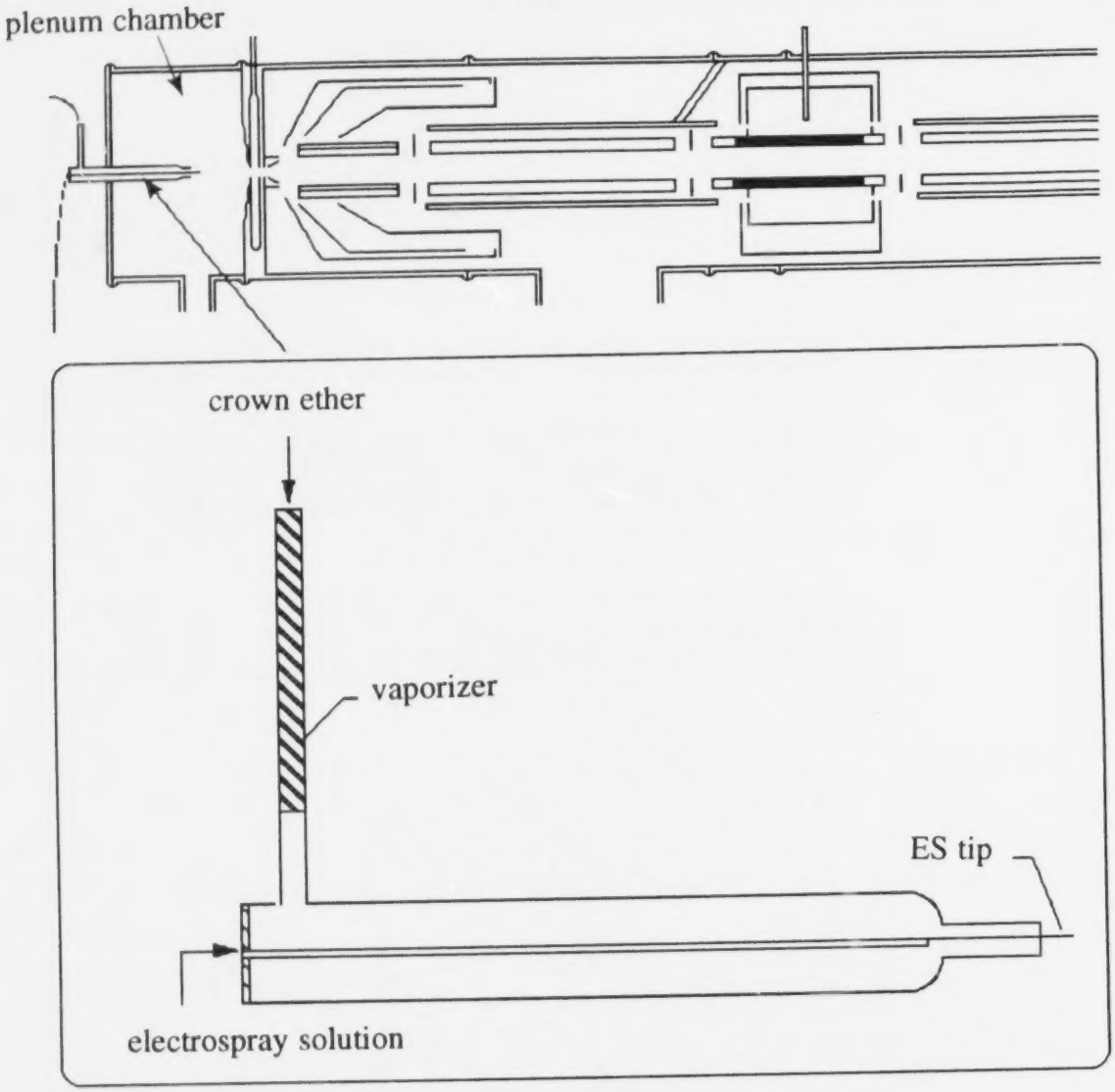

Figure 4-3. Device for the study of gas phase ion molecule reactions. Volatile crown ether is evaporated by vaporizer and transported by air flow to TAGA plenum chamber where it can undergo an exchange reaction with the crown ether-ion from electrospray. ES tip protrudes ca. 1 cm past glass tube. Diameter of glass tube near ES tip is ca. 1 cm (i.d.).

4.3 Results and Discussion

a. Complexation of metal ions and cyclic ligands in solution

The stability constants, K_S, for the complexation of alkali ions with crown ether 18C6 are known (6, 7). Therefore the concentrations of the complex and the free metal ion at equilibrium can be evaluated

$$M^+ + L = M^+L \qquad (4\text{-}1)$$

$$K_s = \frac{[M^+L]}{[M^+]\,[L]}$$

where [M+L]: concentration of complex (mole/L)

[M+]: concentration of free metal ion (or solvated ion) (mole/L)

[L]: concentration of free crown ether (mole/L)

As mentioned in the Introduction, the very small charged droplets that produce the gas phase ions are expected to have lost a large amount of solvent due to solvent molecule evaporation. It was shown in Chapter 3 that the volume ratio, $V_o/V_f = F$, where V_o is the initial volume at the ES tip and V_f is the volume at the point where gas phase ion emission occurs, can be estimated on the basis of certain assumptions. The factor F could be very high $F \approx 4000$ if the fission of the droplets was symmetric or quite low $F \approx 140$ if the ion emitting droplets were due to non-symmetric fission, see Chapter 3. Furthermore, the assumed size of the ion emitting droplets affected the calculation of F. The concentration of solutes in the ion emitting droplets relative to the initial concentration in the solution is expected to increase by the factor F.

The rationale of the present experiments is to use the equilibrium (4-1) and the measured gas phase ion intensity ratio, I_{ML+}/I_{M+}, in order to

obtain an independent experimental estimate of the factor F. Obviously, a large concentration increase due to solvent evaporation will shift the equilibrium (4-1) towards the product side and thus lead to an increase of the ion ratio ML^+/M^+ in the droplet solution. This increase will be reflected in the gas phase ion ratio.

The equilibrium in the ion emitting droplet will be given by:

$$K_s = \frac{C_{M^+L}}{C_{M^+} C_L} \tag{4-2}$$

where C_{M+L}: the concentration of M^+L in the ion emitting droplet,

C_{M+}: the concentration of M^+ in the ion emitting droplet,

C_L:the concentration of L in the ion emitting droplet.

In the present experiments the initial concentrations in the solution to be electrosprayed were chosen as: $[M^+] = 10^{-4}$ M = a, [L] = 10^{-4} M. Because the initial concentrations were equal, the equilibrium in the initial solution can be expressed as:

$$K_s = \frac{x}{(a - x)^2} \tag{4-3}$$

where x: the equilibrium concentration of ML^+;

(a-x): the equilibrium concentration of M^+ or L.

For the ion emitting droplets the concentrations will have increased by a factor F. Thus the initial concentration before equilibrium would be: $Fa = C_{oM+} = C_{oL}$. Calling the concentration at equilibrium $C_{ML+} = Fy$ then

$$C_{M+} = Fa - Fy = F(a - y)$$

$$C_L = Fa - Fy = F(a - y)$$

substituting in equation 4-2 one obtains:

$$K_s F = \frac{y}{(a - y)^2} \qquad (4\text{-}4)$$

Equations 4-3 and 4-4 are of the same form.

The gas phase ion ratio I_{M^+L}/I_L can be related to the concentration ratio in the ion emitting droplet by the equation:

$$\frac{I_{M^+L}}{I_{M^+}} = \frac{k_{M^+L} C_{M^+L}}{k_{M^+} C_{M^+}} \qquad (4\text{-}5)$$

as shown in Chapter 3 (see equation 3-10) provided that the ion with the higher coefficient k is in the "high" concentration range, so that no depletion occurs. This condition is met in the present experiments because M+L is the ion with the higher coefficient, and the concentration of M+L is in the high concentration range, i.e. [M+L] > $5x10^{-5}$ M. The ratio k_{M^+L}/k_{M^+} was determined in experiments where k_{M^+} was obtained with solutions containing only M^+ and k_{M^+L} with solutions of M^+ and L at concentrations such that the dominant ion was M+L, see Figures 4-4, 4-5. The k_{M^+L}/k_{M^+} values are summarized in Table 4-1. Equation 4-5 can be rewritten as,

$$\frac{I_{M^+L}}{I_{M^+}} = \frac{k_{M^+L} C_{M^+L}}{k_{M^+} C_{M^+}} = \frac{k_{M^+L}\, y}{k_{M^+}(a - y)} \qquad (4\text{-}6)$$

and since y is the only unknown it can be evaluated. Once y has been obtained the product K_sF can be obtained from equation 4-4. Since K_s is known, F can be determined.

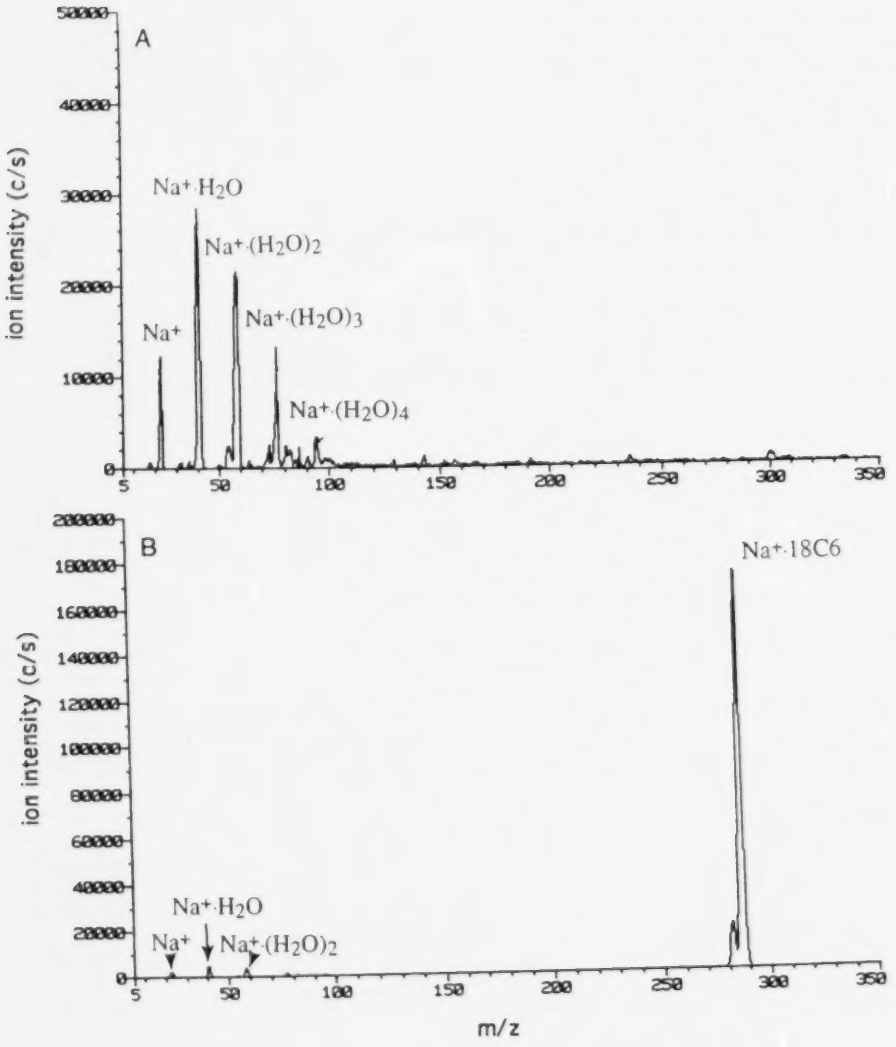

Figure 4-4 Electrospray mass spectra of (A) sodium ion and its solvated clusters from a 10^{-4} M NaCl methanol solution; (B) sodium and crown ether complex ions from a 10^{-4} M NaCl and 10^{-4} M 18C6 methanol solution. Flow rate=20 μL/min.

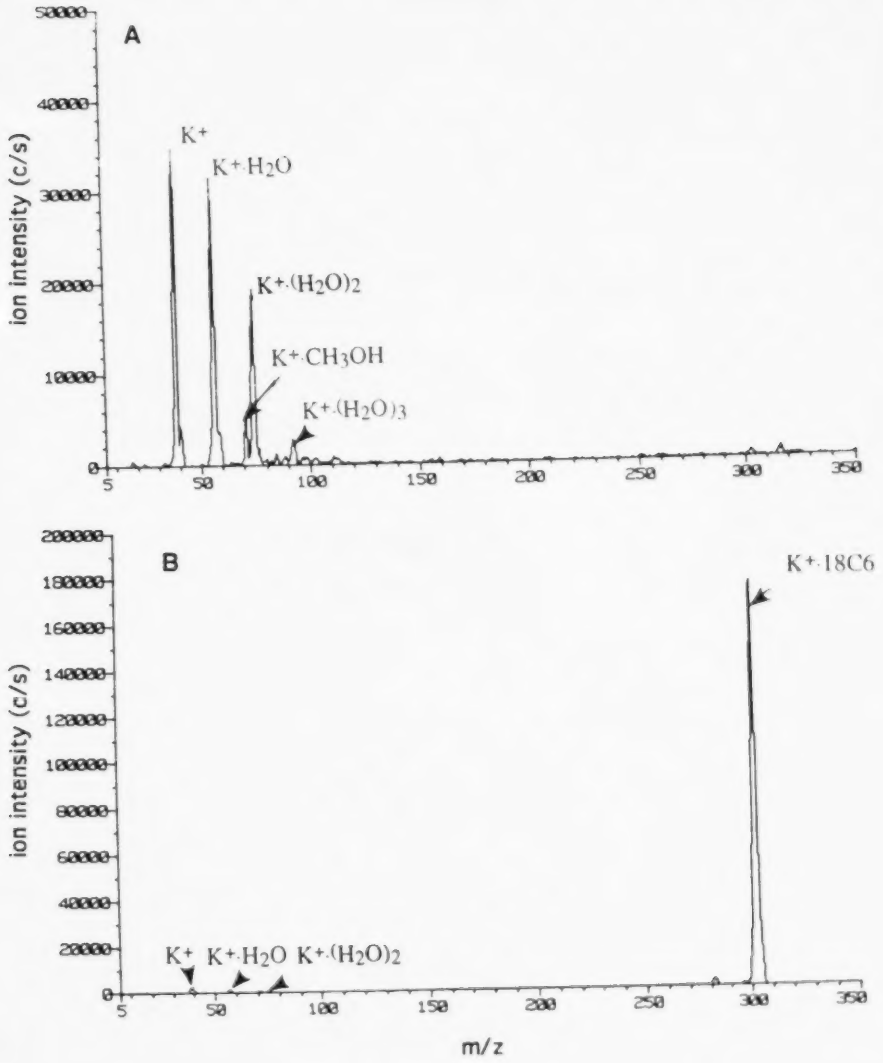

Figure 4-5 Electrospray mass spectra of (A) potassium ion and its solvated clusters from a 10^{-4} M KCl methanol solution; (B) potassium and crown ether complex ions from a 10^{-4} M KCl and 10^{-4} M 18C6 methanol solution. Flow rate=20 μL/min.

Table 4-1. Sensitivity Comparison between Gas Phase Alkali Ion and Complex Ion [a]

M	Li	Na	K	Rb	Cs
$\Sigma M^+(H_2O)_n$ [b] (c/s)	2.0×10^5	2.2×10^5	1.7×10^5	1.7×10^5	1.3×10^5
S.F[c].(18C6)[d]	2.0	2.9	4.1	3.9	2.6

a. Both the metal ion and ligand initial concentrations were 10^{-4} M; Metal ion (or solvated cluster) and crown ether complex were measured using two different solutions.

b. transmission efficiency corrected $\Sigma M^+(H_2O)_n$ in absence of crown ether.

c. sensitivity factor:

$$S.F. = \frac{ML^+}{\Sigma M^+(H_2O)_n} \approx \frac{k_{M^+L}}{k_{M^+}}$$

where L=18C6

d. ratio of total ion currents in presence and absence of crown; total ion current in the presence of crown is mainly of $I(M^+L)$.

Table 4-2. Concentration of Alkali Ion and Crown Ether Complex at Equilibrium in Methanol Solution [a]

M^+	Li	Na	K	Rb	Cs
log K_S[b]	~0	4.32	6.29	5.82	4.44
$[M^+]$[c] (mole/L)		4.93×10^{-5}	6.91×10^{-6}	1.16×10^{-5}	4.48×10^{-5}
$[ML^+]$[c] (mole/L)		5.07×10^{-5}	9.31×10^{-5}	8.84×10^{-5}	5.52×10^{-5}
$\frac{[ML^+]}{[M^+]}$[d]		1.03	13.5	7.64	1.23
$\frac{I_{ML^+}}{I_{M^+}}$[e]		13	48	40	16
$\frac{y}{(a-y)}=\frac{C_{M^+L}}{C_{M^+}}$		4.5	12	10	6.2
y		8.2×10^{-5}	9.2×10^{-5}	9.1×10^{-5}	8.6×10^{-5}
K_SF		2.5×10^{5}	1.5×10^{6}	1.1×10^{6}	4.5×10^{5}
K_S		2.1×10^{4}	1.9×10^{6}	6.6×10^{5}	2.7×10^{4}
F		12	0.8	1.7	16

a. Crown ether (L) is 18C6.

b. K_S (moles/L) values in CH_3OH solution are from references 5 and 6.

c. Calculated concentrations of M^+ and ML^+ in CH_3OH at equilibrium, for initial $[M^+] = [L] = 10^{-4}$ M.

d. Calculated ratio at equilibrium.

e. Ion intensity ratio observed in experiment are corrected for transmission, but not corrected for surface activity and ion emission coefficient differences, see Chapter 3.

Mass spectra obtained with a 10^{-4} M NaCl solution in methanol and with 10^{-4} M NaCl and 10^{-4} M L, when L is the crown ether 18C6, are shown in Figure 4-4. It is evident that the equilibrium is shifted very much to the M^+L complex. The transmission corrected ratio, I_{M^+L}/I_{M^+}, obtained from this experiment where $M^+ = \Sigma M^+(H_2O)_n$ is given in Table 4-2. Similar data obtained for K^+ and 18C6 are given in Figure 4-5, which lead to the ratio I_{K+L}/I_{K+} given in Table 4-2. Results for Rb^+ and Cs^+ obtained in analogous experiments are also included in Table 4-2.

The gradual increase of I_{M+L} and decrease of I_{M+} observed with a series of solutions where $[M^+] = 10^{-4}$ M was kept constant and [L] was increased from $1x10^{-5}$ M to $2x10^{-4}$ M is shown for $M^+ = K^+$ and L = 18C6 in Figure 4-6. The changes are consistent with a shift of the equilibrium towards the product M^+L which is expected to occur with an increase of the initial concentration of L. A small decrease of I_{K+L} at $[L] > 10^{-4}$ M is observed. This can be attributed to the formation of a M^+L_2 complex:

$$M^+L + L = M^+L_2$$

The formation of such a complex was detected in the mass spectrum (see Figure 4-7). Such sandwich complexes are known to form both by reactions both in solution (4) and in the gas phase (12). Also included in Table 4-2 are the calculated ratios, C_{M+L}/C_{M+} (see equation 4-6). The evaluated $y = C_{ML+}$ and the factor F relate to the concentration increase in the droplet due to volume shrinkage by solvent evaporation.

The value F obtained is not constant as might be expected but varies from ~1 to 16. It should be noted that the experimental conditions, particularly for K^+ and Rb^+, were not well suited for a determination of the constant, K_sF, because the equilibrium is shifted almost entirely towards the complex side. To obtain a good value for K_sF, the

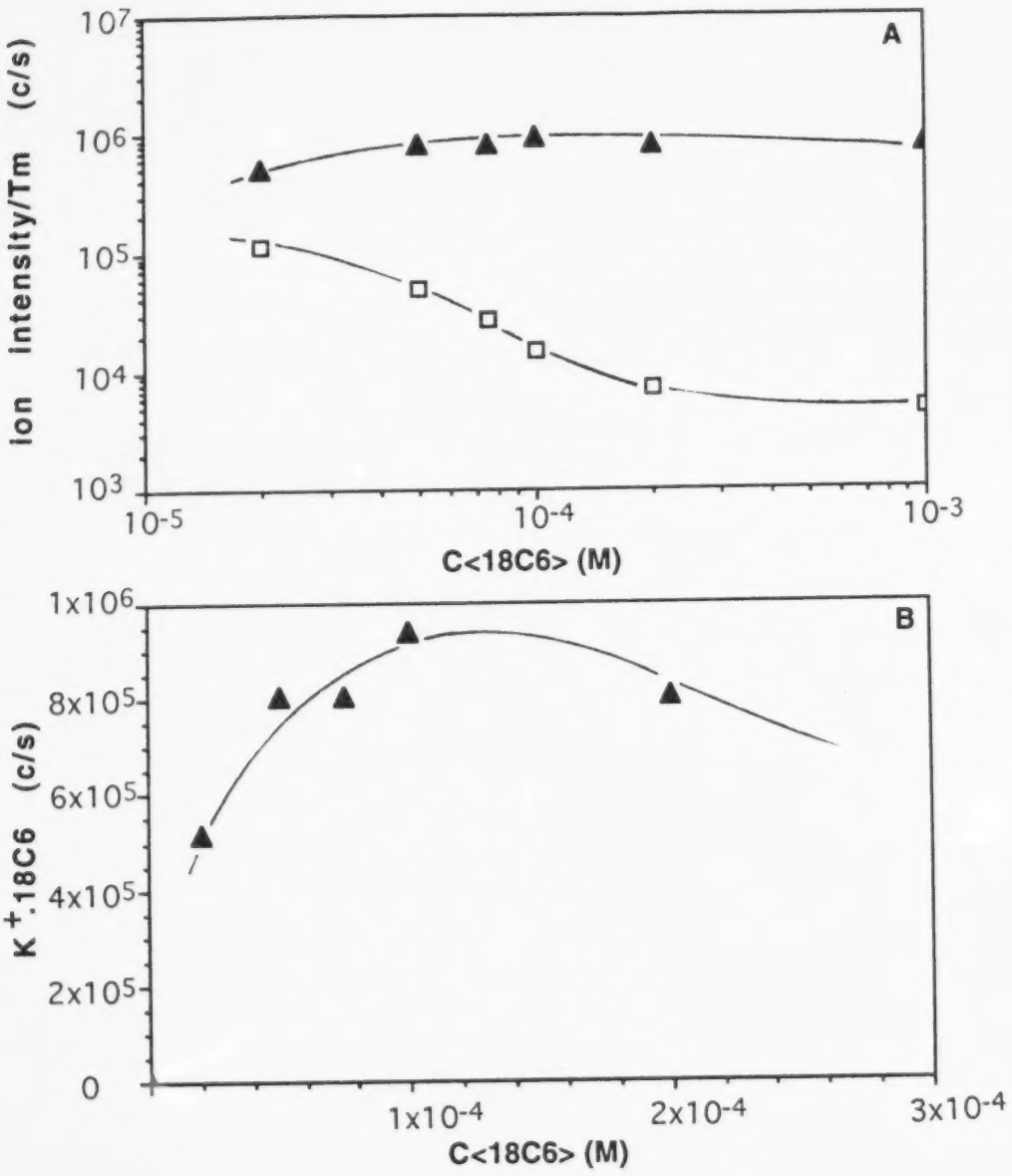

Figure 4-6 Dependence of ion intensities of $K^+(Sol)_n$ and K^+·18C6 on 18C6 concentration: (A) K^+ is transferred to K^+·18C6 with increase of 18C6 concentration; (B) Change of K^+·18C6 intensity on a linear scale illustrates that intensity will no longer increase with excess 18C6 in solution. Initial [KCl]=10^{-4} M. ❑ $\Sigma K^+(Sol)_n$; ▲ K^+·18C6.

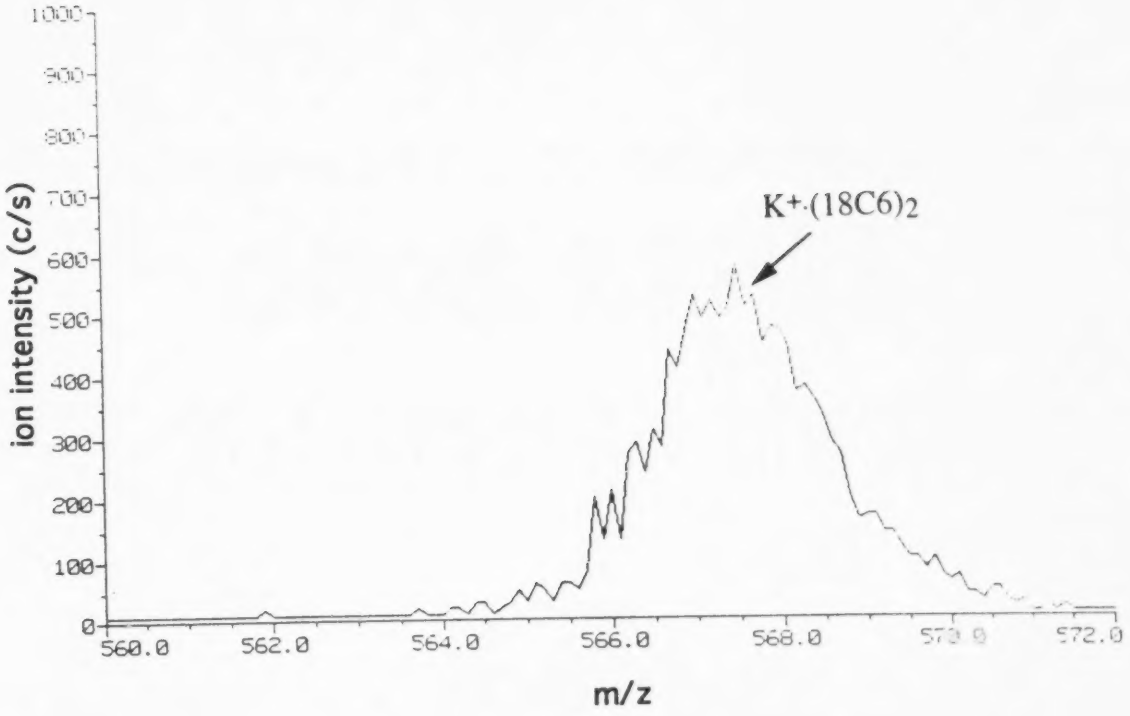

Figure 4-7 Mass spectrum contains a peak due to "sandwich" style complex [$K^+ \cdot (18C6)_2$] (m/z=567) formed when excess crown ether is present in solution; 10^{-4} M KCl and 10^{-3} M 18C6 in methanol solution.

experimental value for I_{M+L}/I_{M+} must be very accurate. But, because I_{M+} is very small, any nonequilibrium source of M^+ ion intensity will have a large effect on the ratio. Sources of nonequilibrium M^+ intensity may be collisional dissociation of the complex in the ion sampling region of the mass spectrometer or slow kinetics for complex formation. An analysis of the kinetics given below indicates that equilibrium may not be attained when K_s is very large as in the case for K^+ and Rb^+. Therefore, we consider the results in Table 4-2 for these two ions unreliable.

Accurate determination of F can be obtained only for cases where C_{M^+L}/C_{M^+} is closer to unity and this requirement is met at least to a certain extent for Na^+ and Cs^+. The F values for these ions are 12 and 16 and thus more in line with the expected concentration increase (see Chapter 3).

The question whether the rate for complex formation is fast enough to allow equilibrium to be attained as the droplets shrink by evaporation, needs to be addressed. Liesegang et al. (16) determined the rate constant for complex formation, $k = 10^9$ (L/mol)s^{-1}. For an initial concentration of $[M^+] = [L] = a$ of 10^{-4} mol/L, this rate constant leads to an initial half-life for the reaction

$$t_{1/2} = \frac{1}{k_2 a}$$

$$\approx \frac{1}{10^9 \times 10^{-4}} = 10^{-5} \text{ sec} \qquad (4\text{-}7)$$

It was shown in chapter 3 that the time between droplet fissions are in the 10 to 100 μs time scale. The largest relative volume changes occur for the small droplets. For example (see Figure 3-19 in Chapter 3), offspring droplets of R = 0.076 μm shrink to R_s = 0.029 μm in 40 μs. The volume

decreases by a factor of 20, which means that the concentration of electrolytes should increase by the same factor. It is clear that an adequate answer requires an accurate analysis involving a solution of the appropriate differential equation which includes the time dependence of the concentration due to droplet evaporation in the reaction rate equation. Here we offer only some qualitative considerations. It is clear that the forward rate will increase as the concentration is increased since the rate depends on the square of the concentration, i.e. the product of C_{M+} and C_L. An increase of the concentration will require a shift of the equilibrium to the product side but this shift will be facilitated due to the increased rate of the reaction with concentration.

The time required for a droplet of radius R_o to decrease its volume by a factor of 2 can be evaluated with equation 3-17. It is given by equation 4-8a, while 4-8b provides the time for a $R_o = 0.076$ μm droplet.

$$t_{\text{volume halflife}} = R_o \times 1.72 \times 10^2 \text{ ses} \qquad (4\text{-}8a)$$

$$= 0.076 \times 10^{-6} \times 1.72 \times 10^2$$

$$= 1.3 \times 10^{-5} \text{ sec} = 13 \text{ μs} \qquad (4\text{-}8b)$$

The time is approximately the same as the reaction halflife, see equation 4-7. However the equilibrium needs to shift less than the concentration shift by a factor of 2 calculated in equation 4-7.

This can be illustrated by the following model calculation for Cs^+. Assume that the concentration before the volume reduction corresponds to $a = 1 \times 10^{-4}$ M, see equation 4-3. The concentrations at equilibrium are shown below on the left most side written as an equilibrium quotient:

$$\frac{C_{M^+L}}{C_{M^+}C_L} = \frac{0.55 \times 10^{-4}}{0.45 \times 10^{-4} \times 0.45 \times 10^{-4}} \xrightarrow{I} \frac{1.1 \times 10^{-4}}{0.9 \times 10^{-4} \times 0.9 \times 10^{-4}}$$

$$\xrightarrow[\Delta t = 3\ \mu s]{II} \frac{1.3 \times 10^{-4}}{0.7 \times 10^{-4} \times 0.7 \times 10^{-4}} \qquad (4\text{-}9)$$

Process I corresponds to an instant volume reduction by a factor of two corresponding to an instant concentration increase by the same factor. Process II is the reactive relaxation towards the new equilibrium concentrations which are shown at the right of equation 4-9. It is seen that the reactive change of concentrations $C_{M+} = C_L$ is only from 0.9×10^{-4} to 0.7×10^{-4} mol/L. The time t required for this concentration change, calculated with the rate equation:

$$\frac{1}{C} - \frac{1}{C_o} = kt \qquad k = 10^9\ LM^{-1}s^{-1} \qquad (4\text{-}10)$$

is t=3.2 μs, i.e. considerably smaller than the 13 μs required for the droplet shrinkage. Therefore, for these conditions near equilibrium concentrations will be maintained closing the droplet shrinkage.

It is important to note that the rate of reactive relaxation to equilibrium may not be fast enough when K_s is vary large or when K_sF is very large, such that the equilibrium is shifted far to the right and the concentration of $C_{M+} = C_L$ is very low. Shown below are the equilibrium quotients for K^+ and 18C6, calculated for $a = 10^{-4}$ M and $K_s = 1.9 \times 10^6$.

$$\frac{C_{M^+L}}{C_{M^+}C_L} = \frac{0.93 \times 10^{-4}}{0.07 \times 10^{-4} \times 0.07 \times 10^{-4}} \xrightarrow{I} \frac{1.86 \times 10^{-4}}{0.14 \times 10^{-4} \times 0.14 \times 10^{-4}}$$

$$\text{II} \rightarrow \frac{1.9 \times 10^{-4}}{0.1 \times 10^{-4} \times 0.1 \times 10^{-4}} \qquad (4\text{-}11)$$

Processes I and II have the same meaning as in the example for Cs^+ above. The time evaluated with equation 4-10 for change II is t = 29 μs. The time is much longer because the initial concentration $C_o = C_{K+} = C_L$ for K^+, which has a much higher K_S, is much smaller. In this case the reaction time is longer than the droplet shrinkage time. Furthermore, the scheme of process I-II leads to shorter reaction times than actually expected since it is assumed in process I that the concentration increases instantaneously. These results show that the complex equilibrium will not be established for K^+ and Rb^+, when the droplet becomes very small and the rate of volume changes is very rapid. Of course, these are tentative conclusions since the rate of solvent evaporation predicted by equation 3-17 and 4-8 is only an estimate (see Chapter 3). Nevertheless it is possible that the disagreement with the expected volume shrinkage factors F for the high K_S ions K^+ and Rb^+ is due to slow kinetics, as illustrated above.

Unfortunately, the experimental results for I_{ML+}/I_{M+} may be affected also by another process which has not been considered so far. The electrospray process is a nebulizing process and neutral solutes present in the solution can be efficiently transferred to the gas phase. For example, the crown ether may be sufficiently volatile that the uncomplexed molecule may enter the gas phase and react with gas phase M^+ ions produced by the electrospray in gas phase ion-molecule reactions: $M^+ + L = M^+L$. The possible effect of such a reaction on the results summarized in Table 4-2 is considered in the next section.

b. Gas phase reactions of metal ions and macrocyclic ligands

It is well known that crown ethers have high proton affinities in the gas phase (8, 9) and that they also have strong tendency to form gas phase ion complexes (10-13). In electrospray, formation of the M^+L complex could occur also in the gas phase from gas phase M^+ ions produced by ES and gas phase L evaporated from the small droplets produced by the ES nebulization process. Therefore, it is necessary to investigate the relative importance of gas phase complexation.

The possibility of gas phase reactions of metal ions (and their solvates) with a crown ether was examined by the method illustrated in Figure 4-3. The spectra in Figure 4-8 show that sodium ion-crown ether complexes do form in the gas phase. However, after the intensities have been corrected for transmission efficiency, only about 10% of the sodium ions do react. In the case where both sodium chloride and crown ether are present in the solution, the solution concentration of Na+ is much smaller. Thus, very much less free Na^+ will result in free Na^+ ions in the gas phase and, equally, less free crown ether is available to contribute to gas phase ion-molecule reactions. The contribution of gas phase complexation to the total gas phase ion Na^+L intensity will be much less than 10%.

Similar considerations should hold also for the potassium, rubidium and cesium complexes. For the Lithium ion, with a much smaller complex formation constant, K_s, the Li^+ and crown ether concentration in the gas phase are higher and the observed I_{Li+L} in Table 4-1 might include a substantial contribution from gas phase ion molecule reaction.

Some additional gas phase reaction related experiments, not directly connected with the interpretation of the data in Table 4-2 will be presented below because they are of some general interest.

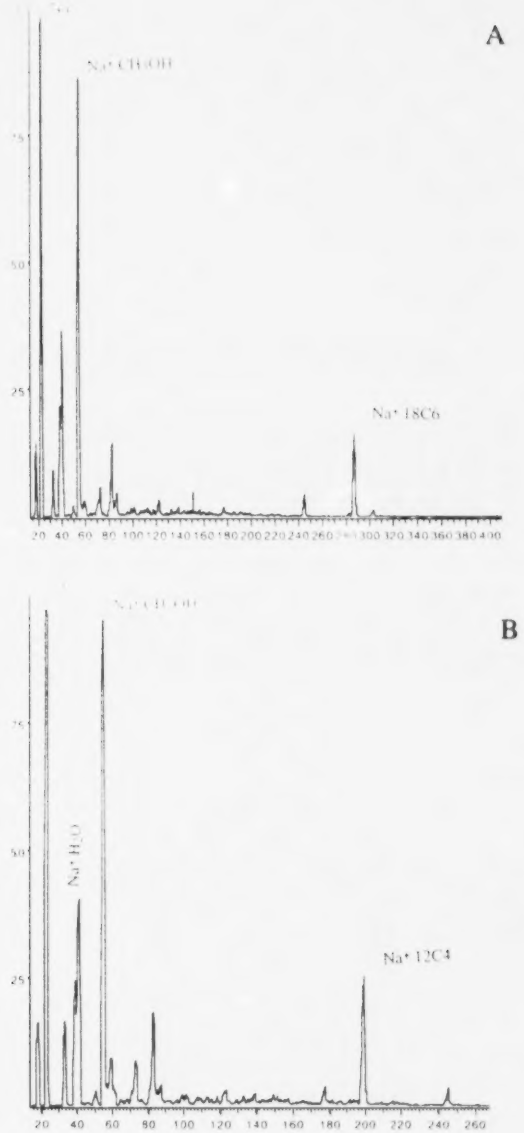

Figure 4-8 Mass spectra obtained from experiment where M^+ is produced by ES and a given crown ether is vaporized as shown in Figure 4-3: (A) Crown ether 18C6, (B) Crown ether 12C4. 10^{-4} M NaCl and 10^{-4} M crown ether are used in (A) and (B). The flow rates of the solution of the ligand L and the solution of NaCl were the same, 20 µl/min.

It is believed that maximum complex stability is obtained when a crown ether has a cavity size similar to that of ion (4). Even though there is still uncertainty as to the solvation contribution in solution (15), it is certain that macrocyclic effects and size-selective reactivity dominate in gas phase (14). Lithium was chosen as an example. Lithium, with the smallest ion radius of all alkali ions, has a large stability constant in lithium 12-crown-4 complex, while 12-crown-4 (12C4) is relative volatile among crown ethers. In the experiment lithium chloride and 18C6 methanol solutions were electrosprayed. At the same time, a pure 12C4 methanol solution was introduced by a vaporizer connected to the glass tubing. It was found that lithium 12C4 complex ion was formed in gas phase. The gas phase reaction can be written as

$$Li^+\cdot 18C6(g) + 12C4(g) = Li^+\cdot 12C4(g) + 18C6(g) \qquad (4\text{-}12)$$

This discovery also supports that the ligand (L) and ion reaction can happen in the gas phase as well as in the liquid phase. The ion intensity of $Li^+\cdot 12C4$ is weaker than the ion intensity of $Li^+\cdot 18C6$ by a factor of 100 although the former is favored because of size-selectivity (14) (see Figure 4-9). Maleknia and Brodbelt found that the selectivity of complexation of crown ether and metal ions in the gas phase is different from that in the liquid phase (10). The best selectivity of a crown ether in solution is for the metal ion whose ionic radius fits best the cavity size of the crown ether. But, the selectivity of crown ether in gas phase will be for a slightly smaller ion due to the achievement of a higher electric field-dipole interaction within the cavity for a given conformation of the ether. This concept is referred as "maximum contact point" (10).

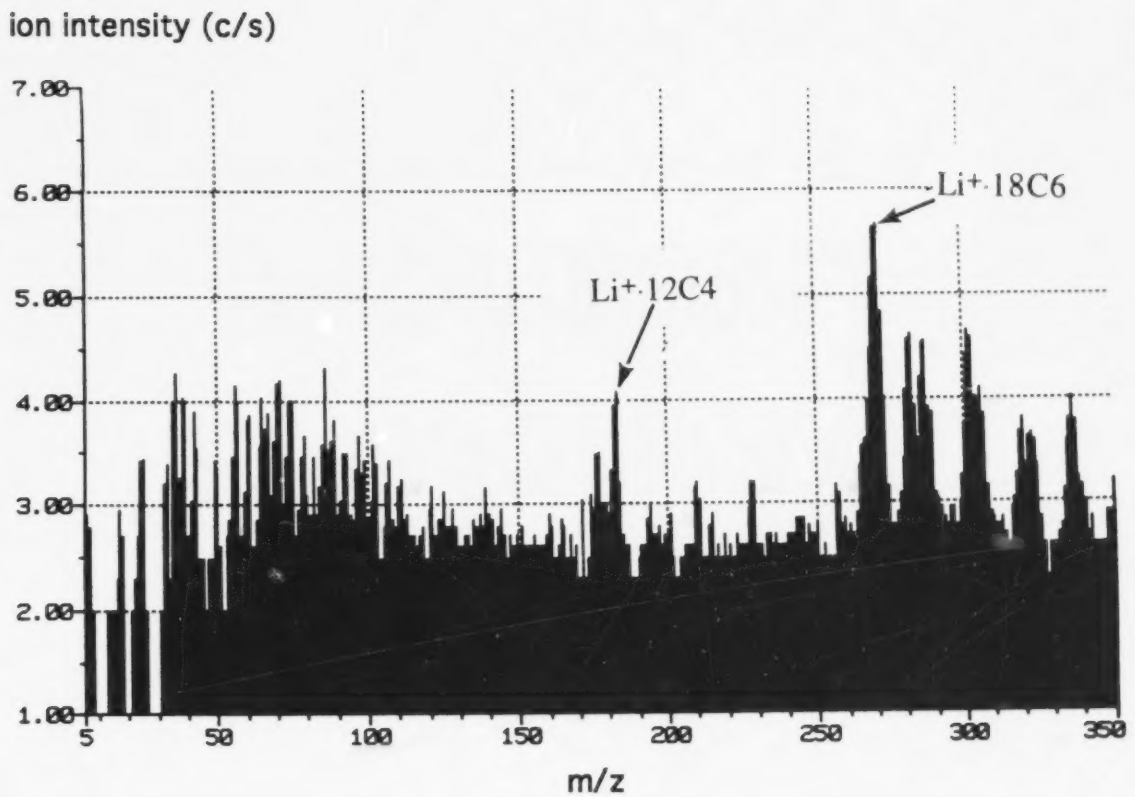

Figure 4-9 Crown ethers 12C4 and 18C6 undergo gas phase ion-molecule exchange reaction: $M^+ \cdot 18C6 + 12C4 = M^+ \cdot 12C4 + 18C6$. Gaseous $M^+ \cdot 18C6$ is produced by electrospray and 12C4 by a vaporizer.

Due to the ion evaporation mechanism, the gas phase metal ions produced by electrospray are actually solvated clusters, see Figure 4-10. If "maximum contact point" dominates the gas phase complexation process of crown ether and metal ion, the formation of the host-guest complex is not favored because most solvated clusters have a larger size than the cavity of 18C6. Thus, most of M^+L complex ions should be formed in solution instead of in gas phase. However, the contribution of gas phase complexation should also be considered when the sensitivity enhancement by complexation is going to be assessed.

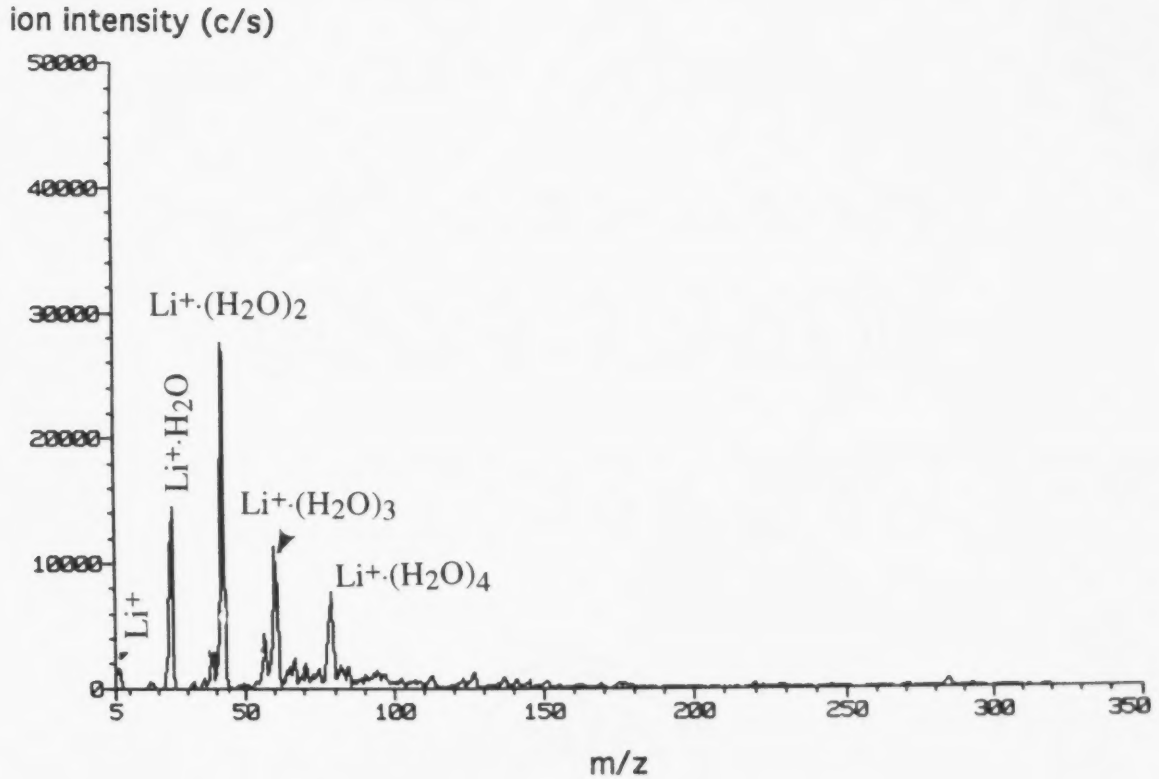

Figure 4-10 Electrospray mass spectra of lithium chloride in methanol solution; gas phase lithium ions are mainly in the form of solvated clusters; [LiCl]=10^{-4} M in methanol.

4.4 Conclusions

Measured ion intensity ratios: I_{ML^+}/I_{M^+} of electrosprayed solutions of M^+ and L in methanol where $M^+ = Na^+, K^+, Rb^+, Cs^+$ and L = 18C6, are compared to the expected ion ratios due to the solution equilibria and due to an increase of solute concentrations because of solvent evaporation from the droplet prior to gas phase ion emission from the droplets. K^+ and Rb^+ have very high stability constants, K_s, and the equilibria are shifted too far to the product (M^+L) side. The I_{ML^+}/I_{M^+} for these systems do not provide a confirmation for a large evaporative solvent loss. The position of the equilibria for Na^+ and Cs^+ which have lower K_s values are more suitable for the measurements and these systems indicate a decrease of solvent volume by a factor of ~15. This factor is smaller than expected in chapter 3 but still of sufficient of magnitude to indicate that there is a large loss of solvent which will lead to important changes of the solute concentration in the droplets.

4.5 References

1. R.J. Pfeifer and C.D. Hendricks, *AIAA Journal*, 6, 496 (1968)
2. J.V. Iribarne and B.A. Thomson, *J. Chem. Phys.*, **64**, 2287 (1976)
3. A. Gomez and K. Tang, *Physics of Fluids A* (in print).
4. I. M. Kolthoff; *Anal. Chem*; **51**, 1R (1974)
5. A.J. Smetana, A.I. Popov; *J. Solution Chem.*, **9**(3) 183 (1980)
6. H. J. Buschmann; *Inorg. Chim. Acta.*, **125**, 31 (1986)
7. H. J. Buschmann; *Inorg. Chim. Acta.*, **105**, 59 (1985)
8. R. B. Sharma and P. Kebarle; *JACS*, **106**, 3913 (1984)
9. R. B. Sharma, A. T. Blades and P. Kebarle; *JACS*, **106**, 510 (1984)
10. S. Maleknia and J. Brodbelt; *JACS*, **114**, 4295 (1992)
11. C. Liou and J. Brodbelt; *JASMS*, **3**, 543(1992)
12. H. Zhang, I. Chu, S. Leming and D.V. Dearden; *JACS*, **113**, 7415 (1991)
13. H. Zhang; D.V. Dearden, *J. Am. Chem. Soc.*, **114** 2754 (1992)
14. D.V. Dearden, H. Zhang, I. Chu, P. Wong and Q. Chen; *Pure & Appl. Chem.*, **65**(3) 423 (1993)
15. G. Michaux and J. Reisse; *JACS*, **104**, 6895 (1982)
16. G. W. Liesegang, et al; JACS, **99**, 3240 (1977)
17. A.Y. Tsivadze, N.B. Generalova and E.N. Pyatova; *Russian J. Inorg. Chem.*, **31**(1), 17 (1986)
18. S. Yanagida, K. Takahashi and M. Okahara; *Bulletin of Chem. Soc. of Japan*, **51**(5) 1294 (1978)
19. a. Chapter 3 in this thesis, b. L. Tang and P. Kebarle; *Anal. Chem.*, (submitted)

Chapter 5 Sampling Efficiency in ESMS

5.1 Introduction

In electrospray, the solution sprayed from the electrospray tip consists of unipolarly charged droplets. For the positive-ion mode of ESMS, the droplets have excess positive ions and a positive electrical current, resulting from the positively charged droplets, flows from the electrospray tip towards the counter electrode on the mass spectrometer. Because this cloud of droplets is charged, it gives rise to a radial electrostatic field E which increases with distance from the axis of the cloud, where it is zero, to a maximum value at the outer edge of the cloud. This field acts upon the charged droplets and drives them radially outwards.

The field strength due to the space charge can be assessed with the Poisson equation (1). Since a cross section of the charged-droplet cloud may be considered to have cylindrical symmetry, the Poisson equation in cylindrical coordinates can be applied:

$$\frac{1}{r}\frac{d}{dr}\left[r\frac{dV}{dr}\right] = -\frac{\rho}{\varepsilon_{o,}} \qquad \text{where} \qquad (5\text{-}1)$$

r: radial distance from the axis of the cloud to the edge of the cloud

V: potential of charged-droplet cloud

ρ: space charge density

ε_o: permittivity of vacuum.

Substituting the field, E = dV/dr, into equation 5-1 and integrating one obtains

$$E = -\frac{\rho r}{2\varepsilon_o} \qquad (5\text{-}2)$$

If the number density of charged droplets in the cloud is n and each droplet is assumed to carry the same quantity of charge q, the charge density ρ is

$$\rho = nq \qquad (5\text{-}3)$$

The radial, coulombic force F on the droplets within the cloud is given by

$$\begin{aligned} F &= qE \\ &= nq^2r/(2\varepsilon_o) \end{aligned} \qquad (5\text{-}4)$$

The effect of the radial field due to the space charge is very noticeable in photographs of the electrospray jet (2) which show that the droplet cloud expands radially very rapidly. Sunner et al. (3) were among the first to propose that the space charge will have an important influence on the observed ion intensities in ESMS. The presence of the radial space charge induced electrical field suggests that it is desirable to sample the ions as close to the ES capillary tip as possible, in order to achieve maximum MS sensitivity. On the other hand it is not desirable to sample too close to the ES tip because gas phase ions may not yet have been formed from the droplets. Also, at close distance, the average droplet size is relatively large and evaporation of the droplet in the sampling region will lead to undesirable high solvent vapor pressure and ion-solvent cluster formation. In practice (4) a compromise between the conflicting requirements is chosen which depends also on the details of the ion sampling arrangement. For example, when the interface to the vacuum is via a capillary (5), heating of the capillary causes solvent evaporation from the droplet and ion

declustering, and in such a case the distance between the ES capillary tip and the sampling orifice can be shorter.

From the above discussion, it is evident that the space-charge effect may influences the mechanism of gas phase ions produced from the charged droplets (see Chapters 3 and 4). For example, one can question whether the space-charge causes relative ion-detection sensitivities to change. In our work, Chapter 3 and 4, we assumed that the relative sensitivity coefficients, k_A/k_B, for various ion species A^+ and B^+ depend only on Iribarne-type ion evaporation differences or differential surface enrichment effects, i.e. the tacit assumption was made that species-selective space charge effects are unimportant.

The effect of the radial field on the ions will change relative intensities if the gas phase ion mobilities of A^+ and B^+ are significantly different. Ion mobilities are approximately proportional to $(\mu/\alpha)^{1/2}$ where α is the polarizability of the ambient gas (N_2, O_2, CH_3OH, etc) and μ is the reduced mass of the ion and ambient gas molecule. For ions whose mass is considerably higher than the mass of the ambient gas (~30) the reduced mass becomes equal to that mass (6). Such ions, which include the majority of ES ions of interest, will have very similar mobilities. On this basis selectivity affecting k_A/k_B due to space charge is not expected. However, the situation may be more complicated.

Hiraoka (7) recently published measurements of relative intensities of ESMS ions as a function of the axial and radial positions of the ion sampling orifice relative to the ES capillary tip. In the measurements, the author changed the position of the ES capillary, leaving the sampling orifice position constant. The solution used was 10^{-3} M acetic acid and 5×10^{-6} M $(CH_3)_4NBr$ in methanol. The author observed large changes in

the positive ion intensities with axial and radial distance. The results for axial distance are given in Figure 5-5 in the Discussion section. The observed major ions were $CH_3OH_2^+$, NH_4^+ and $(CH_3)_4N^+$. The $(CH_3)_4N^+$ ion is expected, as is $CH_3OH_2^+$ due to the protonation of CH_3OH by acetic acid in the solution. However the presence of NH_4^+ is unexpected since this cation was not added to the solution. The NH_4^+ could be formed by the gas phase ion-molecule reaction:

$$CH_3OH_2^+(g) + NH_3(g) = CH_3OH(g) + NH_4^+(g) \qquad (5\text{-}5)$$

where $NH_3(g)$ is due to the presence of ammonia in the ambient air. This reaction is routinely observed in our laboratory whenever NH_3 at concentrations equal to greater than ~10 ppb is present in the laboratory air. Therefore, the presence of NH_4^+ in Hiraoka's results represents a complication and is essentially a flaw in his experiments. In our opinion, he should not have used a precursor ion like $CH_3OH_2^+$ which is due to a base (CH_3OH) of low proton affinity, and is therefore easily deprotonated by gaseous impurities. Also, all the observed $CH_3OH_2^+$ in Hiraoka's experiment may not be due to ion desorption from solution. Corona discharge produces this ion in abundance in the gas phase when a methanol solution is electrosprayed (8). Hiraoka did add CCl_4, as a discharge suppressant, to the methanol solution. However, he provides no specific evidence that the CCl_4 is able to suppress the discharge at small axial distances.

Hiraoka's results interpreted his results on the basis of differential ion-evaporation efficiencies, i.e. k_A/k_B ratios in our nomenclature. It was suggested that $(CH_3)_4N^+$, which is expected to have a high k_A, evaporates from the droplet before the other ions and its ion profile is interpreted on that basis (7).

While the intent and interpretation of Hiraoka's experiment are interesting, they are not concordant with the models of gas phase ion formation considered in Chapter 3, where it was concluded that gas phase ions are formed from very small droplets whose lifetime (several μs) is very much shorter than the total lifetime of the droplets emitted from the ES capillary (~100 μs). The interpretation used Hiraoka implies a rather long duration of the ion emission stage of a droplet, i.e. a duration comparable to the total transit time of a droplet from the ES capillary tip to the sampling orifice (~100-1000 μs).

In an attempt to resolve this contradiction, we decided to perform experiments of the same kind as those of Hiraoka's. We did not use $CH_3OH_2^+$ as one of the ions, but a species that must be produced by the ES process and is not reactive in the gas phase. Therefore, the solution that we used contained equimolar KCl and $(C_2H_5)_4NBr$ at concentrations of $5x10^{-5}$ M in methanol. It should be recalled (Chapter 3) that Et_4N^+ is an ion with a higher sensitivity coefficient than K^+. Therefore, this pair of ions has different ion sensitivity coefficients as was the case in Hiraoka's experiment, but is not affected by gas-phase ion-molecule reactions.

5.2 Experimental

The experiments were performed with the TAGA 6000E which was described in Chapter 3. In the present experiments, the position of the electrospray tip relative to the aperture of the mass spectrometer was changed in three dimensions. The axial distance (L) between the ES tip and the aperture was varied by moving the supporting rod of the ES tip in an axial direction, z, while the radial distance (r) between the ES tip and the

aperture was varied by adjusting the position of the x-y manipulator as shown in Figure 5-1. The flow rate of the spray solution was controlled by changing the selector positions on the syringe pump (syringe pump model 341B, Sage Instrument).

When the effect of axial distance on the detected ion intensity was investigated, the experiments were conducted in two modes. One is the constant voltage mode, which keeps the voltage on the capillary tip constant, the other is the constant current mode, which changes the voltage on the capillary tip to maintain constant ES current. It should be recalled that the ES current is a function of the electrical field on the capillary tip as stated in Chapter 2, while this electrical field depends on both voltage and axial distance (9). The object of the constant voltage mode was to examine the ion intensity dependence on the axial distance. However, the electrical discharge at short distance results in severe interferences. It was found that this problem could be obviated with the constant current mode.

5.3 Results and Discussion

a. Ion intensity dependence on axial distance between ES tip and ion sampling orifice

When a solution of Et_4N^+ and K^+ in methanol was used, the ion intensities changed with axial distance as shown in Figure 5-2 and 5-3. The K^+ ion species were K^+, $K^+{\cdot}H_2O$ and $K^+{\cdot}CH_3OH$. The intensity ratios for these three species change somewhat with distance. Thus, the $K^+{\cdot}CH_3OH$ intensity increased as the distance is decreased. We attribute this effect to penetration of methanol droplets into the interface chamber at short

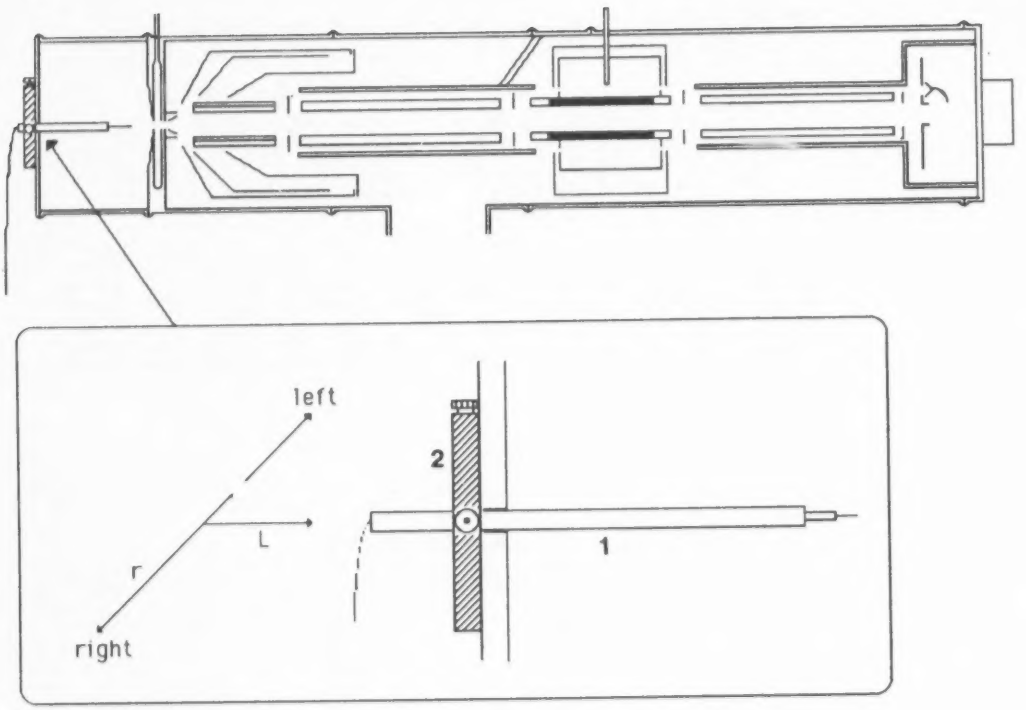

Figure 5-1 The position of electrospray tip is controlled by moving either supporting rod or x-y manipulator. 1. supporting rod; 2. x-y manipulator.

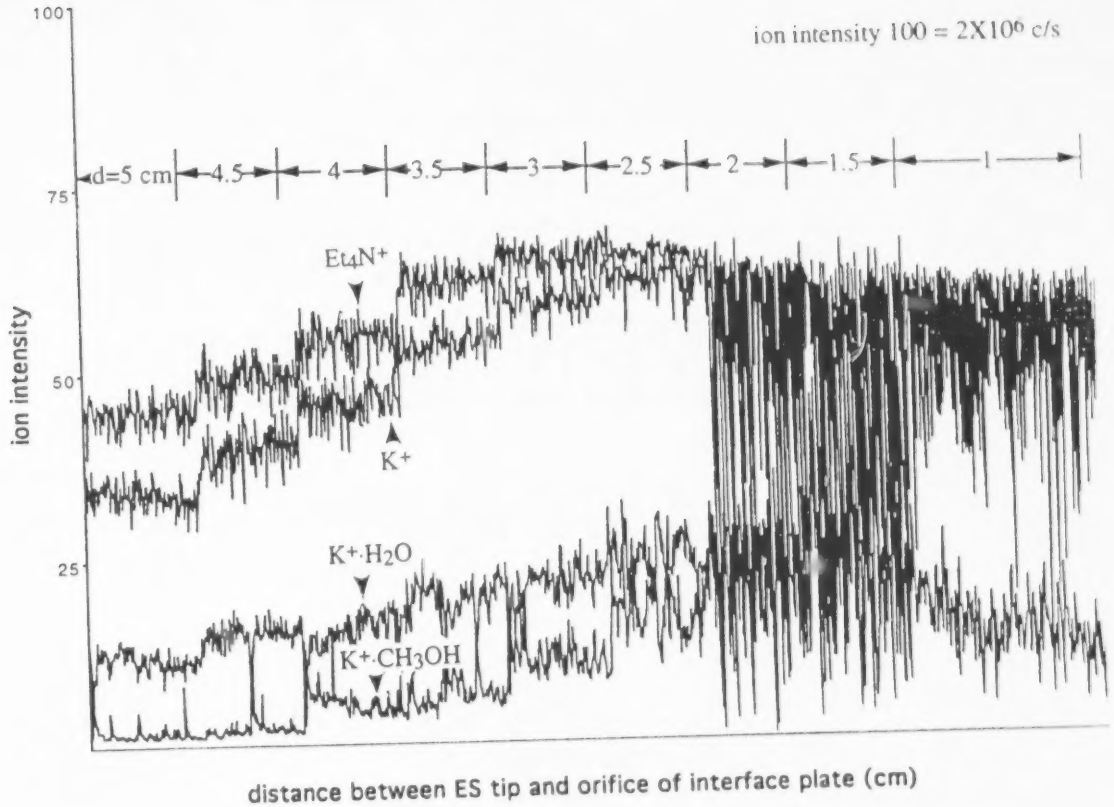

Figure 5-2 The axial distance dependence of ion intensities of Et_4N^+ and $K^+(Sol)_n$ at constant ES voltage. Methanol solution contained $5x10^{-5}$ M Et_4NBr and $5x10^{-5}$ M KCl. Experimental conditions were with r=0 mm, F=20 µL/min and constant capillary voltage V=5 kV.

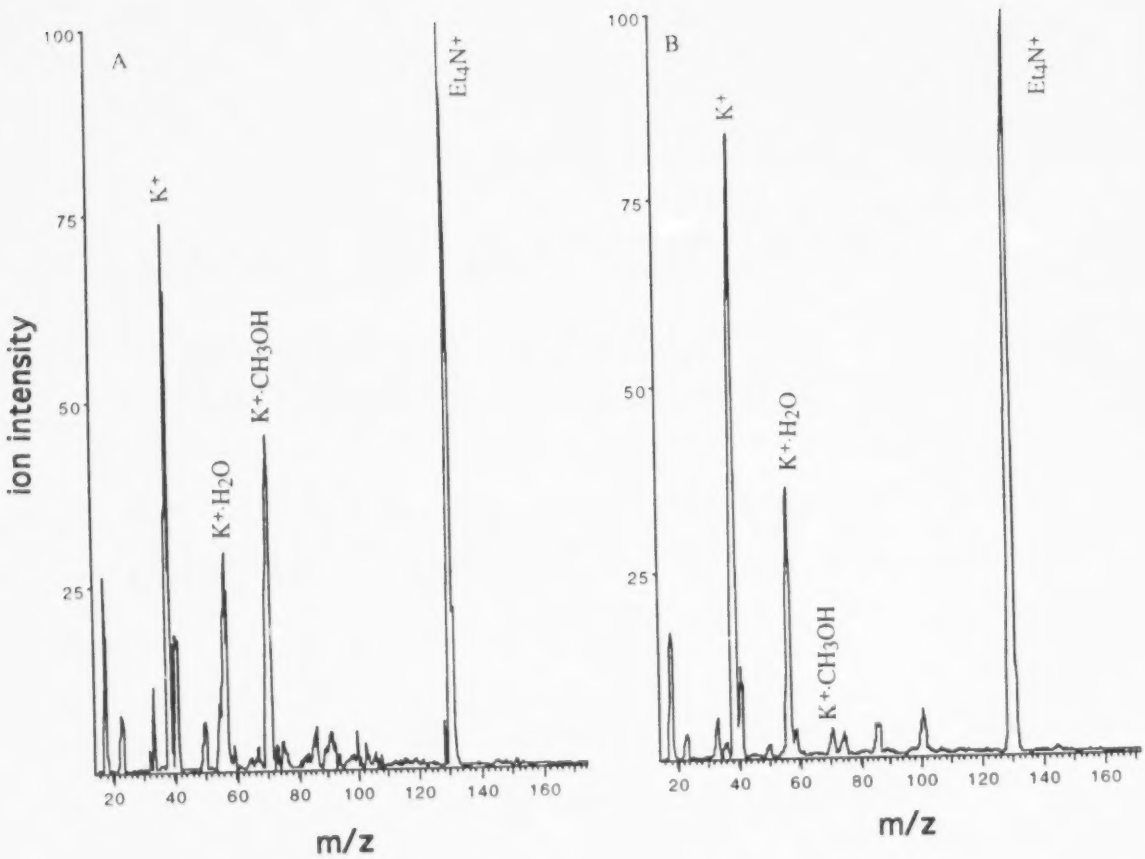

Figure 5-3 The distance (L) change of ES tip from opposite electrode on the mass spectrometer shifts the relative ion intensities of $K^+ \cdot H_2O$ and $K^+ \cdot CH_3OH$. Both KCl and Et_4NBr concentrations were 5×10^{-5} M. (A) L=2.5 cm; (B) L=4 cm.

distances, see Figure 3-1 of apparatus in Chapter 3. Methanol evaporating from these droplets leads to methanol vapor in the interface region which competes with the 2 ppm water vapor in the N_2 gas present in the interface chamber. This leads to a clustering reaction of CH_3OH with the potassium ion.

The Et_4N^+ ion, which has a much larger radius than K^+ and hydrophobic substituents, has much lower binding affinity for a solvent molecule and is observed only as the naked ion Et_4N^+. To compare the Et_4N^+ with K^+ ion intensities, we summed over all the K^+ ion intensities. These data are given in Table 5-1, for both constant voltage and current modes. For constant voltage mode we included data only down to distances of 2.5 cm because electrical discharges apparently occur at smaller distances. This is indicated by the very noisy ion signals at distances less than 2.5 cm in Figure 5-2 in constant voltage mode. As the distance (L) is decreased, the electric field near the capillary tip increases as indicated by equation 2-8 in Chapter 2. Evidently, the field becomes large enough to initiate an electric discharge for d<2.5 cm. The ratio between the ion intensities, Et_4N^+/K^+, at constant V in Table 5-1 is seen to change little, i.e. from 2 at d = 5 cm to 1.4 at d = 3 cm, after correction for mass discrimination. The increase of ES capillary current with the decrease of axial distance is expected, see Hendricks equation

$$I = \left(\frac{4\pi}{\varepsilon}\right)^{3/7} (9\gamma)^{2/7} \varepsilon_o^{5/7} Q^{4/7} (\sigma E_c)^{3/7}$$ in Chapter 2.

The ion intensities shown in Figure 5-4 were obtained in the constant capillary current mode with I = 0.2 μA. In this case an electric discharge at low distance does not occur and undisturbed ion intensities

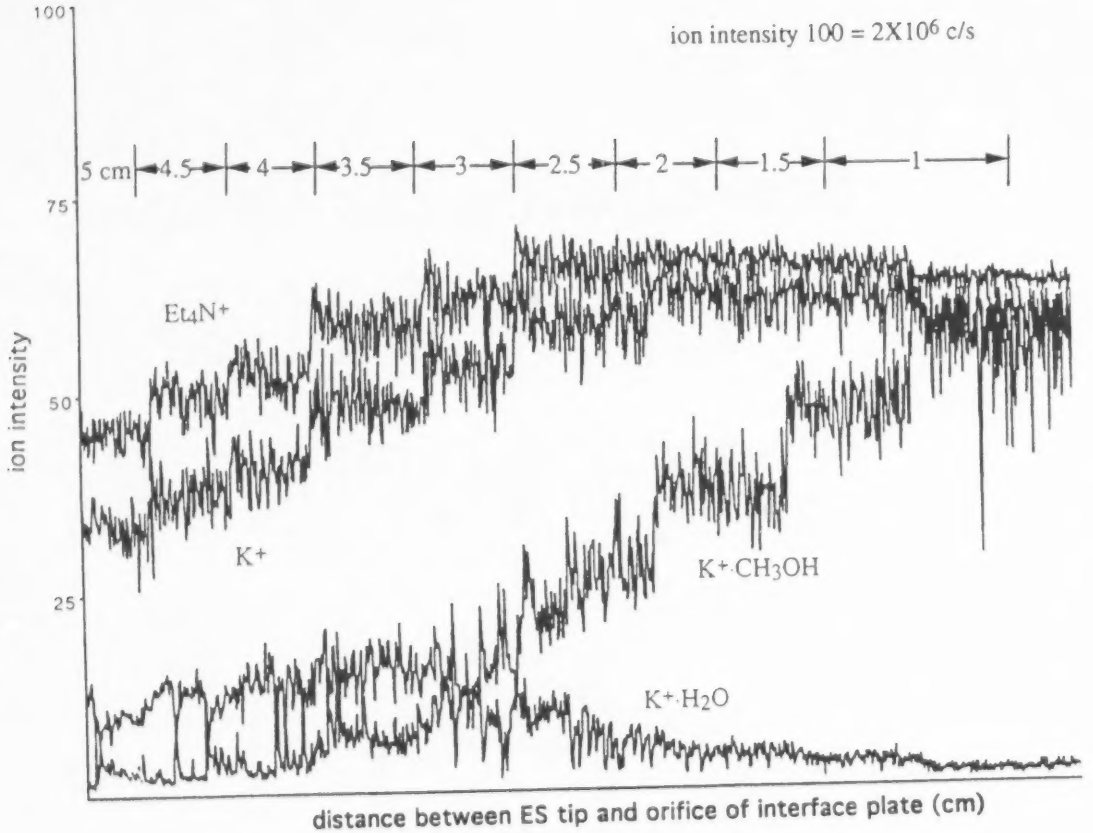

Figure 5-4 The axial distance dependence of ion intensities of Et_4N^+ and $K^+\cdot(Sol)_n$ at constant ES current. Methanol solution contained $5x10^{-5}$ M Et_4NBr and $5x10^{-5}$ M KCl. Experimental conditions were with r=0 mm and constant ES current 0.2 μA.

Table 5-1. Ion Intensity Changes with Axial Distance between ES Capillary and Sampling Orifice

d (cm)	Constant V [a]			Constant I [b]			Ref. 5[c]
	K^+ (c/s)	Et_4N^+ (c/s)	$\frac{Et_4N^+}{K^+}$	K^+ (c/s)	Et_4N^+ (c/s)	$\frac{Et_4N^+}{K^+}$	$\frac{Me_4N^+}{MeOH_2^+}$
5	$6.6x10^5$	$1.3x10^6$	2.0	$6.7x10^5$	1.3x106	2.0	~10
4	$1.0x10^6$	$1.6x10^6$	1.6	$8.8x10^5$	1.5x106	1.7	~3.5
3	$1.4x10^6$	$1.9x10^6$	1.4	$1.2x10^6$	1.8x106	1.5	~0.5
2	-	-	-	$1.6x10^6$	1.9x106	1.2	~0.16
1	-	-	-	$1.9x10^6$	1.9x106	1.0	~0.1

a. Present work. Distance was changed at constant ES voltage. For d<3 cm, electrical discharges were observed, see Figure 5-2. K^+ ion intensities are summed over K^+, $K^+{\cdot}H_2O$ and $K^+{\cdot}CH_3OH$.

b. Present work. Distance was changed at constant ES current I, i.e. capillary voltage was decreased with decrease of distance. Data from Figure 5-4.

c. From Hiroaka's work, see Figure 5-5. Intensities of $CH_3OH_2^+$ include intensity of NH_4^+ because NH_4^+ is probably an ion-molecule reaction product of CH_3OH, see text.

could be observed down to a distance of L = 1 cm. The $Et_4N^+/\Sigma K^+$ ratios, Table 5-1, observed at large L are similar to those obtained with constant capillary voltage. This is to be expected since the conditions for the two sets of experiments are very similar. The ratio $Et_4N^+/K^+ = 1.0$ observed for the smaller distance L = 1 cm is roughly half that for the largest distance. Thus, changes occur but they are not drastic. Hiraoka's data are difficult to interpret because of the presence of the extraneous NH_4^+ ions. If one assumes that NH_4^+ was formed by the ion-molecule reaction (equation 5-5) from $CH_3OH_2^+$, the sum of intensities for $CH_3OH_2^+$ and NH_4^+ should be representative of the $CH_3OH_2^+$ intensity produced by the ES process in the absence of an electric discharge. The ratio $Me_4N^+/CH_3OH_2^+$ given in Table 5-1 was calculated from Figure 5-5 with this assumption. The ratio changes drastically with distance from 10 at L = 5 cm to 0.1 at L = 1 cm, i.e. by a factor of 100! The presence of a weak electric discharge in Hiraoka's experiments at short distance would give high protonated-ion densities and provide an explanation for the low ratio of intensities. The high ratio at L = 5 cm is more difficult to explain. The solution contained $5x10^{-6}$ M of Me_4N^+ and about $3x10^{-5}$ M of $CH_3OH_2^+$ calculated for a 10^{-3} M CH_3COOH solution (assuming a $pK_a = 6$ in methanol-water solvent (10, 11)), i.e. the protonated species dominate the Me_4N^+ six-fold. Since the solution concentrations are low, the $k_{Me_4N^+}/k_{CH_3OH_2^+}$ effectively observed due to depletion will not be larger than 3 one expects an ion intensity ratio: $Me_4N^+/CH_3OH_2^+ = 1/2 = 0.5$ in the absence of distance effects. Therefore, it appears that the large value, 10, at large distance is the unexpected value, although we don't know the mass dependent discrimination present in his quadrupole. For the present, we are unable to rationalize the large difference between Hiraoka's

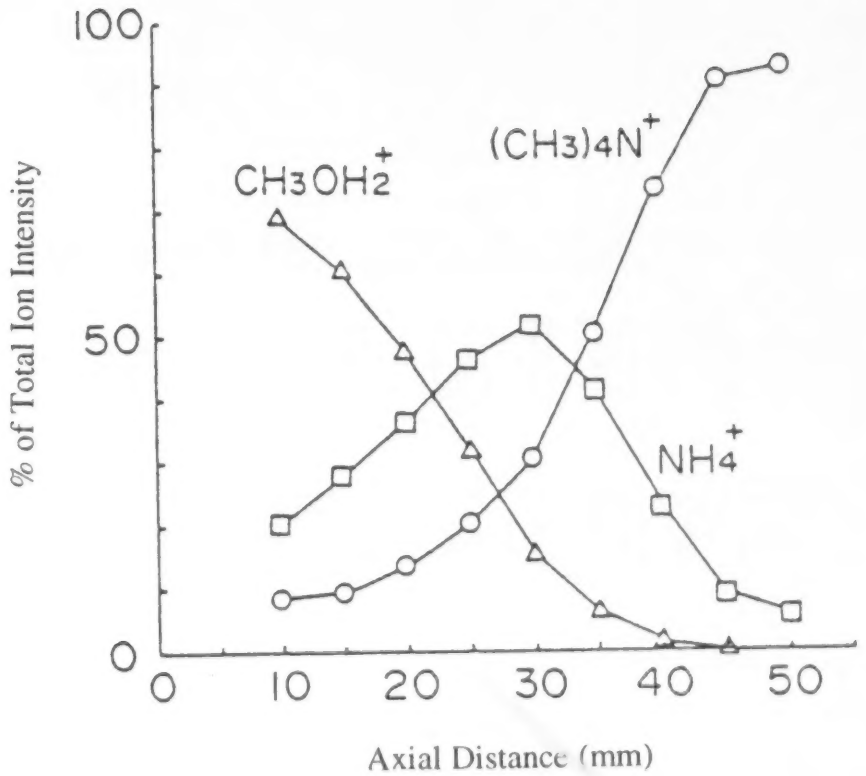

Figure 5-5 Ion intensities change with axial distance observed by Hiraoka (7). ES solution is $5x10^{-6}$ M $(CH_3)_4NBr$ and $1x10^{-3}$ M CH_3COOH in $CH_3OH+H_2O+CCl_4$ (8/2/0.5 v/v/v); Flow rate=10 μL/min; Capillary voltage V=3.1 kV.

data and our own.

b. Ion intensity dependence on radial distance between the ES tip and ion sampling orifice

The study of the effect of radial distance on the relative ion intensities was carried out with Et_4N^+ and K^+ as analyte ions since Hiraoka's work demonstrated that radial distance between ES tip and sampling orifice can cause a large difference in analyte ion intensity. He investigated the effect of radial distance on the detected ion intensities with $5x10^{-6}$ M $(CH_3)_4NBr$ and $1x10^{-3}$ M CH_3COOH as analytes in ESMS solution. His findings, shown in Figure 5-6, suggest that careful consideration of radial distance is necessary when analyzing the detected ions. For example, all $(CH_3OH)_n{\cdot}H^+$ (n = 1~3) ion intensities are sensitive to radial distance. The intensities are at a maximum at the axis of the droplet cloud and decreases rapidly with the distance from the axis. On the contrary, NH_4^+ from ambient air has its lowest ion intensity in the center of droplet cloud and reaches its highest intensity near the edge of the cloud. The ion intensity of $(CH_3)_4N^+$ is relatively insensitive to the change of radial distance if compared to $(CH_3OH)_n{\cdot}H^+$, even though it eventually decreases at a large radial distance (of about 10 mm). Thses results can be rationalized in terms of gas phase ion-molecule reactions. The ions near the edge of charged droplet cloud are subject to reactions with air-born molecules more than the ions in the center of the cloud. In Figure 5-6, the molecule NH_3 in the ambient air can penetrate the charged droplet cloud and, since NH_3 is a stronger base than CH_3OH, it will remove the protonated analyte ion produced by electrospray. The ions in the central

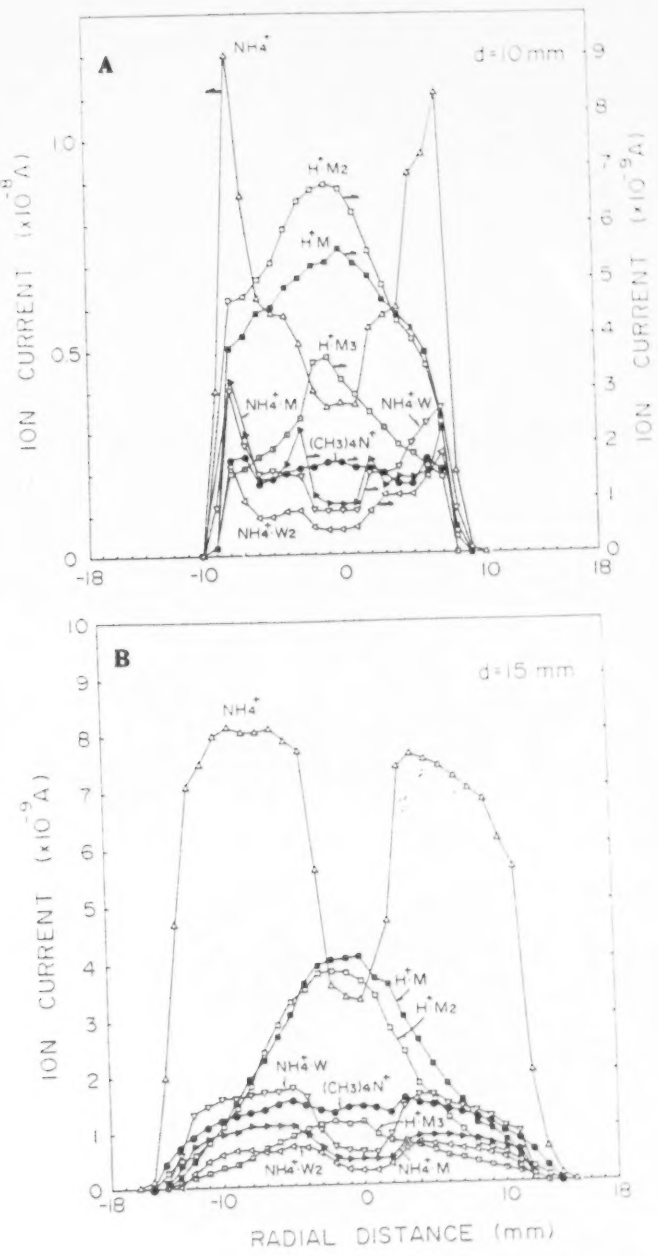

Figure 5-6 Ion intensities change with radial distance observed by Hiraoka. ES solution was $5x10^{-6}$ M $(CH_3)_4NBr$ and $1x10^{-3}$ M CH_3COOH in $CH_3OH+H_2O+CCl_4$ (8/2/0.5 v/v/v); Flow rate=10 µl/min; Capillary voltage V=3.1 kV. (A) L=1 cm; (B) L=1.5 cm.

region of the cloud are less affected by the reaction, since the NH_3 concentration is relatively low. In this sense, sampling at the center of the charged droplet cloud will provide optimum conditions for the detection of ES produced ions. The interference from impurity gases in ESMS is also alleviated if the analyte ion, such as $(CH_3)_4N^+$, is unable to transfer its charge to other gaseous molecules. Proton transfer from NH_4^+ to analyte was not a problem in our research on the ES mechanism as all the experiments in Chapter 3 used analytes which either had a high proton affinity or can not transfer charge to neutral molecules.

The radial distance effect was evaluated again with the consideration of gas phase reaction. Figure 5-7 shows that ion intensities of both Et_4N^+ and K^+ essentially remain constant in the whole range of radial distance change which is available on the modified TAGA 6000E. From equation 5-3, we know that the charge density ρ is proportional to the number density n. According to Hendricks equation, the capillary current is determined by distance and voltage. We found that charge density ρ in electrospray is constant everywhere in the cloud at a specific distance with our experimental conditions, which maintain total ES ion current constant. The ion intensity might eventually decrease if the distance could be adjusted further away from the aperture on TAGA 6000E. However, our concern is with the ion intensity which arises from electrospray. The constant ion intensity relative to the radial distance indicates that the ion intensity detected in the experiments reflects the gas phase ion density.

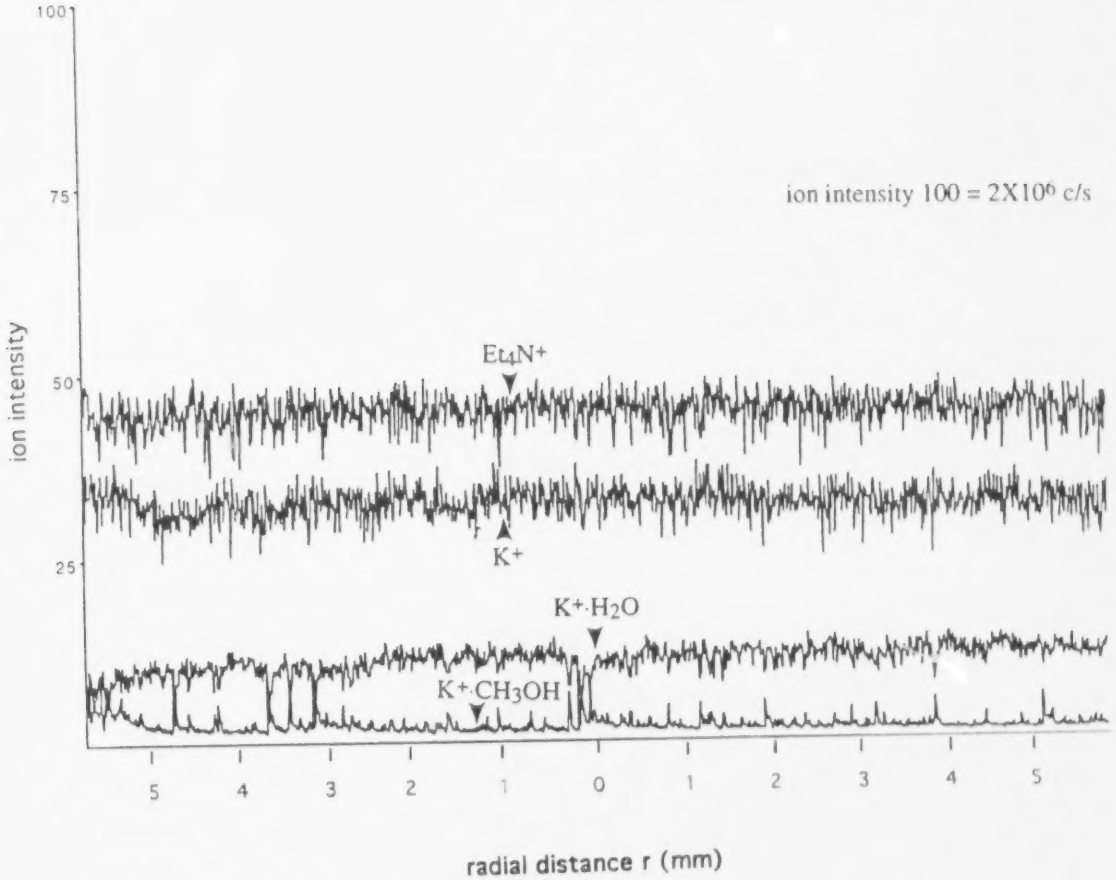

Figure 5-7 The radial distance dependence of ion intensities of Et_4N^+ and $K^+(Sol)_n$. Methanol solution contains $5x10^{-5}$ M Et_4NBr and $5x10^{-5}$ M KCl with L=5 cm, F=20 μL/min and V=5 kV.

c. Influence of flow rate on relative ion intensities

In Chapter 3, the flow rate used in the experiments was unchanged. Although 20 μL/min is a reasonable flow rate in the ESMS experiments under the conditions developed in our group, it was subjected to verification of its effect on sampling efficiency. After the flow rate was reduced 50%, the ion intensity changed in a pattern similar to the original flow rate. Figure 5-8 illustrates that both Et_4N^+ and K^+ intensities maintain a similar ratio but increase with the decreasing axial distance. Figure 5-9 shows that radial distance has almost no effect on ion intensity. When L = 1 cm, there is little difference for $K^+{\cdot}CH_3OH$, which shows a bit higher intensity at r = 0 mm. Therefore, a higher flow rate (20 μL/min) is more suitable in the ESMS mechanism study.

5.4 Conclusions

The space charge in ESMS exerts a force on charged species which moves them radially outwards in the droplet cloud. The detected ion intensities decrease with increase of axial distance due to the expansion of the droplet cloud when the ES current is constant. As ion mobilities at atmospheric pressure are very similar, the relative ion intensities among gas phase ions are relatively stable with change in axial distance. The ion density seems constant in the droplet cloud with our experimental conditions and the ion intensities are independent of the radial distance, although ion intensity will eventually decrease outside the cloud. Gas phase ion-molecule reactions must be taken into account in order to avoid interference from impurity gases of high proton affinity in the ambient air.

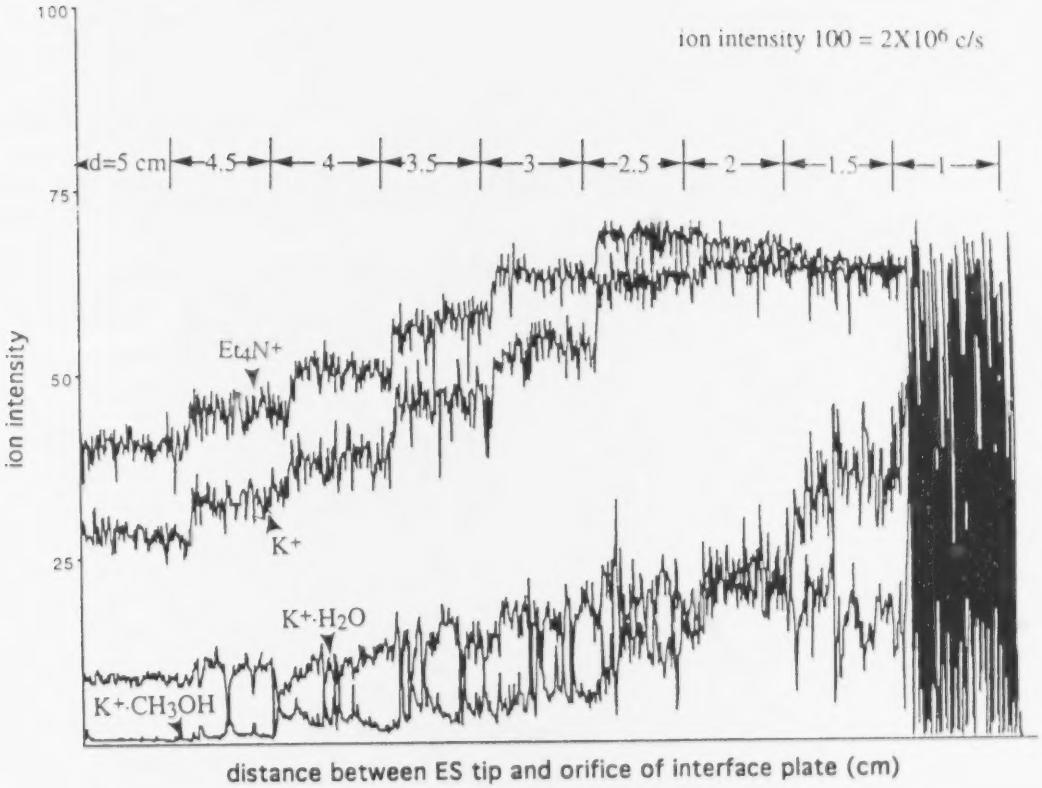

Figure 5-8 The axial distance dependence of ion intensities of Et_4N^+ and $K^+\cdot(Sol)_n$. Methanol solution contains $5x10^{-5}$ M Et_4NBr and $5x10^{-5}$ M KCl with r=0 mm, F=10 µl/min and V=4 kV.

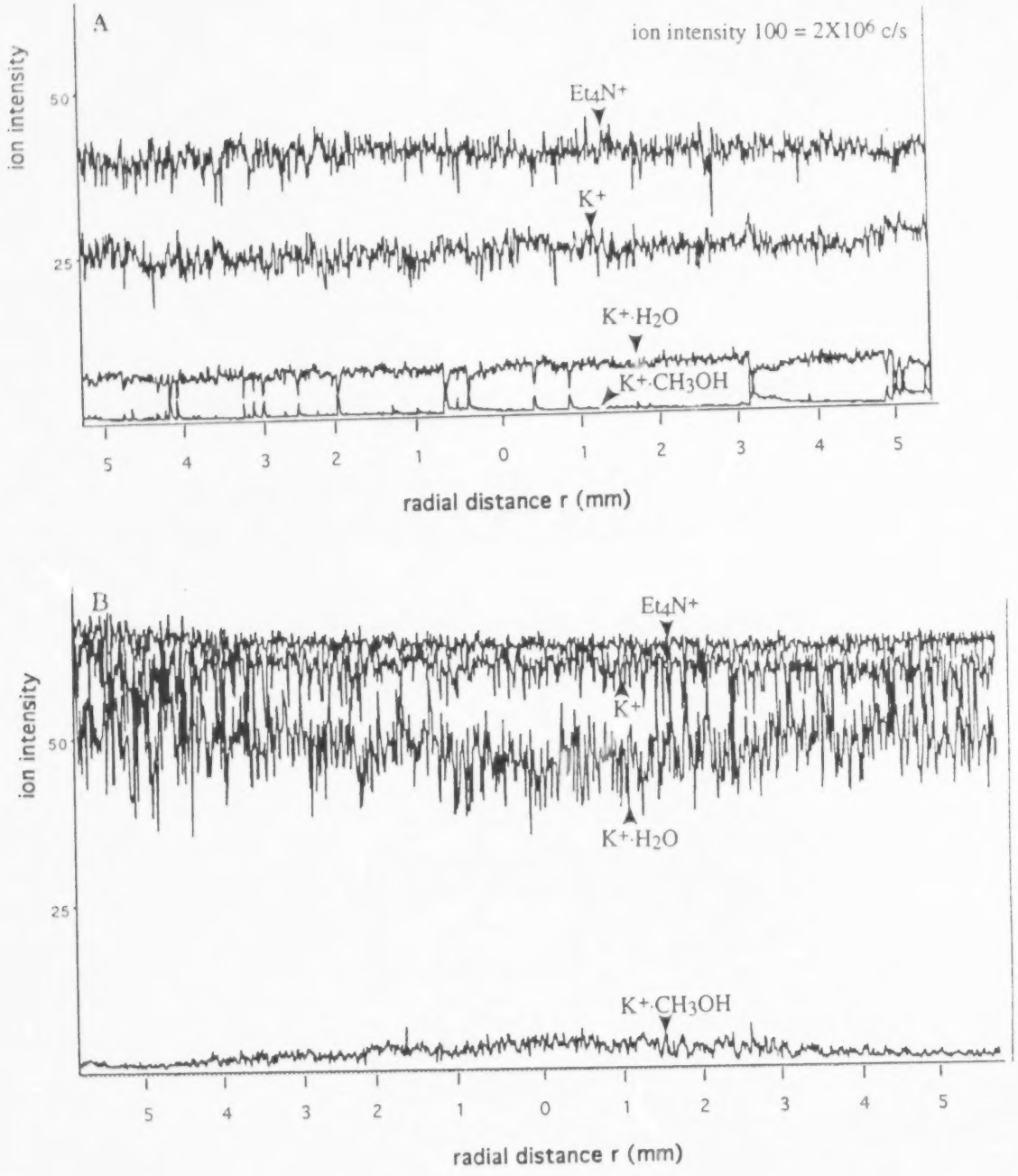

Figure 5-9 The radial distance dependence of ion intensities of Et_4N^+ and $K^+(Sol)_n$. Methanol solution contains $5x10^{-5}$ M Et_4NBr and $5x10^{-5}$ M KCl with (A) L=5 cm, F=10 µl/min and V=4 kV and (B) L=1 cm, F=10 µl/min and V=3.1 kV.

5.5 References

1. Bailey, A.G.; Chapter 5 in *Electrostatic Spraying of Liquids*, John Wiley & Sons, Inc. (1988)
2. Sheehan, E.W.; Willoughby, R.; Photographic Studies of Electrospray Aerosols presented in *The 41th ASMS Conference on Mass Spectrometry and Allied Topics* (1993)
3. Busman, M.; Sunner, J. and Vogel, G.R.; *J. Am. Soc. Mass Spectrom.*, **2**, 1 (1991)
4. Mirza, U.A.; Cohen, S.L. and Chait, B.T.; *Anal. Chem.*, **65**, 1 (1993)
5. Yamashita, M.; Fenn, J.B.; *J. Phys. Chem.*, **88**, 4671 (1984)
6. McDaniel, E.W.; Chapter 9 in *Collision Phenomena in Ionized Gases*, John Wiley & Sons Inc. (1964)
7. Hiraoka, K.; *Rapid Commu. Mass Spetrom.*, **6**, 463 (1992)
8. Ikonomou, M.G.; Blades, A.T. and Kebarle, P.; *J. Am. Soc. Mass Spectrom.*, **2**, 497 (1991)
9. Smith, D.P.H.; *IEEE Trans. Ind. Appl.*, **IA-22**, 527 (1986)
10. Goodhue, L.D.; Hixon, R.M., *J. Am. Chem. Soc.*, **56**, 1329 (1934)
11. Paabo, M.; Robinson, R.A.; Bates, R.G., *J. Am. Chem. Soc.*, **87**, 415 (1965)